AD-A146 393 RADAR BEAMSPLITTING EXPERIMENTS AND FEASIBILITY DEMONSTRATION OF A COMBIN.. (U) GEORGIA INST OF TECH ATLANTA ENGINEERING EXPERIMENT STATION W A HOLM ET AL. 1/2

UNCLASSIFIED JUL 78 GIT/EES-A-2047-000 SBI-AD-E001 604 F/G 17/9 NL

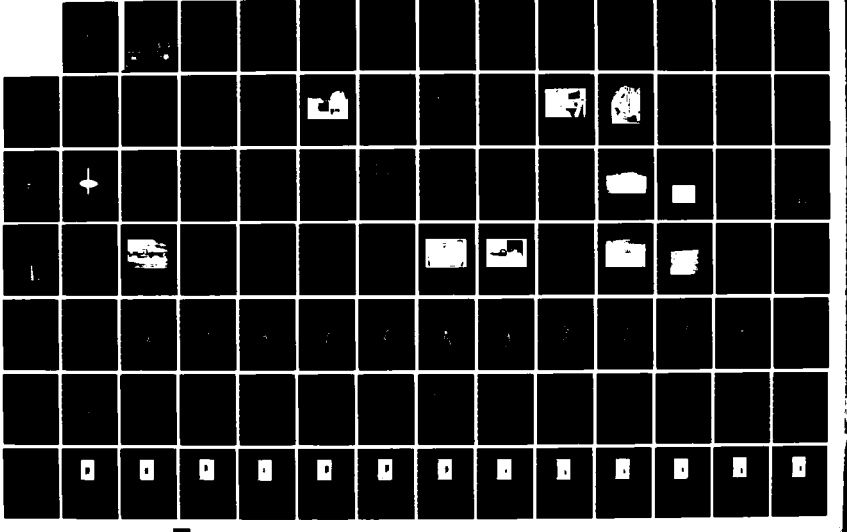

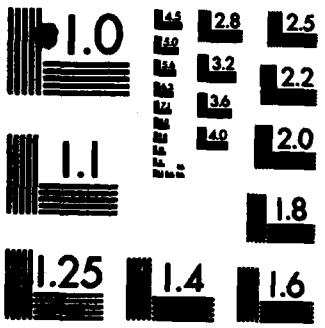

OPY RESOLUTION TEST CHART

AD-E001604

RADAR BEAMSPLITTING EXPERIMENTS AND FEASIBILITY DEMONSTRATION OF A COMBINED ELECTRO-OPTICAL/RADAR SENSOR SYSTEM

AD-A146 393

Final Technical Report for Period 1 September 1977 – 31 March 1978

By

W. A. Holm, R. C. Michelson, W. S. Foster, and B. A. Lafitte

REPORT N00014-77-C-0683

EES/GIT PROJECT A-2047-000

Prepared for

DEPARTMENT OF THE NAVY
OFFICE OF NAVAL RESEARCH
ARLINGTON, VIRGINIA 22217

U. S. ARMY ELECTRONICS COMMAND
FT. MONMOUTH, NEW JERSEY 07703

DTIC
ELECTE
SEP 28 1984
S D
A

JULY 1978

GEORGIA INSTITUTE OF TECHNOLOGY
Engineering Experiment Station
Atlanta, Georgia 30332

DTIC FILE COPY

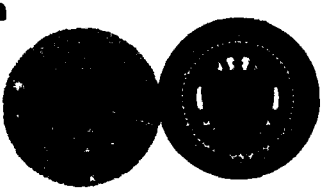

This document has been approved for public release and sale; its distribution is unlimited.

84 09 26 171

UNCLASSIFIED

SECURITY CLASSIFICATION OF THIS PAGE (When Data Entered)

REPORT DOCUMENTATION PAGE		READ INSTRUCTIONS BEFORE COMPLETING FORM
1. REPORT NUMBER	2. GOVT ACCESSION NO. ADA146393	3. RECIPIENT'S CATALOG NUMBER
4. TITLE (and Subtitle) RADAR BEAMSPLITTING EXPERIMENTS AND FEASIBILITY DEMONSTRATION OF A COMBINED ELECTRO-OPTICAL/ RADAR SENSOR SYSTEM		5. TYPE OF REPORT & PERIOD COVERED Final: 9/1/77 - 3/31/78
		6. PERFORMING ORG. REPORT NUMBER A-2047-000
7. AUTHOR(s) W. A. Holm, R. C. Michelson, W. S. Foster, and B. A. Lafitte		8. CONTRACT OR GRANT NUMBER(s) N00014-77-C-0683
9. PERFORMING ORGANIZATION NAME AND ADDRESS Engineering Experiment Station Georgia Institute of Technology Atlanta, Georgia 30332		10. PROGRAM ELEMENT, PROJECT, TASK AREA & WORK UNIT NUMBERS
11. CONTROLLING OFFICE NAME AND ADDRESS U.S. Army Electronics Command Fort Monmouth, New Jersey 07703		12. REPORT DATE July 1978
		13. NUMBER OF PAGES 115
14. MONITORING AGENCY NAME & ADDRESS(if different from Controlling Office) Department of the Navy Office of Naval Research Arlington, Virginia 22217		15. SECURITY CLASS. (of this report) UNCLASSIFIED
		15a. DECLASSIFICATION/DOWNGRADING SCHEDULE

16. DISTRIBUTION STATEMENT (of this Report)

APPROVED FOR PUBLIC RELEASE.
DISTRIBUTION UNLIMITED.

17. DISTRIBUTION STATEMENT (of the abstract entered in Block 20, if different from Report)

18. SUPPLEMENTARY NOTES

19. KEY WORDS (Continue on reverse side if necessary and identify by block number)

Dual Mode Sensor, Radar Sensor, Electro-Optical Sensor, Radar Beamsplitting, Radar Target Locating Accuracy, Target Handoff, Target Classification.

20. ABSTRACT (Continue on reverse side if necessary and identify by block number)

A dual mode sensor concept for precise target location and identification was investigated by combining an electro-optical sensor with a millimeter wave radar sensor. The combined sensor system was tested using corner reflectors, a pickup truck, and a shop van as targets. Targets were located using beam-splitting techniques with an accuracy of 1 milliradian during system integration tests and with an accuracy of 1/2 milliradian in azimuth during field tests, representing a 19-to-1 improvement in azimuth resolution. The overall feasibility of the dual mode sensor concept was demonstrated by handoff experiments.

DD FORM 1 JAN 73 1473 EDITION OF 1 NOV 65 IS OBSOLETE

UNCLASSIFIED

SECURITY CLASSIFICATION OF THIS PAGE (When Data Entered)

ENGINEERING EXPERIMENT STATION
Georgia Institute of Technology
Atlanta, Georgia 30332

RADAR BEAMSPLITTING EXPERIMENTS AND FEASIBILITY DEMONSTRATION OF A COMBINED ELECTRO-OPTICAL/RADAR SENSOR SYSTEM

Final Technical Report On
EES/GIT Project A-2047-000

By

W. A. Holm, R. C. Michelson, W. S. Foster and B. A. Lafitte

Prepared for:

DEPARTMENT OF THE NAVY
OFFICE OF NAVAL RESEARCH
Arlington, Virginia 22217

and

U. S. ARMY ELECTRONICS COMMAND
Ft. Monmouth, New Jersey 00703

Under

Contract N00014-77-C-0683

July, 1978

ACKNOWLEDGMENT

The authors wish to acknowledge the following people who contributed to this research effort: N. T. Alexander, J. E. Davidson, G. R. Loefer, J. A. McKenzie, J. E. Matthews and P. W. Schwotzer. The authors would also like to express their appreciation to the Deputy Commanding Officer, Ft. Gillem, Georgia and to the personnel under his command for their cooperation and assistance during the system integration tests and field tests conducted in this program.

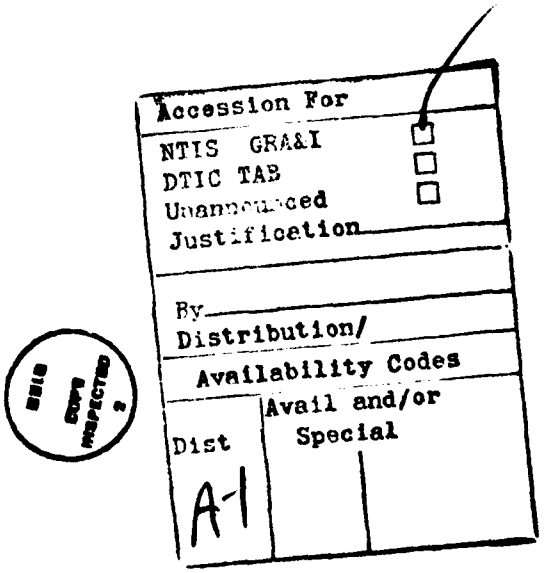

TABLE OF CONTENTS

LIST OF FIGURES

LIST OF FIGURES continued

LIST OF FIGURES continued

LIST OF FIGURES continued

LIST OF TABLES

I. INTRODUCTION

Background

A military commander in a hostile environment requires real time information for avoiding or targeting weapons against enemy forces that pose a high threat to the survivability of his command or the success of his mission. This information has traditionally been supplied by conventional surveillance and targeting systems using microwave radar as the primary sensor. The rapid proliferation of sophisticated weapon systems deployed by foreign countries is being countered by development of precision guided weapons as a force multiplier. Conventional microwave sensors, however, are severely limited in their ability to precisely locate targets and have practically no capability for target identification. The tactical commander may therefore determine that he is surrounded by hostile forces but the radar sensor cannot provide him the information he needs to determine which weapons or forces pose the highest threat; the commander needs more information if he is to make the best use of his resources.

One approach for providing tactical commanders with improved target information is the use of electro-optical (EO) sensors such as low light level television, forward looking and other infrared devices and laser radar. Since these sensors operate at, or are sensitive to, frequencies in the infrared and visible region of the electromagnetic spectrum, they can provide greater target resolution than conventional microwave radar sensors and therefore, offer a potential solution to the problems of precise target location and identification. Two basic limitations of EO sensors, however, prevent these sensors from completely replacing the radar sensor in tactical operations. The length of time required for the high resolution EO sensors to scan a given spatial volume limits their effectiveness for rapid search and target acquisition. High atmospheric attenuation losses also limit the effectiveness of EO sensors, particularly in adverse weather conditions and in battlefield environments including smoke, fog, and erosols. These losses can be so severe that a tactical vehicle without additional sensors would be literally blind to the tactical environment.

The concept being investigated by the Georgia Institute of Technology Engineering Experiment Station (GIT/EES) is based on the use of a dual mode sensor for precise target location and identification. The dual mode sensor is based on combining an EO sensor with a millimeter wave radar sensor. This approach offers the potential for overcoming some of the inherent disadvantages and limitations of the EO sensors and at the same time taking full advantage of their basic distinguishing characteristic of high resolution. The radar sensor would complement the EO sensor by performing the all-weather search and target acquisition function as well as providing moderate target location accuracy in adverse atmospheric conditions. In this dual mode sensor system, the radar sensor would perform its conventional role of searching large spatial volumes to acquire and crudely locate a target. Once the target is acquired, the higher resolution EO sensor would be directed toward the target for accurate and precise target location, target identification and weapons targeting.

Objectives

The long range goal of the GIT/EES research program being conducted for the U. S. Army Electronics Research and Development Command (ERADCOM) is to develop a dual mode (EO/radar) sensor system for surveillance and targeting applications. The intent is to use a pulsed, heterodyned CO_2 laser radar suitable for weapon guidance as the EO sensor in the final system.

The basic target locating accuracy of the radar in a clutter and multipath environment is of critical importance in determining the angle of view (AOV) to be scanned by the laser radar in both azimuth and elevation. These AOV's must be kept to a minimum because of the long time required for laser radar to scan a large spatial volume. The radar sensor must also effectively locate the target when the EO sensor is ineffective due to adverse environmental conditions. The primary objectives of this initial phase of the dual mode sensor research program were, therefore, to:

1. Experimentally determined the minimum angular (azimuth and elevation) uncertainty of target position as measured with the radar sensor alone by use of beamsplitting techniques.

2. Experimentally investigate the problems associated with the handoff of targets from the radar sensor to the EO sensor and demonstrate the overall feasibility of the dual mode sensor concept for surveillance and targeting applications.

Summary

The initial phase of the dual mode sensor research program was conducted by modifying a GIT/EES instrumentation radar facility to add an EO sensor and other measurement equipment. A conventional television camera was chosen to simulate the laser radar for the initial experiments and feasibiliby demonstration. The primary tasks accomplished were system integration including the development of radar beamsplitting techniques, system integration tests and field tests.

The system integration tests demonstrated that a radar operator could use the dual mode sensor to locate a target in elevation and azimuth to an accuracy of approximately one milliradian by simply visually centering the angle cursor over the target return displayed on the radar B-scope. Since the radar beamwidth was 9.6 milliradians (mrad), the 1 mrad beamsplitting accuracy represented over a 9:1 improvement in target resolution. Targets included corner reflectors and a small pickup truck at ranges that varied from 112 to 1026 meters. A summary of the beamsplitting experiments during the system integration tests is presented in Table I.

Beamsplitting experiments conducted during the field tests were based on using radar azimuth and elevation profiles rather than the B-scope display and angle cursor. This approach reduced the subjectivity of the measurements and increased the beamsplitting accuracy. The target, a M-109 shop van, was located in elevation to an accuracy of less than one milliradian and it was located in azimuth to an accuracy of approximately one-half milliradian. This represented a 19:1 beamsplit improvement in azimuth resolution. Target (shop van) ranges during the experiments varied from 438 meters to 1430 meters. A summary of the beamsplitting results for the field tests is given in Table II.

TABLE I: SUMMARY OF BEAMSPLITTING RESULTS (System Integration Tests)

ELEVATION BEAMSPLITTING

TARGET	NO. OF TRIALS	RANGE (meters)	RESOLUTION (ONE STANDARD DEVIATION) (mrad)
Corner Reflector	30	168	1.047
Corner Reflector	30	168	1.066
Truck	6	112 - 408	0.544
Truck	8	455 - 1026	1.009

AZIMUTH BEAMSPLITTING

TARGET	NO. OF TRIALS	RANGE (meters)	RESOLUTION (ONE STANDARD DEVIATION) (mrad)
Corner Reflector	30	356	1.116

TABLE II: SUMMARY OF BEAMSPLITTING RESULTS (Field Tests)

ELEVATION BEAMSPLITTING

TARGET	NO. OF TRIALS	RANGE (meters)	RESOLUTION (ONE STANDARD DEVIATION) (mrad)
M109 Shop Van	15	588 - 1430	0.982†
M109 Shop Van	14	588 - 1430	1.731*

AZIMUTH BEAMSPLITTING

TARGET	NO. OF TRIALS	RANGE (meters)	RESOLUTION (ONE STANDARD DEVIATION) (mrad) ††
M109 Shop Van	10	438	0.508
M109 Shop Van	10	542	0.797**
M109 Shop Van	10	731	0.503
M109 Shop Van	10	1311	0.466

†Visual beamsplitting of elevation profile data.

*Electronic beamsplitting of elevation profile data.

††Visual beamsplitting of azimuth profile data.

**Shop van head-on; in all other runs, shop van is broadside.

An automated electronic beamsplitter was developed and tested during the field tests. The beamsplitter automatically calculates the geometrical center of the radar return from a target and places the angle cursor at the center of the target displayed on the B-scope. Resolution inadequacies in the beamsplitter circuit, however, limited the target location accuracy. Using the beamsplitter, the target (shop van) was located in elevation to an accuracy of approximately 1.75 mrad.

The overall feasibility of the dual mode sensor concept was demonstrated by handoff experiments during both the system integration tests and the field tests. The radar sensor and EO sensor boresights were aligned in azimuth. Several targets were then acquired by the radar and the radar sensor was aligned to accurately locate the targets using the appropriate beamsplitting techniques. The EO sensor was then activated to determine whether the targets were in the EO sensor angle of view. The dual mode sensor performed well during these tests; the EO boresight was always on the target and was usually centered on the target.

II. DUAL MODE SENSOR DESCRIPTION

The dual mode (electro-optical/radar) sensor was implemented by modifying the GIT/EES 70 GHz mobile instrumentation radar facility to integrate an electro-optical sensor, elevation scanning reflectors, a theodolite, monitoring and recording equipment and electronic beamsplitting devices.

Radar Sensor

The radar sensor is a high resolution rapid scan millimeter wave radar which was initially developed for Harry Diamond Laboratories [1] and later installed in a M-109 shop van (Figure 1) and modified for use as an instrumentation radar facility [2]. Saliant parameters of the basic radar are listed in Table III. The radar antenna and radar console are linked together and revolve about a common vertical axis. The operator moves with the radar console and faces the area illuminated by the radar; the operator may also view this area through a telescope that has its optical axis aligned with the radar antenna electro-magnetic axis.

Electro-Optical Sensor

The electro-optical sensor chosen for the initial implementation is a conventional television camera (vidicon), Sony Model AVC-3200 and a telephoto zoom lens, Swift Model No. 888522. This configuration was chosen to provide an economical simulation of the laser radar which will be used as the electro-optical sensor during later phases of the program. The electro-optical sensor was mounted in the radar van and aligned with the periscope to coboresight the EO sensor optical axis with the radar antenna electromagnetic axis (Figure

---

1. R. M. Goodman, Jr. and F. B. Dyer, "Millimeter Wave Radar", Final Report on Contract DA-49-186-AMC-275(A), Engineering Experiment Station, Georgia Institute of Technology, February, 1968.

2. N.T. Alexander, T.S. Craven and W.S. Foster, "Target Acquisition Experiments Employing a Millimeter Wave Rapid Scan Radar," Final Report on Contract N00014-76-C-0860, Mod. P00001, Engineering Experiment Station, Georgia Institute of Technology, October, 1976.

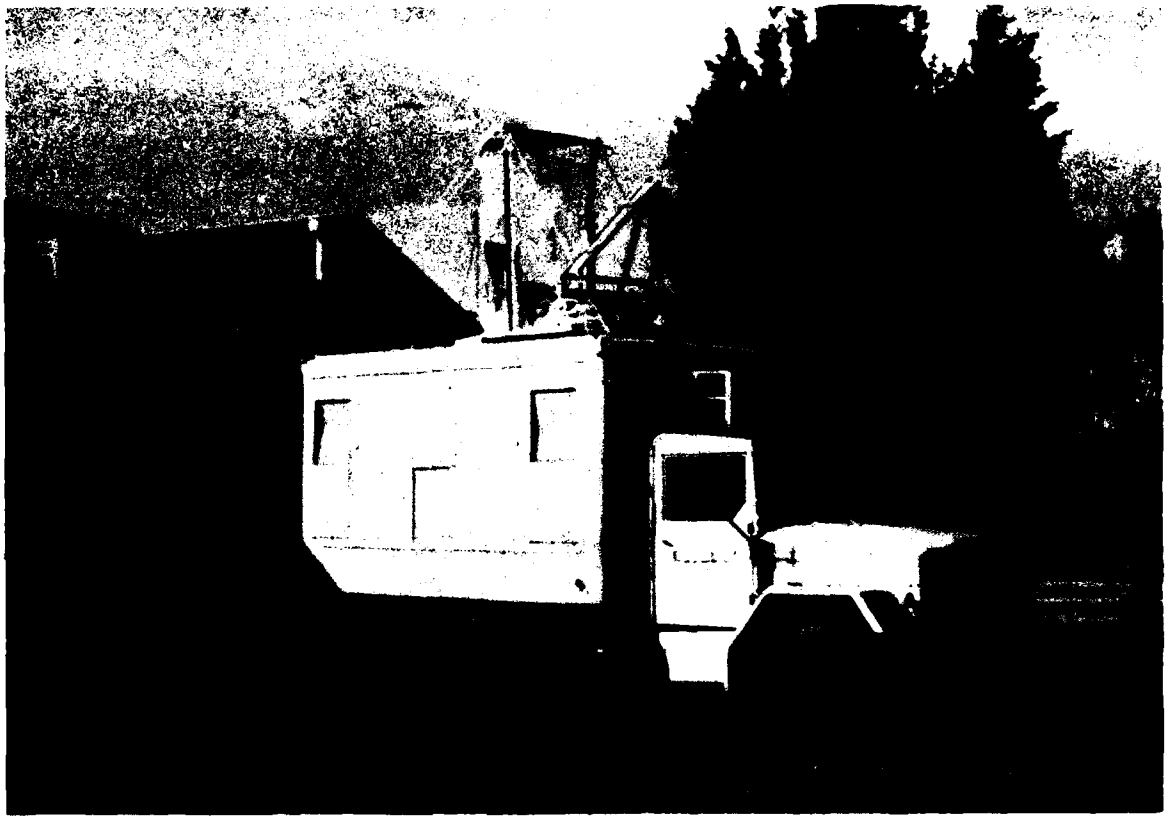

Figure 1. M-109 shop van containing 70-GHz radar system.

TABLE III: BASIC RADAR SYSTEM PARAMETERS

1. Antenna: Folded, geodesic lens feeding a parabolic cylinder reflector. The antenna is 24 inch diameter by 3.5 inch height. Gain: 43.2 dB (corrected for loss)

2. Scanning Modes: Scanning by a seven ring switch which allows a scan rate of approximately 1 rpm to 50 rps

   Azimuth Scan Mode:

   Scan Angle: 45° (±22.5° about boresight)
   Azimuth Beamwidth: 0.55° (positionable through 360°)
   Vertical Beamwidth: 3.5° (positionable from -10° to 20°)

   Vertical Scan Mode

   Scan Angle: 15° (approximately)
   Azimuth Beamwidth: 3.5° (positionable through 360°)
   Vertical Beamwidth: 0.55° (positionable through ±5°)

3. Transmitter:

   Magnetron: Bomac BL 234C
   Peak Power: 500 watts
   Frequency: 69 to 71 GHz
   RF Pulse Width: 20 and 45 nanoseconds (adjustable)
   Pulse Repetition Frequency: 5 KHz to 25 KHz (variable)
   Modulator: Triggered blocking oscillator
   Duplexer: Bomac BL-P-017D

4. RF Component Loss: 6 dB (Total)

5. Local Oscillator: Varian VA 250 Klystron

6. Mixer: Philco IN2792 Mixer crystal; conversion loss 15 dB
   Equivalent noise figure 18 dB minimum
   Equivalent noise figure with IF 25 dB maximum

7. IF: Gain: 70 dB
   Center Frequency: 400 MHz
   Bandwidth: 60 MHz
   Noise Figure: 5 dB

8. Video Amp:

   Bandwidth: 50 MHz
   Gain: 150 (Voltage)

9. Displays-indicator units:

   Sector scan
   B-scan mode
   Non-coherent Doppler aural display

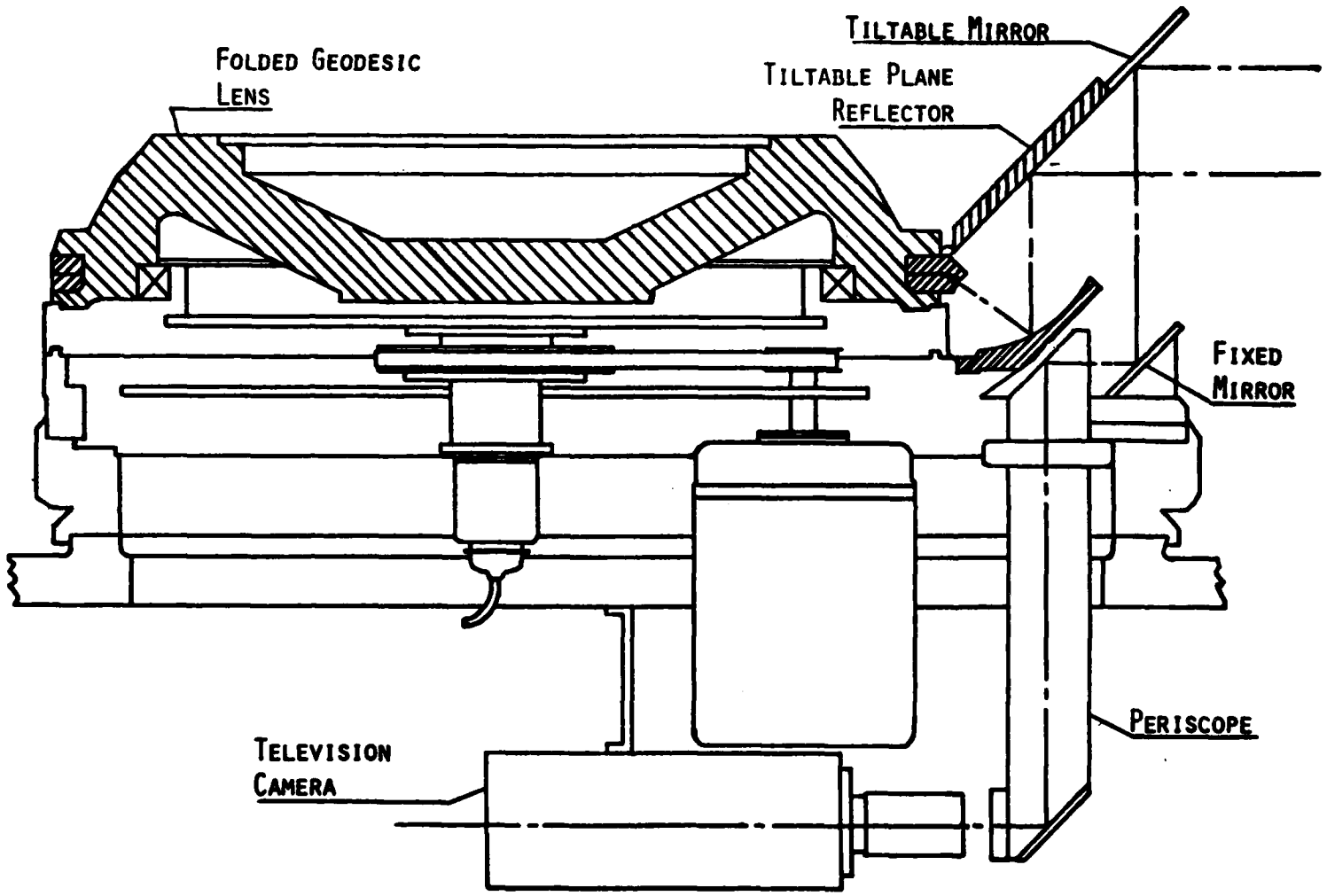

Figure 2. 70 GHz folded geodesic lens antenna with TV camera mounted for viewing through periscope. (Actual method of camera mounting varied from that shown here.)

2). The camera and lens were installed by using a rifle scope mount and a fabricated base plate assembly (Figure 3) that allow translation of the camera and lens in both directions of the horizontal plane and rotation in azimuth and elevation. This mounting method allowed the camera to be aligned with the periscope to reduce optical aberrations.

A mirror system was added so that the radar and EO sensors remained co-boresighted during movement of the radar tiltable plane reflector. The mirrors were necessary because the line of sight through the periscope was originally fixed in elevation. A 25.4 cm by 35.56 cm (10 inch by 14 inch) mirror was attached to the top of the tiltable plane reflector and a 12.7 cm by 17.78 cm (5 inch by 7 inch) mirror was mounted in an adjustable yoke in front of the top port of the periscope (Figures 2 and 4).

Elevation Scanning Reflectors

Electromagnetic reflectors were added to permit investigation of elevation beamsplitting techniques. Two plane reflectors were added to the radar antenna as shown in Figure 4. The reflectors rotate the radar beam radiated by the folded geodesic lens through 90°, thus, changing the azimuth scan to elevation scan. The reflector assembly was mounted with an adjustable knee brace that permitted forward and backward movement of the assembly for adjustment of the radar beam elevation boresight.

The elevation scan mode is activated by folding the tiltable plane reflector mirror assembly back out of the way so that the electromagnetic field radiated by the lens antenna can reach the elevation scanning reflectors. In the elevation scan mode, the EO sensor is inoperative and the radar B-scope display becomes a range versus elevation angle display so that the azimuth cursor becomes an elevation cursor. Note that targets must first be located to within 3.5° of boresight in the azimuth scan mode before they can be displayed in the elevation scan mode, i.e., the azimuth beamwidth in the elevation scan mode is only 3.5°.

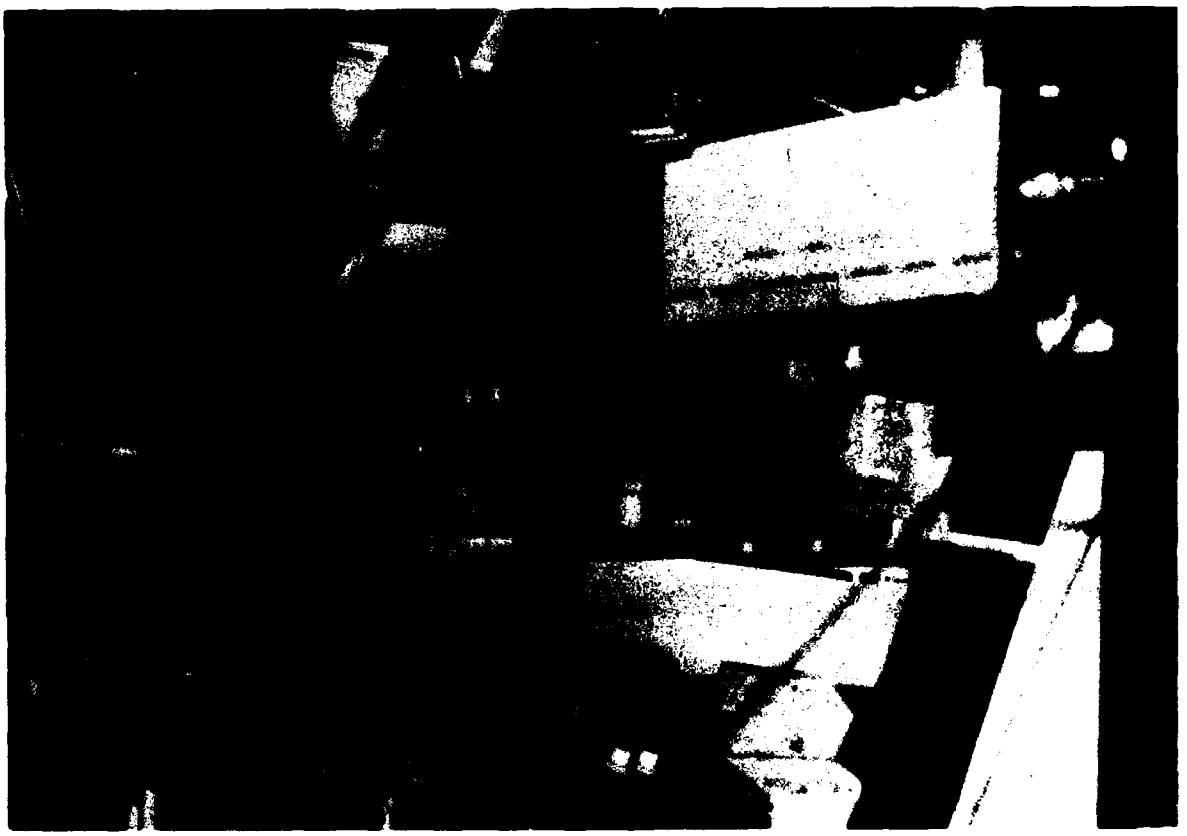

Figure 3. TV camera aligned with periscope and radar display and controls.

Figure 4. 70 GHz antenna assembly with vertical scan reflectors mounted on top of geodesic lens antenna

The elevation scanning reflectors were machined to a flatness tolerance of 0.0076 cm (0.003 inches) and polished to a mirror surface to ensure that the inherent accuracy of the radar in the azimuth mode was retained in the elevation mode. Care was taken to maintain the reflectors at the appropriate 45° angles to provide a proper 90° beam rotation.

Theodolite

The theodolite, an optical instrument used to accurately measure angles, was manufactured by the Keuffel and Esser Company. The theodolite was mounted on the radar antenna assembly behind the elevation scanning reflectors to permit its use in determining the angular positions of various targets. The theodolite measurements provided the means for evaluating the radar's angular locating accuracy.

Monitoring and Recording Equipment

The monitoring and recording equipment included a second television camera, a special effects generator, a video tape recorder, a video monitor and an X-Y recorder. The television camera was focused on the radar display. The special effects generator accepted inputs from the monitor (radar) camera and the EO sensor camera and provided an output to the video tape recorder and video monitor as shown in Figure 5. Composite displays of the radar and EO sensor images could be displayed in a variety of split screen modes. The X-Y recorder was later installed to plot radar elevation and azimuth profiles.

Electronic Beamsplitting Devices

The radar sensor was initially configured to use the B-scope azimuth/elevation cursor as a beamsplitting technique for determining the minimum angular uncertainty of target position as measured by the radar. When system integration test results indicated that operator perception and subjectivity had a significant effect on the angular position measurements, research was initiated to mitigate or eliminate the human factors element. This research included investigation of the use of an optical comparator and two electronic beamsplitting devices, i.e., a peak detector and an edge detector.

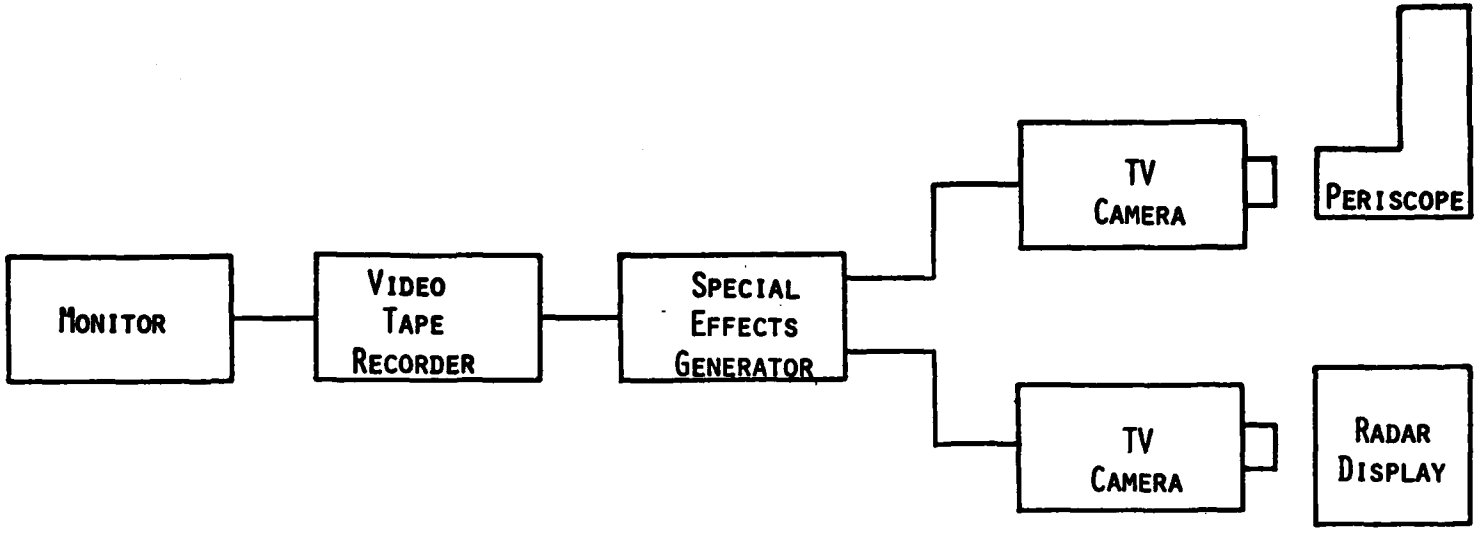

Figure 5. Schematic drawing of EO/radar monitoring and recording system.

Optical Comparator. The first attempt at reducing both the subjectivity and inaccuracies associated with visual beamsplitting involved using an optical comparator to provide a frame of reference and decrease operator eye fatigue. The initial display format shown in Figure 6 lacked a stationary reference and forced the operator to use the nebulous angular boundaries of the target as limits between which the angle cursor must be placed for beamsplitting. The display format using the optical comparator is shown in Figure 7; the stationary precision grid of the optical comparator is superimposed on the magnified B-scope display. The grid provided a reference for measuring the angular width of the displayed target so that the center of the target display could be accurately computed for placement of the angle cursor. Minimum paralax was obtained by using the comparator in direct contact with the B-scope C.R.T. surface. Unfortunately, radar-induced jitter (Figure 7) prevented accurated measurement of the target angular width using the grid marks. Beamsplitting with the aid of the optical comparator was, therefore, highly subjective.

Peak Detector Beamsplitter. The second attempt at improving beamsplitting accuracy involved development and evaluation of a beamsplitting circuit comprising a digital peak detector as shown in Figure 8. This circuit enabled the operator to determine the value of the target return for various cursor positions and would then alert the operator to the largest peak value encountered for placement of the cursor over the angular center of target display.

The peak detector beamsplitter measures the amplitude of the video return corresponding to the coincidence of the range and angle cursors. As the angle (or range) cursor is moved across the displayed target, video amplitude measurements are made at the display refresh rate. Each measured value is compared to the previous value and the largest value is retained for comparison with the next measured value. When the peak value is found by manually sweeping the cursor across the displayed target, the operator switches the circuit from the learning mode to the lock mode to prevent further updating of the peak video value stored by the circuit.

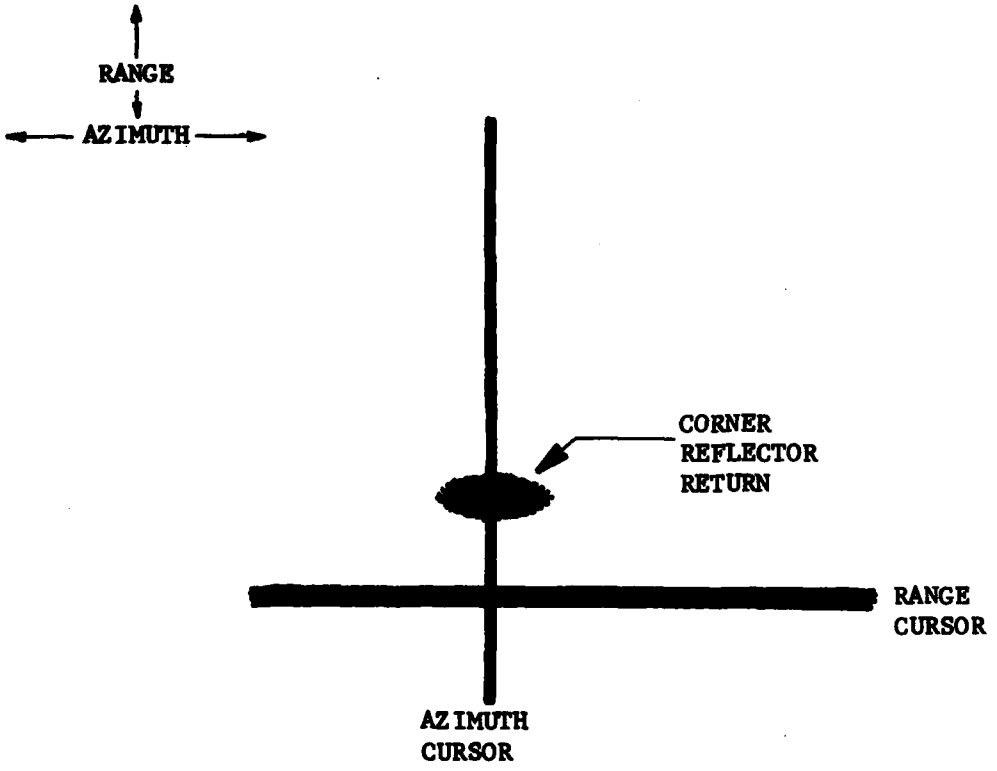

Figure 6. Drawing of B-scope display as it appeared to the unaided eye.

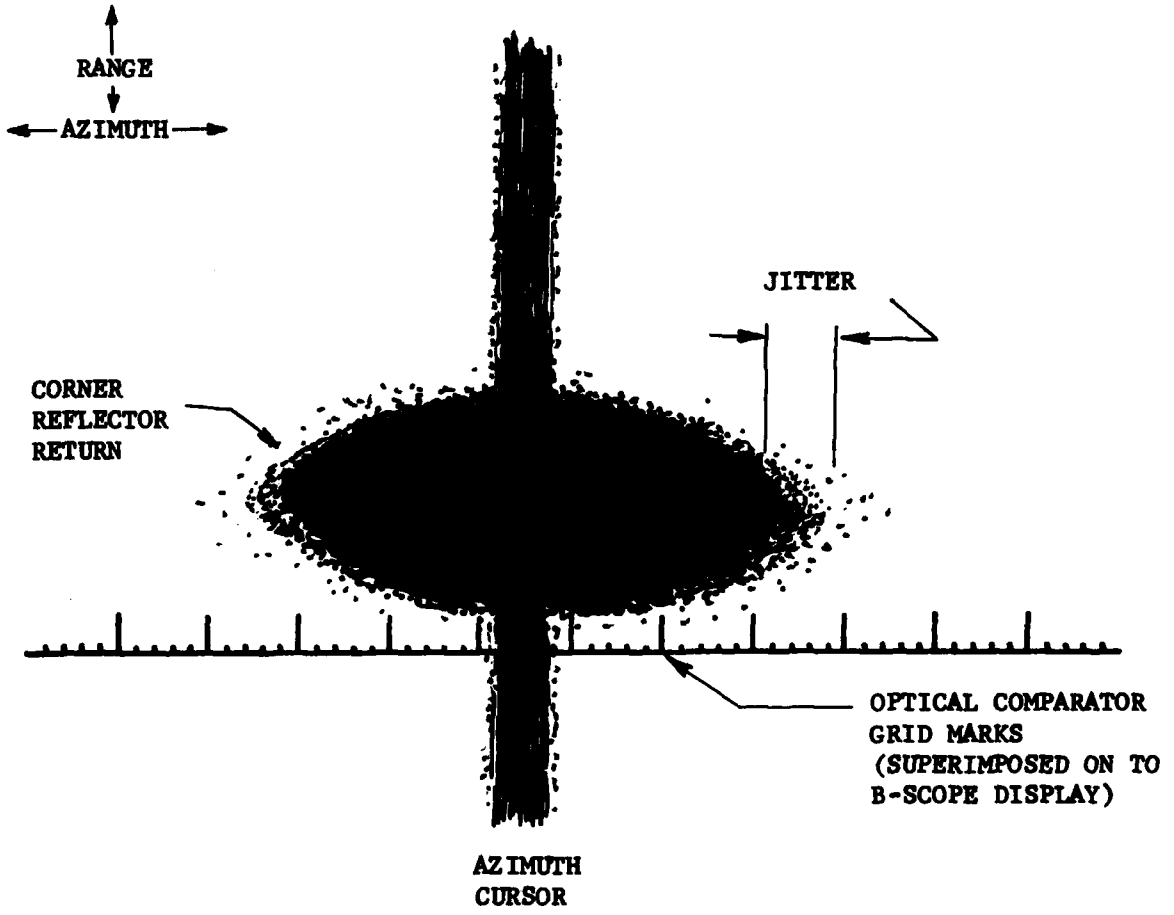

Figure 7. Drawing of B-scope display as viewed through an optical comparator.

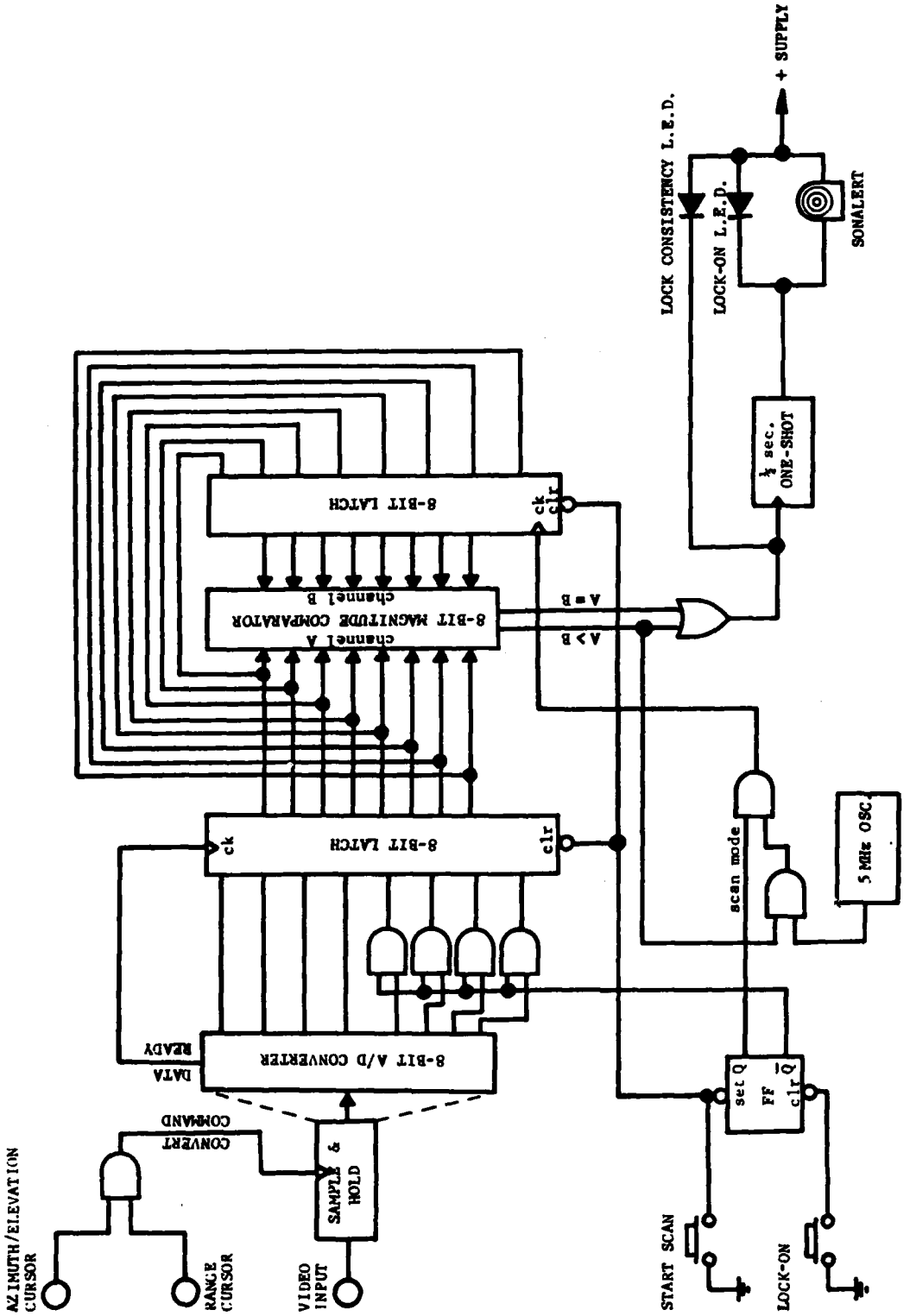

Figure 8. Block diagram of one card digital peak detector.

The operator then sweeps the cursor across the target with the circuit in the lock mode. The circuit will continue to measure the video signal amplitude coincident with the range and angle cursors at the display refresh rate, but each measured value will be compared to the peak value obtained in the learning mode rather than the previous value measured in the lock mode. An alarm is sounded when a measured video value equals or exceeds the peak learned video value. By scanning the target several times with the angle cursor, the operator can observe a point of consistency for the alarms; this point will be the angular center of the displayed target. The circuit operation is based on the assumption that the target response has a unique maximum in the main lobe.

Noise near the angular center of the displayed target could cause inaccuracies in learning the peak video amplitude and the point of consistent alarms in the lock mode. The inaccuracies due to noise can be reduced by using 4- to 7-bit resolution in the learning mode and 8-bit resolution in the lock mode; i.e., the least significant bits (LSB) of the analog-to-digital (A/D) converter could be zeroed during the learning mode and enabled in the lock mode. The A/D converter has a resolution of 8 millivolts (mV). Zeroing the 4 LSB's in the learning mode will change the resolution to 128 mV so that the video samples must differ significantly for a new peak to be learned but the 8 mV resolution in the lock mode would cause an alarm for lock mode samples as much as 128 mV below the peak learned value. This would tend to improve lock consistency but it would also broaden the consistent lock range.

In theory, this peak detection technique is quite viable. When tested in the laboratory using a triangle wave to simulate the target video, the circuit was able to catch the peak consistently and reliably. In the field, however, performance was varied. The video return from a point target is reasonably peaked with the maximum received energy occurring near beam center. This is shown in part (a) of Figure 9 along with the peak detector's "learning response" represented by the shaded region. Note that a peak value indicating the relative target center is correctly identified. The circuit's response to the return of an extended target, however, resulted in an ambiguous set of maxima. As shown in Figure 9(b) and discovered in practice, the peak

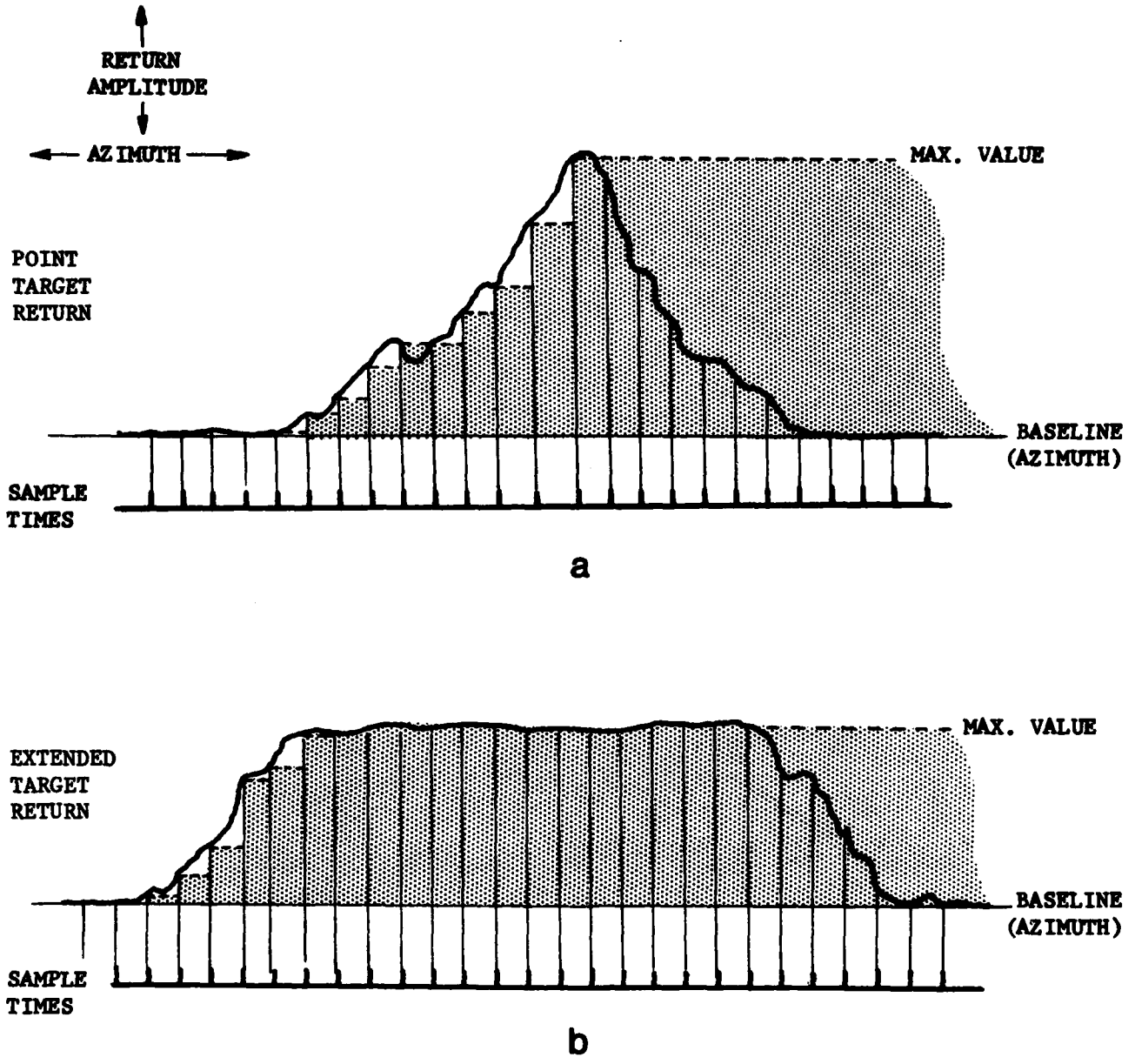

Figure 9. Drawing of the radar azimuth profiles from (a) a point target and (b) an extended target.

detector circuit is unable to pinpoint the center of a distributed or extended target in azimuth. In the case of such a target, the circuit's response was to indicate lock consistency over a range of azimuth values encompassing as much as a degree.

Edge Detector Beamsplitter. The final attempt at improving beamsplitting accuracy involved development and evaluation of a beamsplitting circuit based on an edge sensing concept and on automated cursor scan. This approach shown in Figure 10 is insensitive to target angle distribution (width) and totally eliminates operator interaction. Once initiated, this circuit automatically causes the azimuth cursor to scan across the target. Circuitry similar to that employed by the peak detector is used to sample the video voltage at the intersection of the azimuth and range cursors (samples once per display refresh). Unlike the peak detector, however, the video is not digitized. Instead, the sampled video is channeled through a video boxcar unit (analog sample and hold) whose output is compared to an adjustable threshold by an analog comparator. The output of the comparator then detects (in a binary form) the passage of a significant rising or falling voltage edge such as those encountered in the video as the azimuth cursor is scanned across a target. Figure 10 is a block diagram of this circuit showing the input sensing scheme detailed above. Basically, the circuit scans the target video and records the position of the rising and falling edges of the voltage waveform referenced to the internal count which generates the azimuth cursor sweep. Exactly where on the rising and falling edges of the waveform that the circuit defines as "the edge" is determined by the adjustable threshold. This is shown in Figure 11. The threshold is chosen at the point of fastest rise time and minimum noise for best results.

Once the positions of the rising and falling edges have been determined, the following arithmetic function is performed to determine the absolute center of the target video waveform relative to the edge of the PPI or B-scope

$$\text{Absolute Center} = [(AZ2 - AZ1)/2] + AZ1$$

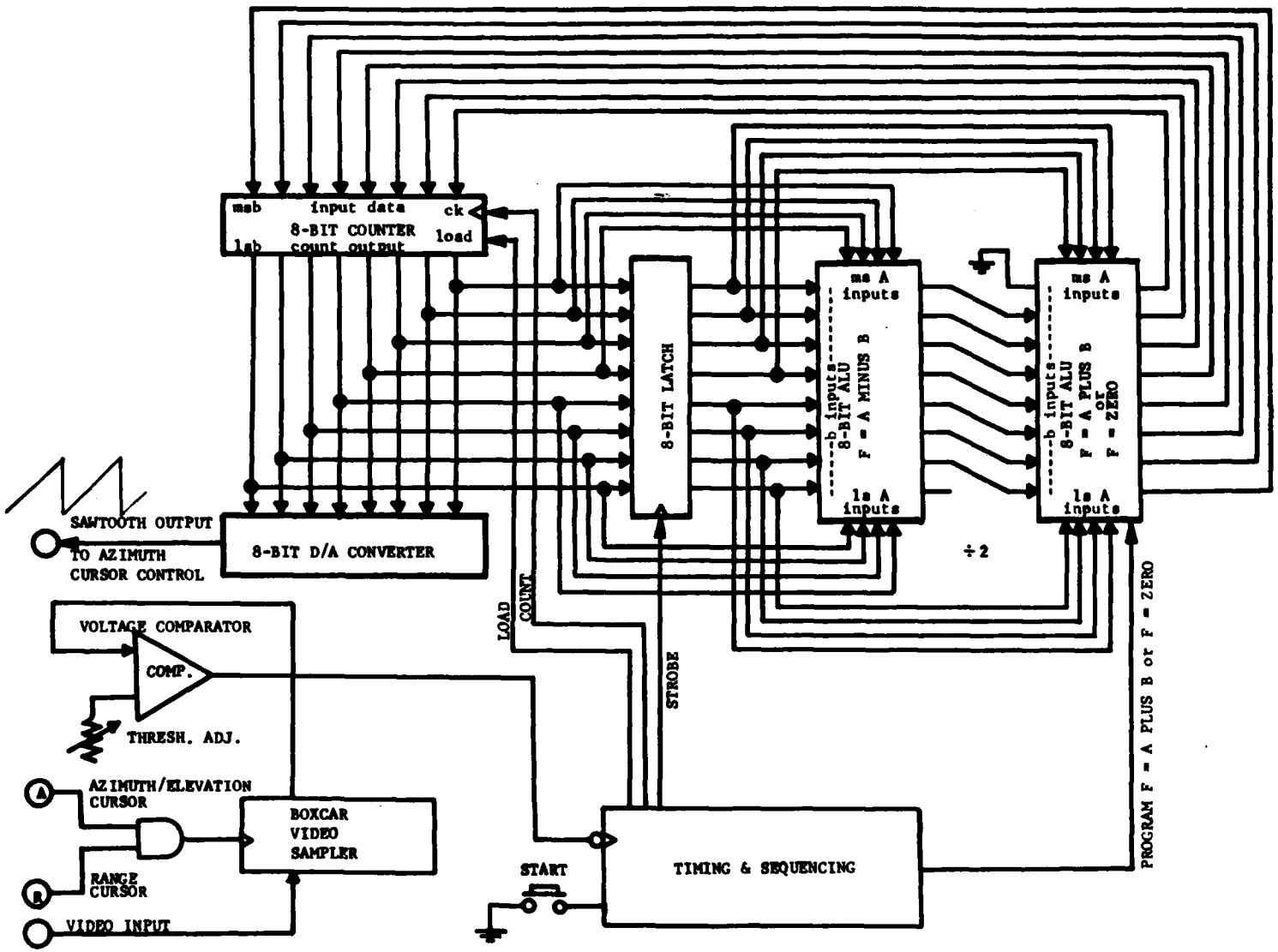

Figure 10. Block diagram of electronic beamsplitter.

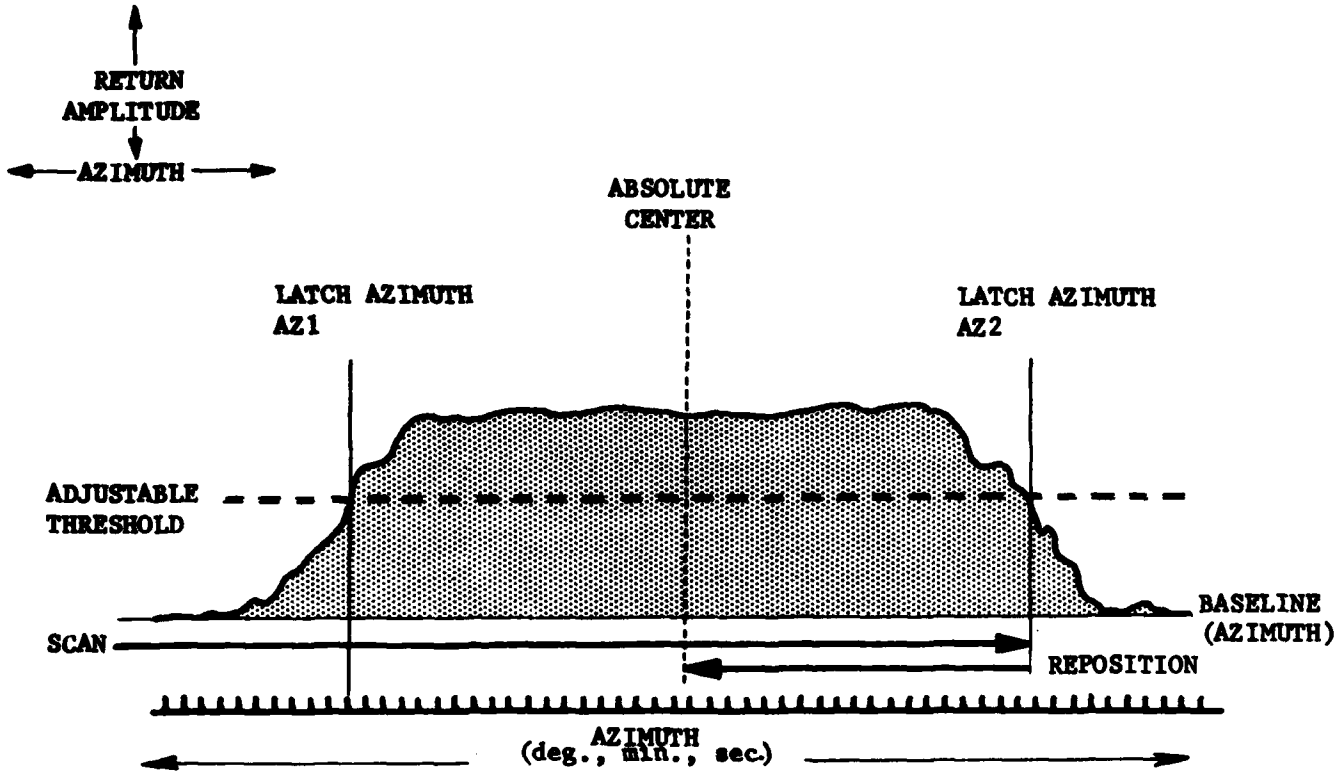

ABSOLUTE CENTER = [(AZ2 - AZ1)/2] + AZ1

Figure 11. Drawing depicting "cursor centering" scheme employed by electronic beamsplitter.

display, where AZ1 is the location of the rising edge and AZ2 is the location of the falling edge when scan direction is defined from rising to falling edge.

Immediately upon determining the absolute center, the circuit ceases the azimuth cursor scan and automatically repositions the cursor at the computed absolute center point. Operation is then suspended until the operator reinitiates the process upon command. By monitoring the azimuth cursor voltage, the absolute center can be measured directly with a digital voltmeter. Surprising accuracy can be achieved with only eight bits (e.g., the number of counter and processing bits carried forth by the prototype circuit). Note that the processing algorithm is independent of target width and can be made tolerant of unevenly distributed returns by proper adjustment of the threshold.

Two modes of operation were used with this automated circuit. The first and intended mode involved "hands-off" operation where the circuit was allowed to scan and determine target center automatically. The second mode used only the cursor scanning ability of the circuit. As the cursor scanned over the video return from the target, this video was simultaneously plotted on an X-Y plotter to provide azimuth or elevation profiles (depending on the radar's scan mode) of the target. Beamsplitting was then accomplished visually by the operator. While still subject to human error, visually beamsplitting using azimuth or elevation profiles should be less subjective than trying to center the cursor over the return as displayed in a B-scope. Both modes of operation were used in the elevation beamsplitting experiments.

III. SYSTEM INTEGRATION TESTS

System integration tests of the dual mode sensor were conducted at Fort Gillem, Georgia, during the Fall of 1977 (20 - 30 September). The test site was a field having a very gently undulating terrain bounded by trees as shown in Figure 12 and providing a maximum range of over 1500 meters. The system integration tests included elevation beamsplitting, azimuth beamsplitting and radar sensor-to-EO sensor handoff experiments.

Elevation Beamsplitting Experiments

The elevation beamsplitting experiments included tests using corner reflectors and a pickup truck as targets. The elevation of the targets as measured by the radar was determined by having the radar operator position the elevation cursor over the center of the target displayed on the "B-scope" (range vs. elevation display). The elevation of the targets was also measured by the theodolite. The accuracy of the radar was then determined by comparing the elevation of the targets as measured by the radar to the elevation of the targets as measured by the theodolite.

The angle represented by the elevation cursor position was determined from measurements of the elevation cursor potentiometer voltage. The elevation angle as a function of cursor potentiometer voltage was determined by using two corner reflectors placed at a range of 168 meters from the radar but at different elevations. The elevation cursor was centered over the "B-scope" display of each target (corner reflector) and the corresponding elevation cursor potentiometer voltages were recorded.

Due to the proximity of the corner reflectors to the radar, multipath effects essentially only resulted in the appearance of two additional distinct indirect returns on the radar display rather than a broadening or other alteration of the direct returns themselves. A photograph of the "B-scope" (range vs. elevation) display showing the return from the two corner reflectors is presented in Figure 13 along with the geometry of the direct and indirect multipath returns. Careful analysis shows that the maximum difference in one

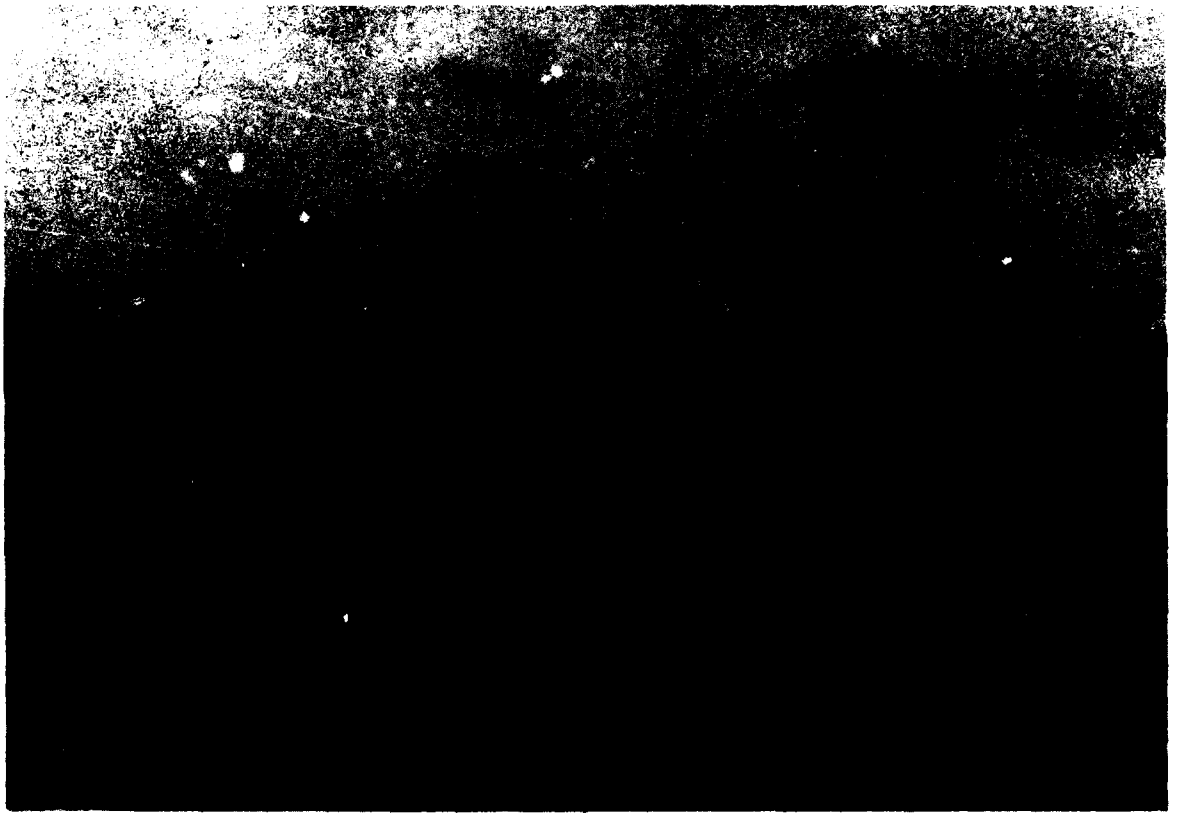

Figure 12. Field test site at Ft. Gillem, Georgia.

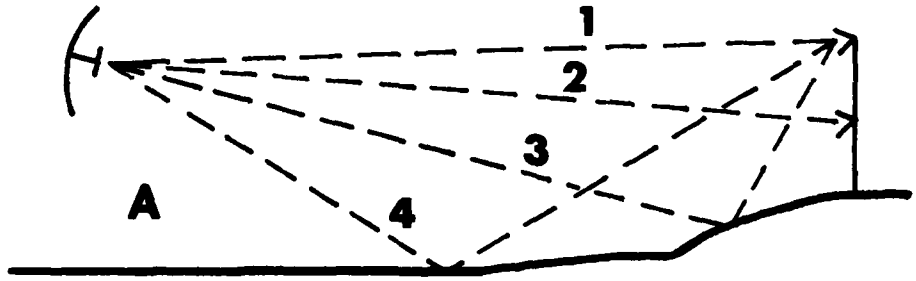

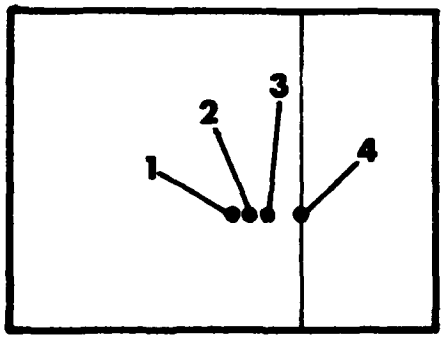

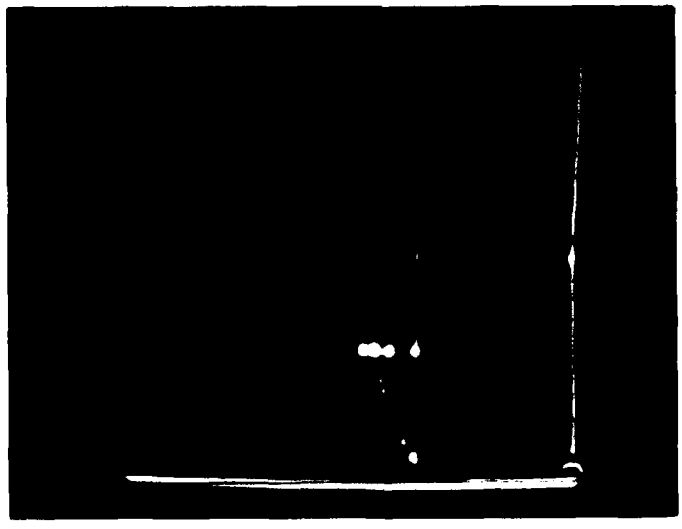

Figure 13. Multipath effects in the vertical scan mode showing (a) multipath geometry, (b) labeling of target returns on B-scope and, (c) photograph of B-scope display.

way path lengths between any two returns is less than 1/3 meter; thus, all returns will be in the same range bin.

The number one and number two corner reflectors were measured by the theodolite to be at elevation angles of θ_1 = 16.338 mrad above horizontal and θ_2 = 1.188 mrad below horizontal, respectively.

The elevation cursor was centered over the direct return from the number one corner reflector and the cursor (potentiometer) voltage was noted. The results of repeating this procedure 30 times are shown in Figure 14; the average cursor voltage was $\langle V_1 \rangle$ = 2.606 volts with a standard deviation of σ_1 = 0.008183 volts. This procedure was then repeated for the number two corner reflector with the results shown in Figure 15. The average cursor voltage was $\langle V_2 \rangle$ = 2.469 volts with a standard deviation of σ_2 = 0.008334 volts.

The voltage to elevation angle conversion constant, α, was then computed as follows:

$$\alpha = \frac{\theta_1 - \theta_2}{\langle V_1 \rangle - \langle V_2 \rangle} = 127.93 \ \frac{\text{mrad}}{\text{volt}} \qquad (1)$$

The constant, α, represents the slope of the cursor voltage versus elevation angle curve. Checks were later made to insure that this curve was indeed a straight line. The absolute functional relationship between the elevation cursor voltage and the elevation angle did not remain over a long (day to day) period of time due primarily to movements of the shop van in which the radar was housed. Therefore, the only reliable long term result from the above calibration is the value of the conversion constant, α, which did remain constant.

Using the conversion constant, α, from Equation 1 and the standard deviation in cursor voltages, the corner reflectors were located in elevation with a resolution of

$$\sigma_1 = (0.008183 \text{ volts}) \left(127.93 \ \frac{\text{mrad}}{\text{volt}}\right) = 1.047 \text{ mrad}$$

CORNER REFLECTOR NO. 1

RANGE: 168 meters

ELEVATION ANGLE: 16.34 mrad
(Above Horiz)

$\langle V_1 \rangle$ = 2.606 volts

σ_1 = 0.008183 volts

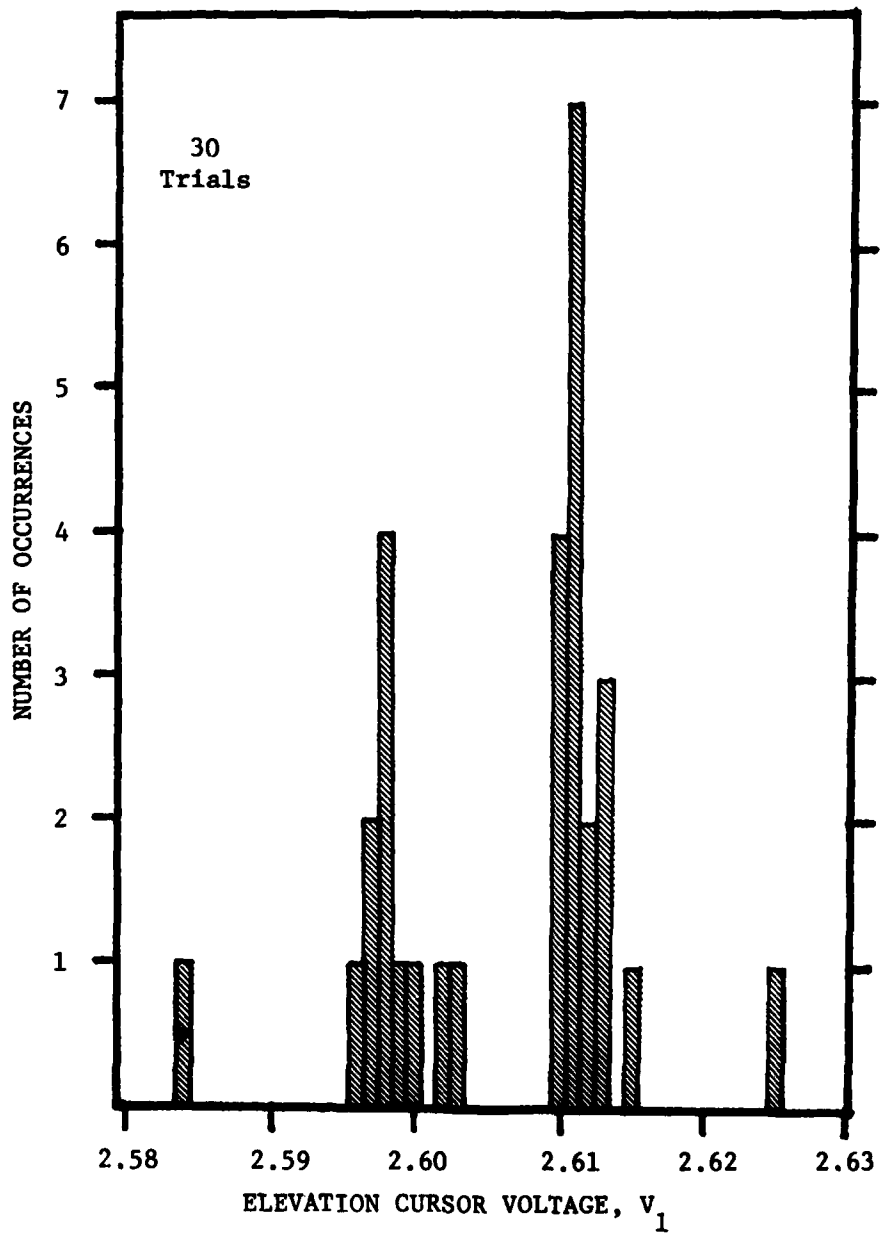

Figure 14. Histogram of cursor voltage for elevation beamsplitting trials on corner reflector No. 1.

CORNER REFLECTOR NO. 2

RANGE: 168 meters

ELEVATION ANGLE: 1.188 mrad
(Below Horiz)

$\langle V_2 \rangle$ = 2.469 volts

σ_2 = 0.008334 volts

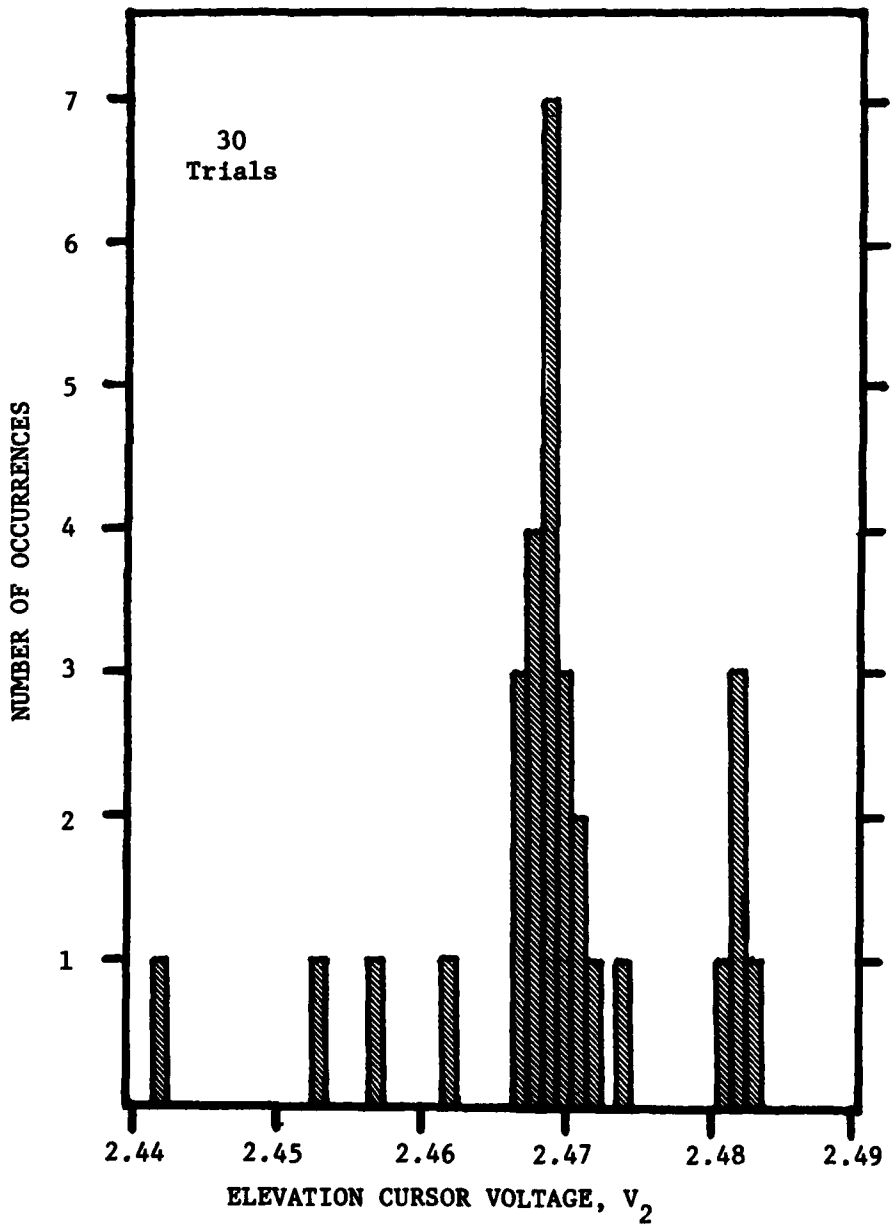

Figure 15. Histogram of cursor voltage for elevation beamsplitting trials on corner reflector No. 2.

$$\sigma_2 = (0.008334 \text{ volts}) \left(127.93 \frac{\text{mrad}}{\text{volt}}\right) = 1.066 \text{ mrad}$$

Given the radar's 9.6 mrad elevation beamwidth, this represents approximately a nine-fold increase in resolution, i.e., a 9:1 beamsplit ability.

The small pickup truck used as a target is shown in Figure 16. The first set of elevation beamsplitting measurements consisted of six measurements with the range of the truck varying from 112 meters to 408 meters. At each of the six truck positions, the elevation cursor was centered over the return of the truck and cursor voltage noted. The actual elevation angle of the truck as measured by the theodolite was also noted. As mentioned above, unless a calibration immediately preceded the test run, no absolute elevation angle could be determined from the cursor voltage. Instead, a relative elevation angle, $\tilde{\theta}_T$, was calculated by means of the equation:

$$\tilde{\theta}_T = \theta_T + \alpha[\langle V \rangle - V] \tag{2}$$

where: $\langle \theta_T \rangle$ = average truck elevation angle as measured by the theodolite (over the 6 measurements)

$\langle V \rangle$ = average elevation cursor voltage (over the 6 measurements)

V = elevation cursor voltage of a given measurement.

Thus, the difference, $\Delta\theta$, in the theodolite measured elevation angle, θ_T, and the radar-measured relative elevation angle, $\tilde{\theta}_T$, could be obtained for each truck position. This angular difference, $\Delta\theta$, is given by:

$$\begin{aligned} \Delta\theta \equiv \theta_T - \tilde{\theta}_T &= \theta_T + \alpha V - [\langle \theta \rangle + \alpha \langle V \rangle] \\ &= \theta_T + \alpha V + \text{constant} \end{aligned} \tag{3}$$

While the absolute value of $\Delta\theta$ is a relatively meaningless quantity (since it depends on the average values of θ_T and V), the dispersion in $\Delta\theta$ is meaningful because it is independent of these averages and gives an indication of the elevation beamsplitting resolution of the radar. The dispersion in $\Delta\theta$ for Test A was such that the standard deviation was:

$$\sigma(\Delta\theta) = 0.544 \text{ mrad}$$

The data from these experiments are summarized under Test A in Table IV.

Figure 16. Radar target for system integration tests.

TABLE IV: RESULTS OF ELEVATION BEAMSPLITTING EXPERIMENTS (System Integration Tests)

CORNER REFLECTOR NO. 1: σ_1 = 1.047 mrad

CORNER REFLECTOR NO. 2: σ_2 = 1.066 mrad

RUN NUMBER	TEST A					TEST B				
	TRUCK					TRUCK				
	RANGE (meters)	θ_T † (mrad)	V * (volts)	$\tilde{\theta}_T$ †† (mrad)	$\Delta\theta$ ** (mrad)	RANGE (meters)	θ_T † (mrad)	V * (volts)	$\tilde{\theta}_T$ †† (mrad)	$\Delta\theta$ ** (mrad)
1	112	44.9806	2.35	44.3217	0.6589	455	12.2993	2.401	12.0772	0.2221
2	112	44.0696	2.35	44.3217	-0.2521	504	11.7513	2.410	10.9258	0.8255
3	173	29.5833	2.46	30.2497	-0.6664	577	11.6204	2.410	10.9258	0.6946
4	267	19.3679	2.55	18.7362	0.6317	696	11.3883	2.410	10.9258	0.4624
5	269	21.9615	2.52	22.5741	-0.6126	804	10.6849	2.411	10.7979	-0.1130
6	408	12.5803	2.60	12.3399	0.2404	896	9.9292	2.426	8.8790	1.0502
7						936	7.1122	2.423	9.2628	-2.1506
8						1026	8.1455	2.424	9.1349	-0.9894
		$\sigma(\Delta\theta)$ = 0.544 mrad						$\sigma(\Delta\theta)$ = 1.009 mrad		

†Elevation angle in milliradians below horizontal as measured by theodolite.

*Elevation cursor voltage.

††$\tilde{\theta}_T = \langle\theta_T\rangle + \alpha[\langle V\rangle - V]$; α = 127.93 mrad/volt

**$\Delta\theta = \theta_T - \tilde{\theta}_T$

The second set of elevation beamsplitting experiments consisted of eight measurements with the range of the truck varying from 455 meters to 1026 meters. The dispersion in $\Delta\theta$ for Test B was such that the standard deviation was:

$$\sigma(\Delta\theta) = 1.009 \text{ mrad}$$

The data from these experiments are summarized under Test B in Table IV.

Azimuth Beamsplitting Experiments

Since the radar console and antenna are linked together and revolve in azimuth about a common vertical axis, the azimuth beamsplitting experiments could be performed without having to resort to the cursor voltage scheme used in elevation beamsplitting experiments. The test plan scenario for the azimuth beamsplitting experiments was as follows:

1. Locate the corner reflector in azimuth on B-scope display and center cursor on corner reflector return.
2. Align theodolite on corner reflector and set zero.
3. Locate target in azimuth on B-scope display and center azimuth cursor on target by moving entire radar console.
4. Finally, measure the target's true angular position relative to theodolite zero.

If the radar has located the target accurately, the theodolite should be zeroed on the target. Any angular deviation of the target from this zero, as measured by the theodolite, is a direct indication of the azimuth beamsplitting resolution of the radar. Again, this procedure is subjective in that it is a function of the radar operator's ability to visually beamsplit a radar return as it appears on the B-scope display.

During the system integration tests, the only reliable azimuth beamsplitting data was taken for two corner reflector targets. These two corner reflectors were placed at different azimuth angles at a range of 356 meters. The radar return from the first corner reflector was located on the B-scope and the azimuth cursor was centered over this return. The theodolite was zeroed on this corner reflector. By moving the radar console, the azimuth

cursor was then centered over the return of the second corner reflector and the angular deviation, $\Delta\phi$, from zero of the second corner as measured by the theodolite was noted. Then, by moving the radar console, the azimuth cursor was recentered over the first corner reflector and the angular deivation noted. The results of repeating this procedure for 30 measurements are given in Table V; the standard deviation in $\Delta\phi$ was found to be:

$$\sigma(\Delta\phi) = 1.116 \text{ mrad}$$

Radar to EO Sensor Handoff Experiments

Several "handoff" experiments were performed to demonstrate the overall feasibility of combining an EO sensor with a radar sensor. The EO sensor and radar boresights were aligned and then the target (corner reflector or truck) was acquired in azimuth by the radar. Once a target had been acquired and aligned on the radar's boresight, the EO sensor was activated to determine whether the target was in the EO sensor's AOV and, if so, to identify the target. During these tests, the zoom lens was kept at its maximum AOV, approximately 14.2 milliradians. The combined sensor system performed very well with the target being centered on the monitor. Figures 17 and 18 are still frames taken from the video taped record of these test results.

TABLE V: RESULTS OF AZIMUTH BEAMSPLITTING EXPERIMENTS (System Integration Tests)

TWO CORNER REFLECTORS

RANGE: 356 meters

TRIALS: 30

	$\Delta\phi$ (mrad)		$\Delta\phi$ (mrad)		$\Delta\phi$ (mrad)
1.	-2.696	11.	-0.708	21.	0.286
2.	-2.671	12.	-0.708	22.	0.305
3.	-2.633	13.	-0.659	23.	0.359
4.	-2.506	14.	-0.417	24.	0.373
5.	-1.687	15.	-0.378	25.	0.412
6.	-1.299	16.	-0.238	26.	0.587
7.	-1.207	17.	-0.208	27.	0.766
8.	-1.144	18.	-0.0436	28.	0.781
9.	-1.120	19.	0.00485	29.	0.785
10.	-0.916	20.	0.145	30.	1.716

$\langle\Delta\phi\rangle$ = -0.491 mrad $\sigma(\Delta\phi)$ = 1.116 mrad

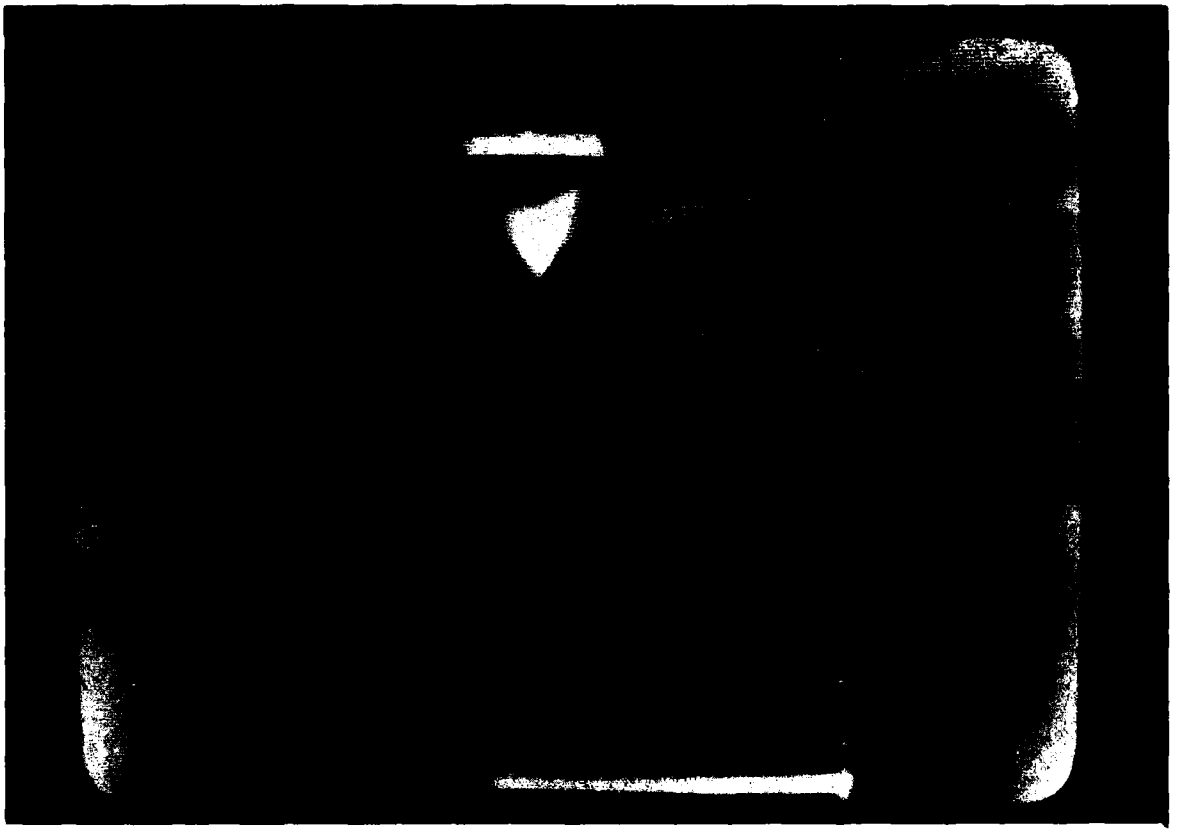

Figure 17. Still frame photo of video tape recording showing split screen of corner reflector as simultaneously imaged by EO sensor (top) and displayed by radar on B-scope.

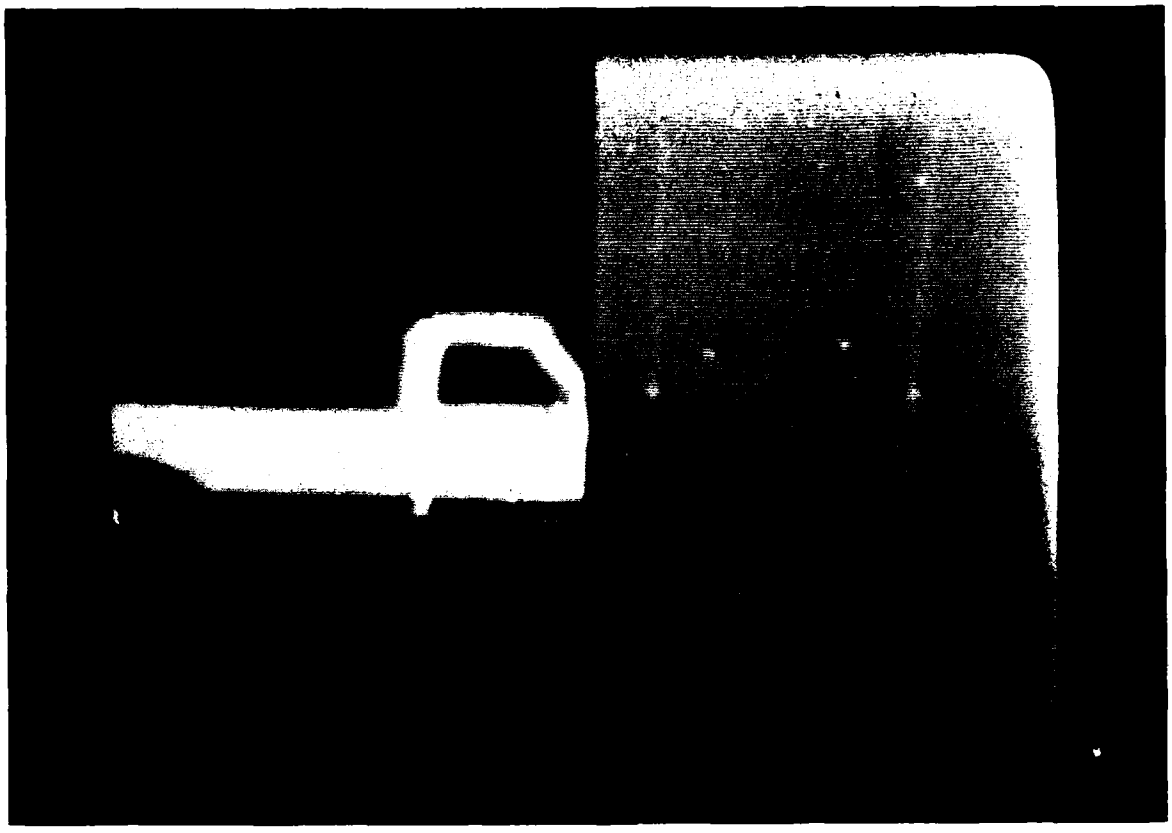

Figure 18. Still frame photo of video tape recording showing split screen of truck as simultaneously imaged by EO sensor (top) and displayed by radar on B-scope.

IV. FIELD TESTS

Field tests of the dual mode sensor were conducted during the Winter of 1978 (11 January to 16 March) at the same field site at Fort Gillem, Georgia where the system integration tests were conducted. The results of the system integration tests and discussions with ERADCOM personnel led to several changes in the test plan scenario. These changes included:

1. Reducing or removing the operator subjectivity from the beamsplitting experiments,

2. Using a grid system on the monitor to estimate the target azimuth location relative to radar boresight for the radar to EO sensor handoff experiments,

3. Using a M-109 shop van instead of a pickup truck as a target.

The initial period of field tests was primarily directed toward experiments and developments for reducing or removing operator subjectivity. These experiments and developments are described under electronic beamsplitting devices in the dual mode sensor description (Chapter II). The actual field tests included elevation beamsplitting, azimuth beamsplitting and radar to EO sensor handoff experiments.

Elevation Beamsplitting Experiments

The elevation beamsplitting experiments consisted of five tests with three runs per test. The target, a M-109 shop van shown in Figure 19, was placed at a different range (from 588 meters to 1430 meters) for each test. For all of the tests, the shop van was oriented broadsides to the boresight of the radar. Two corner reflectors were also placed in the field at different ranges and elevations (see Figure 20). The test plan scenario for the elevation beamsplitting experiments was as follows:

1. Obtain a radar elevation profile (REP) of the near corner reflector, far corner reflector and shop van, all on the same plot.

2. Determine the geometrical center of each REP as calculated by the electronic beamsplitter and note the respective elevation cursor (potentiometer) voltages of these centers.

3. Measure with the theodolite the true elevation angles of the near corner reflector, far corner reflector and shop van. (The elevation angle

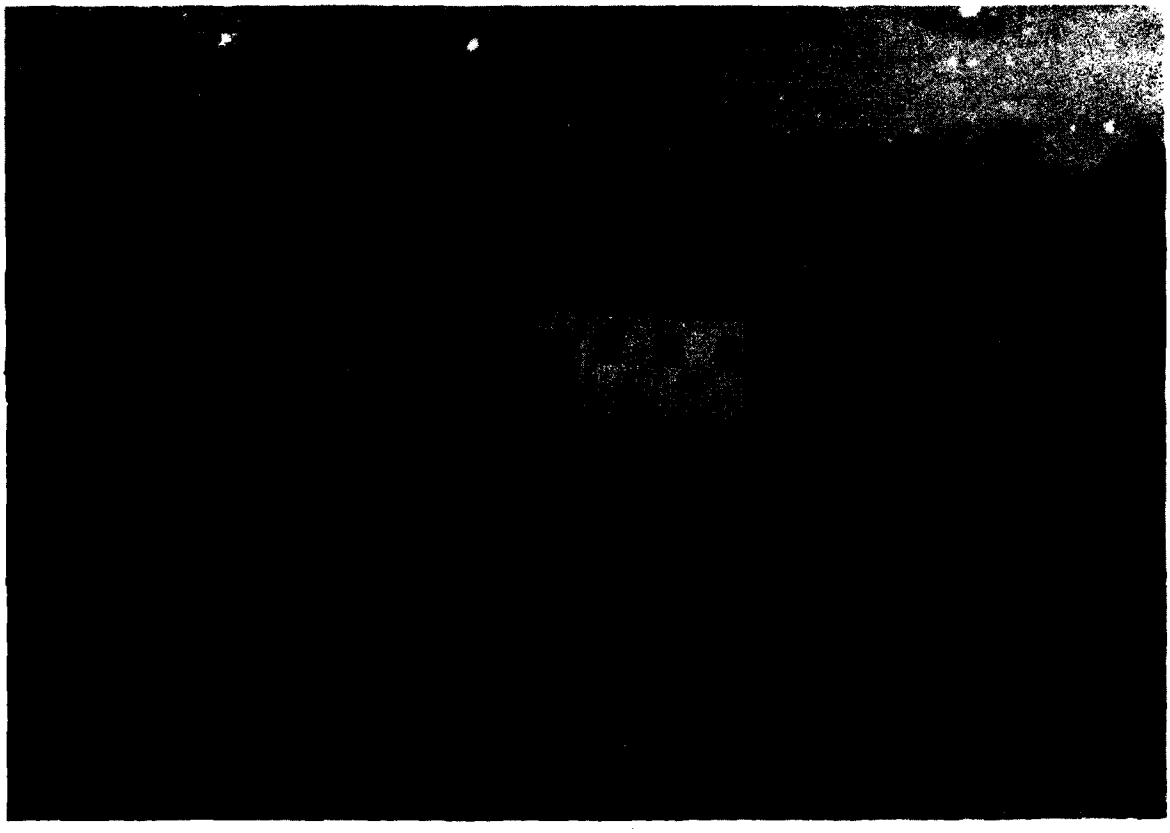

Figure 19. M-109 shop van used as target in field tests.

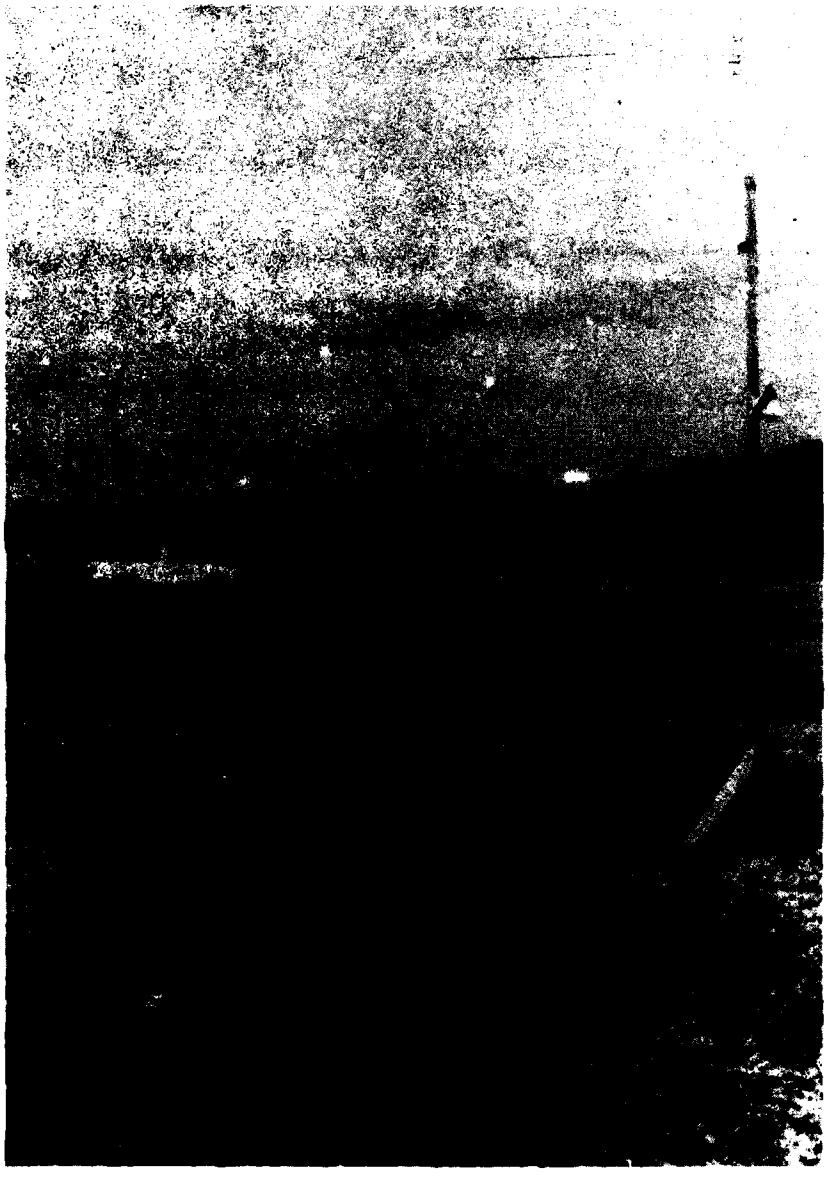

Figure 20. Two reference corner reflectors for elevation beamsplitting experiments.

of the shop van was taken to be the elevation angle of the horizontal line that insected the top of the shop van's cab).

The consistency of the measurements made by the theodolite operator was checked by having him repeatedly measure a fixed angle. The standard deviation of these measurements was less than 10 arc-seconds (0.05 mrad).

A curve of elevation angle versus cursor voltage was generated for each run by relating the true elevation angle of a corner reflector to the voltage of the elevation cursor when centered by the electronic beamsplitter over the REP of that corner reflector. This curve is given by:

$$\theta = \left[\frac{\theta_N - \theta_F}{V_N - V_F}\right] (V - V_F) + \theta F \qquad (4)$$

where: $\theta_N(\theta_F)$ = elevation angle of the near (far) corner reflector as measured by the theodolite

$V_N(V_F)$ = voltage of elevation cursor when centered by the electronic beamsplitter over the REP of the near (far) corner reflector

θ = elevation angle variable

V = cursor voltage variable

An elevation angle, θ_R^E, for the shop van was determined from this curve by replacing V in Equation (4) by the cursor voltage when the electronic beamsplitter centered the cursor over the REP of the shop van. This elevation angle, determined solely by the radar and electronic beamsplitter, gave a measure of the radar's elevation locating ability using an electronic beamsplitter when compared to the true elevation angle, θ_S, of the shop van as determined by the theodolite. The standard deviation in $\theta_S - \theta_R^E$ for 14 runs was found to be:

$$\sigma(\theta_S - \theta_R^E) = 1.731 \text{ mrad}$$

A visual beamsplitting method was also employed which essentially did manually what the electronic beamsplitter did automatically. A visual threshold level (VTL) was arbitrarily drawn by the operator through the REP's of a given run. Then the geometrical center of a given REP was chosen to be the

midway point (along the VTL) between the points where the rising and falling edges of the REP intersected the VTL. A distance along the VTL could then be associated with the center of each REP. A curve of elevation angle versus distance along the VTL was generated for each run by relating the true elevation angle of a corner reflector to the distance along the VTL of the center of the REP of that corner reflector. This curve is given by:

$$\theta = \left[\frac{\theta_N - \theta_F}{D_N - D_F}\right] (D - D_F) + \theta_F \qquad (5)$$

where: $D_N(D_F)$ = distance along VTL of the center of the REP of the near (far) corner reflector

D = distance along VTL variable

An elevation angle, θ_R^V, for the shop van was determined from this curve by replacing D in Equation (5) by the distance along the VTL of the center of the REP of the shop van.

The only subjectivity involved in employing this visual beamsplitting method was in choosing the height of the VTL through the REP plots. The standard deviation in $\theta_S - \theta_R^V$ for the 15 runs was found to be:

$$\sigma(\theta_S - \theta_R^V) = 0.982 \text{ mrad}$$

The more accurate results in elevation beamsplitting obtained with the visual method was due primarily to resolution inadequacies in the electronic beamsplitter.

The results of these elevation beamsplitting experiments are summarized in Table VI. The REP's for the 15 experimental runs are shown in Figures 21 through 35. The VTL is indicated on each plot and the center of each REP as determined by the electronic beamsplitter is shown on the elevation axis in each figure.

Azimuth Beamsplitting Experiments

No electronic beamsplitting was performed in the azimuth experiments. These experiments consisted of four tests, labelled A through D, with ten

TABLE VI: RESULTS OF ELEVATION BEAMSPLITTING EXPERIMENTS (Field Tests)

TEST	RUN NUMBER	NEAR CORNER REFLECTOR RANGE (meters)	NEAR CORNER REFLECTOR θ_N † (mrad)	FAR CORNER REFLECTOR RANGE (meters)	FAR CORNER REFLECTOR θ_F † (mrad)	SHOP VAN RANGE (meters)	SHOP VAN θ_S † (mrad)	θ_R^V * (mrad)	θ_R^E †† (mrad)	$\theta_S - \theta_R^V$ (mrad)	$\theta_S - \theta_R^E$ (mrad)
A	1	372	13.92	392	4.03	588	7.30	7.45	9.04	-0.155	-1.75
	2	372	13.90	392	4.07	588	7.31	9.28	8.81	-1.98	-1.50
	3	372	13.92	392	4.07	588	7.33	8.94	8.87	-1.62	-1.55
B	1	372	13.90	392	4.01	804	9.06	8.40	5.69	0.659	3.37
	2	372	13.88	392	4.12	804	9.09	8.96	10.66	0.126	-1.57
	3	372	13.88	392	4.09	804	9.13	9.48	9.28	-0.349	-0.147
C	1	299	11.02	354	4.76	1127	7.12	8.37	8.19	-1.26	-1.07
	2	299	11.02	354	4.70	1127	7.11	6.36	5.09	0.751	2.01
	3	299	11.02	354	4.70	1127	7.19	7.56	7.80	-0.364	-0.607
D	1	299	11.04	354	4.63	1315	2.40	3.61	3.32	-1.20	-0.914
	2	299	11.03	354	4.51	1315	2.35	2.41	4.16	-0.0630	-1.81
	3	299	10.98	354	4.38	1315	2.35	2.25	**	0.102	**
E	1	299	11.02	354	4.65	1430	1.97	2.99	0.407	-1.02	1.56
	2	299	11.01	354	4.72	1430	1.99	1.36	3.46	0.630	-1.48
	3	299	11.04	354	4.73	1430	2.02	0.228	-0.566	1.79	2.59

$\langle \theta_S - \theta_R^V \rangle$ = -0.264 mrad $\qquad$ $\langle \theta_S - \theta_R^E \rangle$ = -0.205 mrad

$\sigma(\theta_S - \theta_R^V)$ = 0.982 mrad $\qquad$ $\sigma(\theta_S - \theta_R^E)$ = 1.731 mrad

†Elevation angle in milliradians below horizontal as measured by theodolite.

*Elevation angle in milliradians below horizontal as determined by visual beamsplitting of radar elevation profile data.

††Elevation angle in milliradians below horizontal as determined by electronic beamsplitting of radar elevation profile data.

**Data not taken.

RANGE (METERS)		ELEVATION ANGLE (MRAD BELOW HORIZ)
588	SHOP VAN (SV)	7.30
392	FAR CORNER REFLECTOR (FCR)	4.03
372	NEAR CORNER REFLECTOR (NCR)	13.92

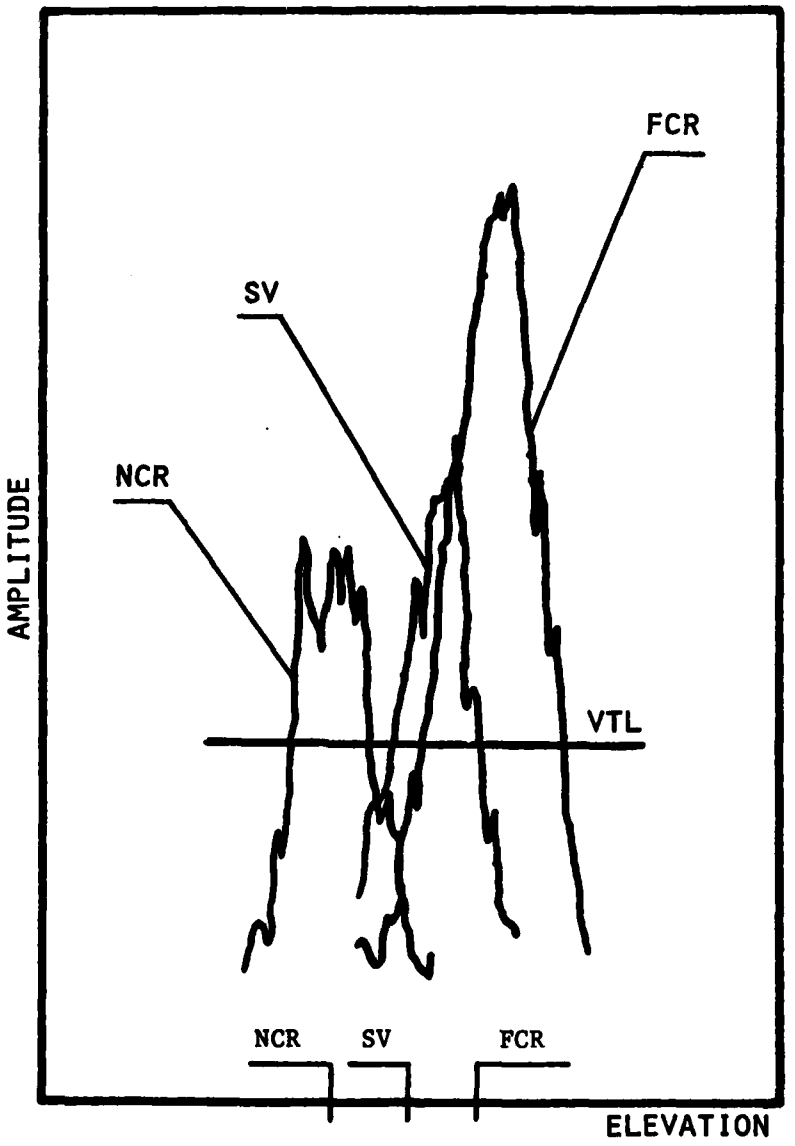

Figure 21. Radar elevation profiles: Run number A-1.

RANGE (METERS)		ELEVATION ANGLE (MRAD BELOW HORIZ)
588	SHOP VAN (SV)	7.31
392	FAR CORNER REFLECTOR (FCR)	4.07
372	NEAR CORNER REFLECTOR (NCR)	13.90

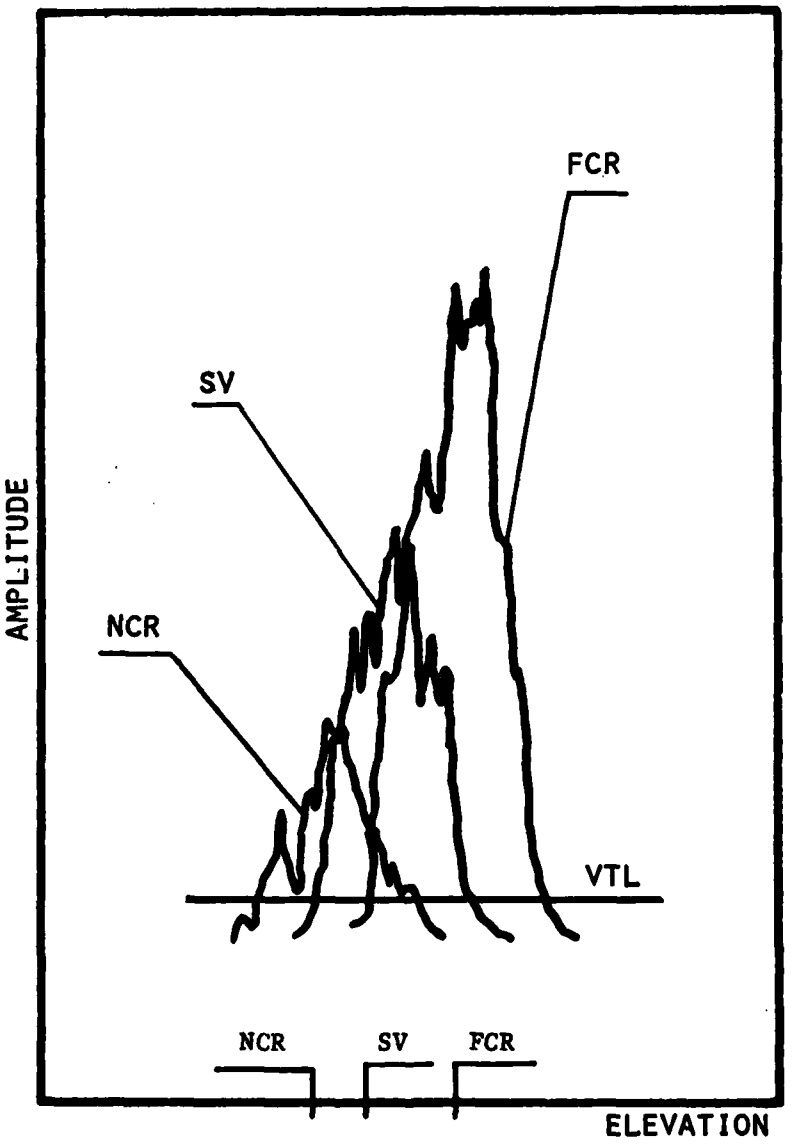

Figure 22. Radar elevation profiles: Run number A-2.

RANGE (METERS)		ELEVATION ANGLE (MRAD BELOW HORIZ)
588	SHOP VAN (SV)	7.33
392	FAR CORNER REFLECTOR (FCR)	4.07
372	NEAR CORNER REFLECTOR (NCR)	13.92

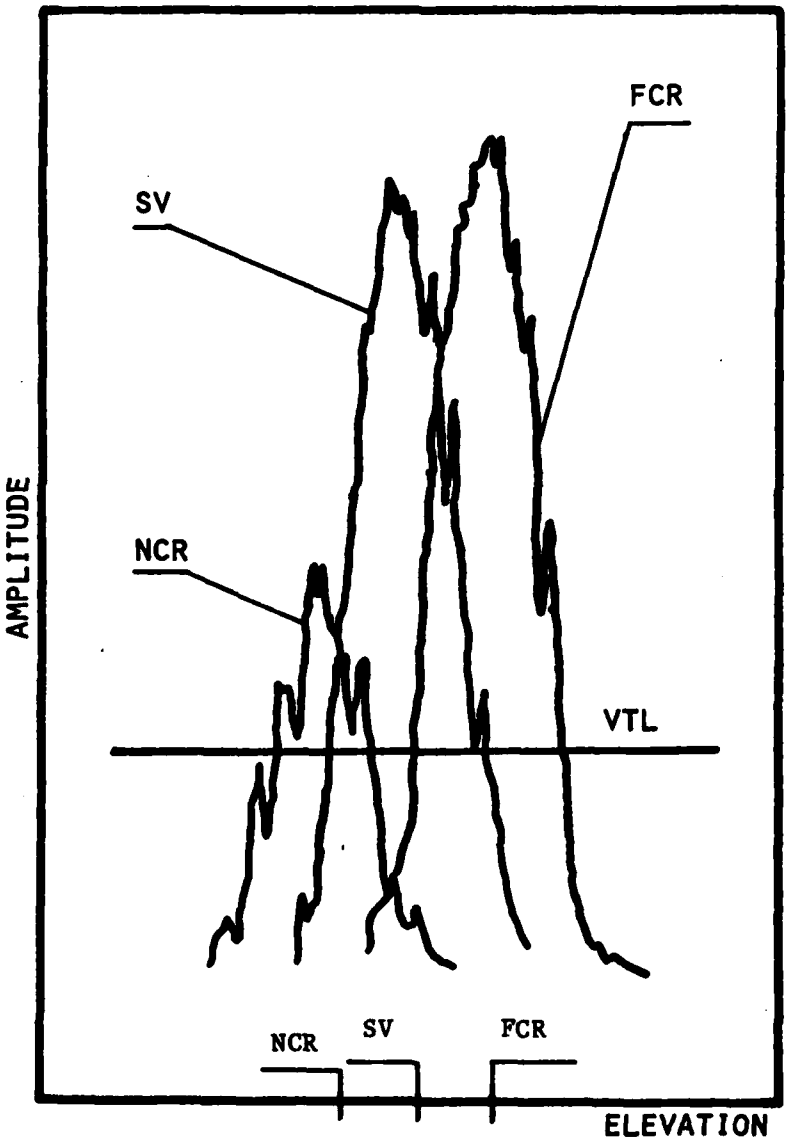

Figure 23. Radar elevation profiles: Run number A-3.

RANGE (METERS)		ELEVATION ANGLE (MRAD BELOW HORIZ)
804	SHOP VAN (SV)	9.06
392	FAR CORNER REFLECTOR (FCR)	4.01
372	NEAR CORNER REFLECTOR (NCR)	13.99

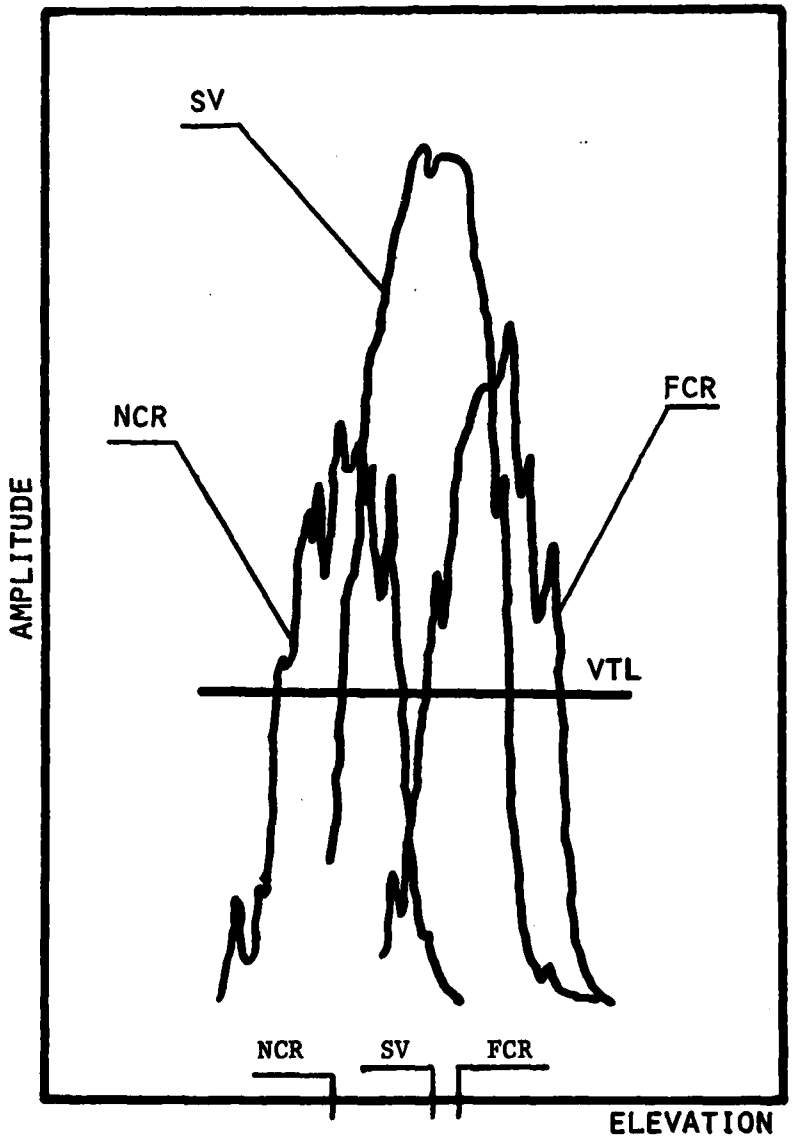

Figure 24. Radar elevation profiles: Run number B-1.

RANGE (METERS)		ELEVATION ANGLE (MRAD BELOW HORIZ)
804	SHOP VAN (SV)	9.09
392	FAR CORNER REFLECTOR (FCR)	4.12
372	NEAR CORNER REFLECTOR (NCR)	13.88

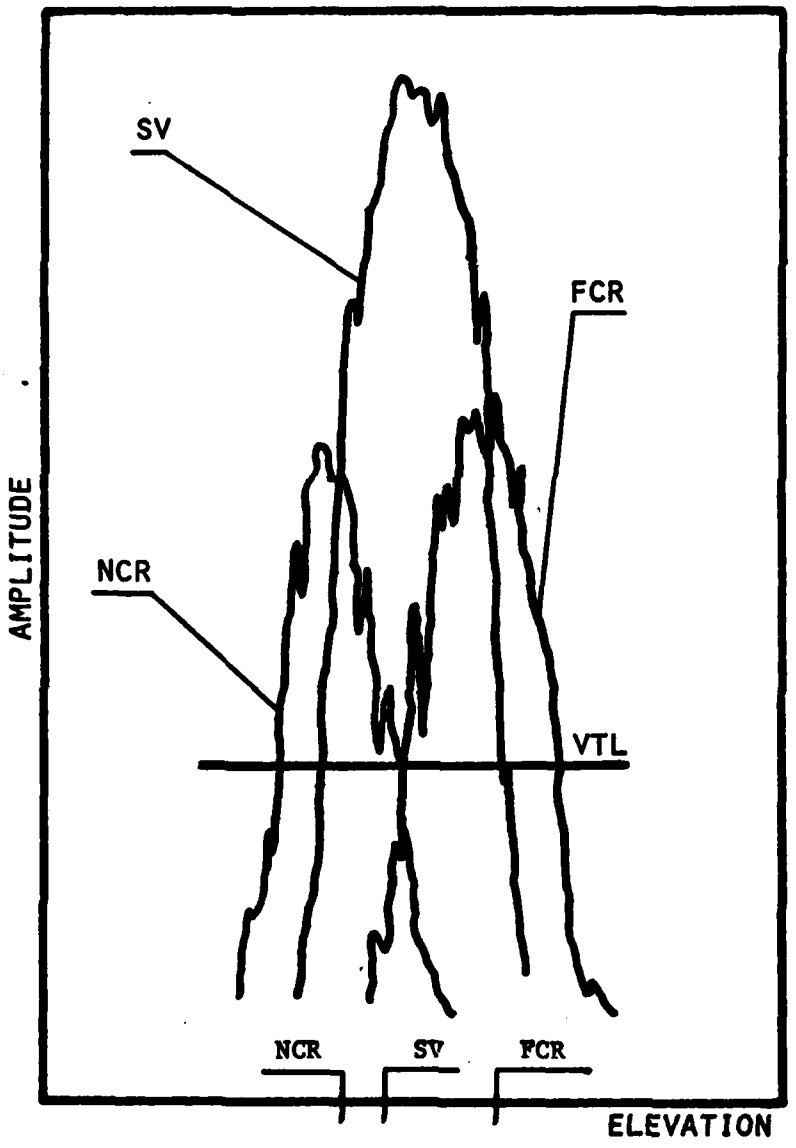

Figure 25. Radar elevation profiles: Run number B-2.

RANGE (METERS)		ELEVATION ANGLE (MRAD BELOW HORIZ)
804	SHOP VAN (SV)	9.13
392	FAR CORNER REFLECTOR (FCR)	4.09
372	NEAR CORNER REFLECTOR (NCR)	13.88

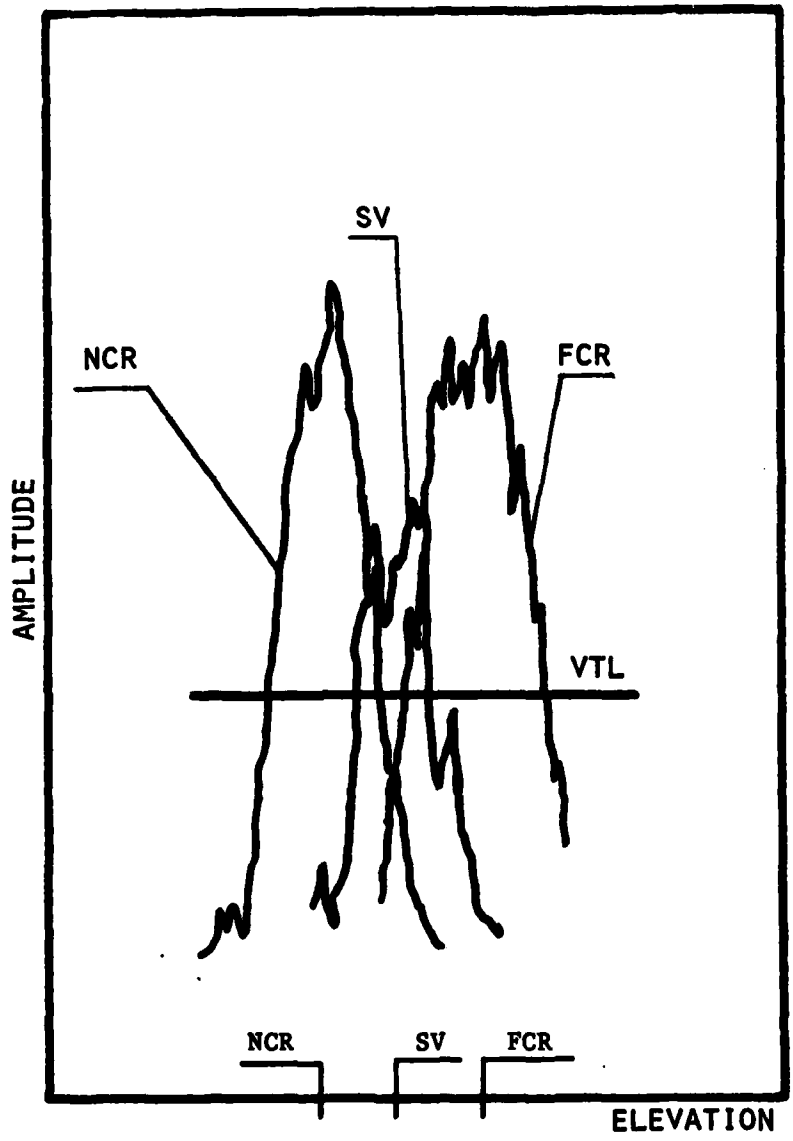

Figure 26. Radar elevation profiles: Run number B-3.

RANGE (METERS)		ELEVATION ANGLE (MRAD BELOW HORIZ)
1127	SHOP VAN (SV)	7.12
354	FAR CORNER REFLECTOR (FCR)	4.76
299	NEAR CORNER REFLECTOR (NCR)	11.02

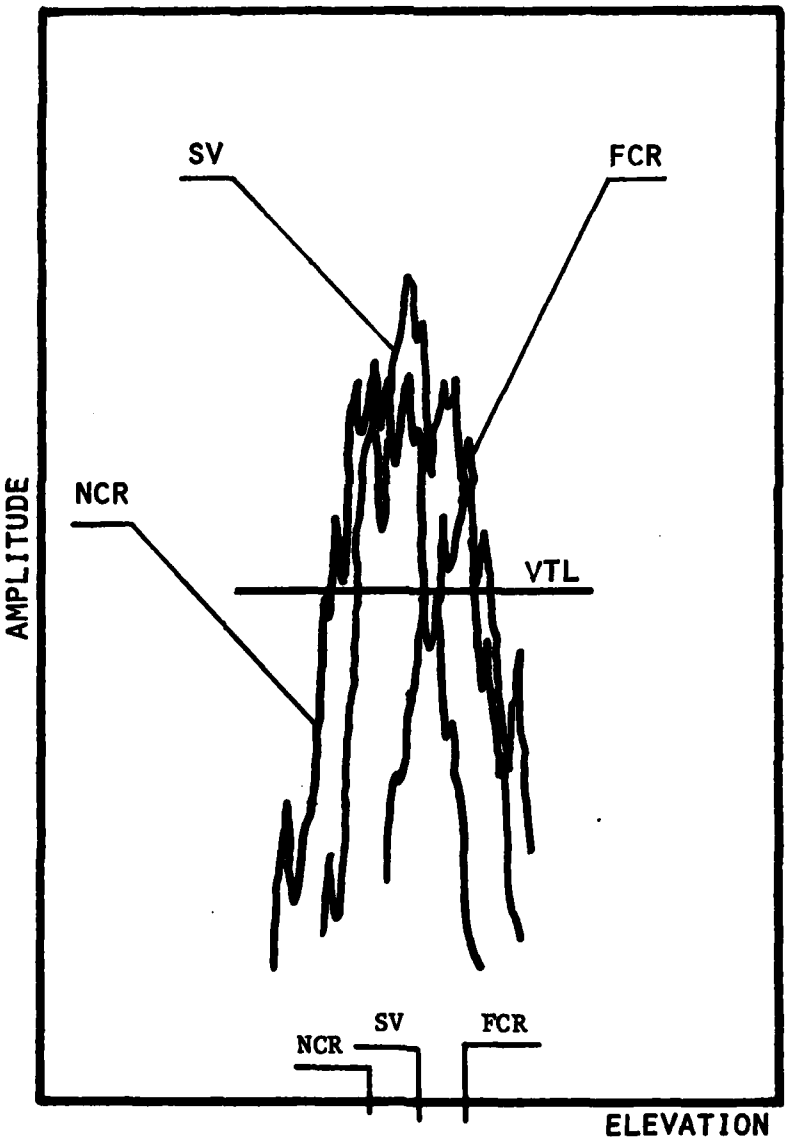

Figure 27. Radar elevation profiles: Run number C-1.

RANGE (METERS)		ELEVATION ANGLE (MRAD BELOW HORIZ)
1127	SHOP VAN (SV)	7.11
354	FAR CORNER REFLECTOR (FCR)	4.70
299	NEAR CORNER REFLECTOR (NCR)	11.02

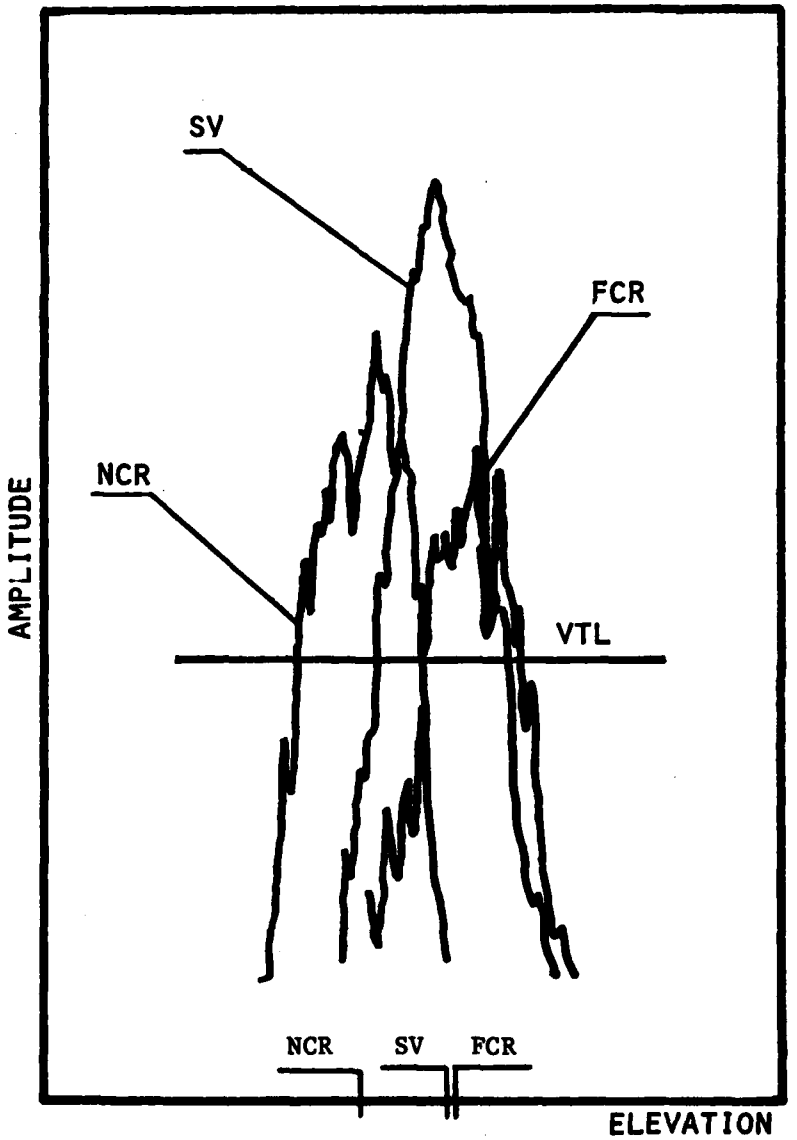

Figure 28. Radar elevation profiles: Run number C-2.

RANGE (METERS)		ELEVATION ANGLE (MRAD BELOW HORIZ)
1127	SHOP VAN (SV)	7.19
354	FAR CORNER REFLECTOR (FCR)	4.70
299	NEAR CORNER REFLECTOR (NCR)	11.02

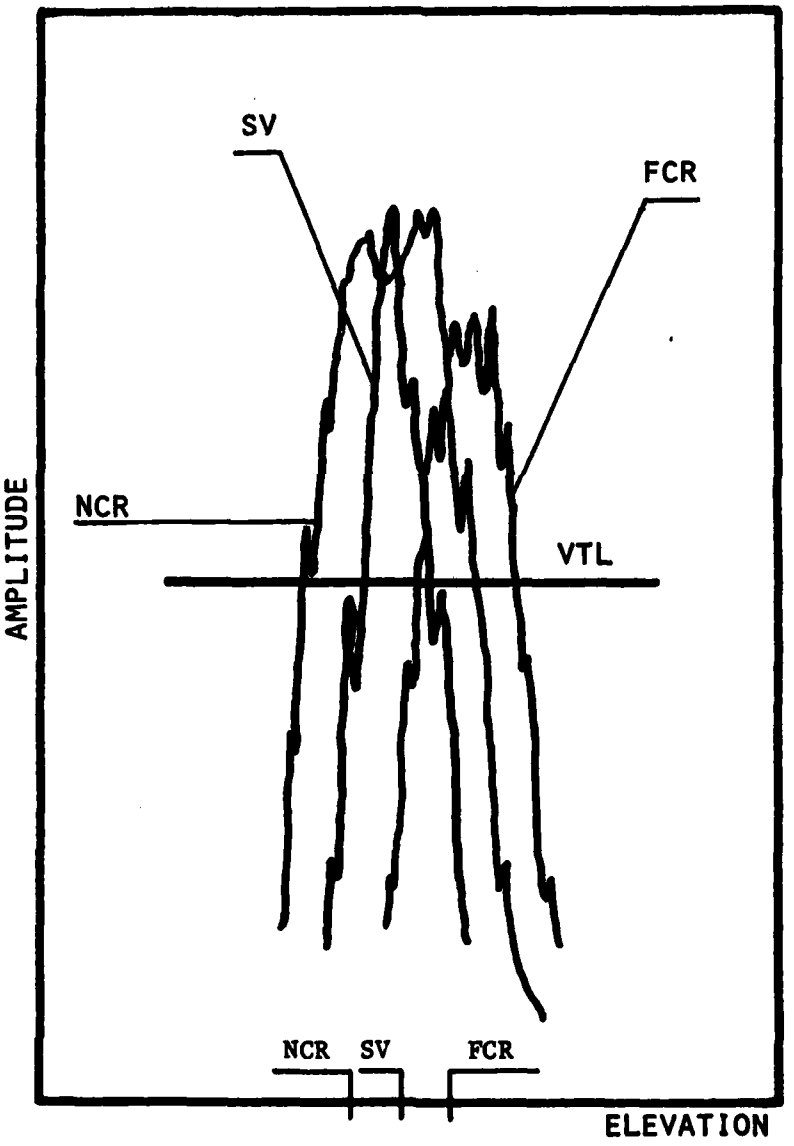

Figure 29. Radar elevation profiles: Run number C-3.

RANGE (METERS)		ELEVATION ANGLE (MRAD BELOW HORIZ)
1315	SHOP VAN (SV)	2.49
354	FAR CORNER REFLECTOR (FCR)	4.63
299	NEAR CORNER REFLECTOR (NCR)	11.04

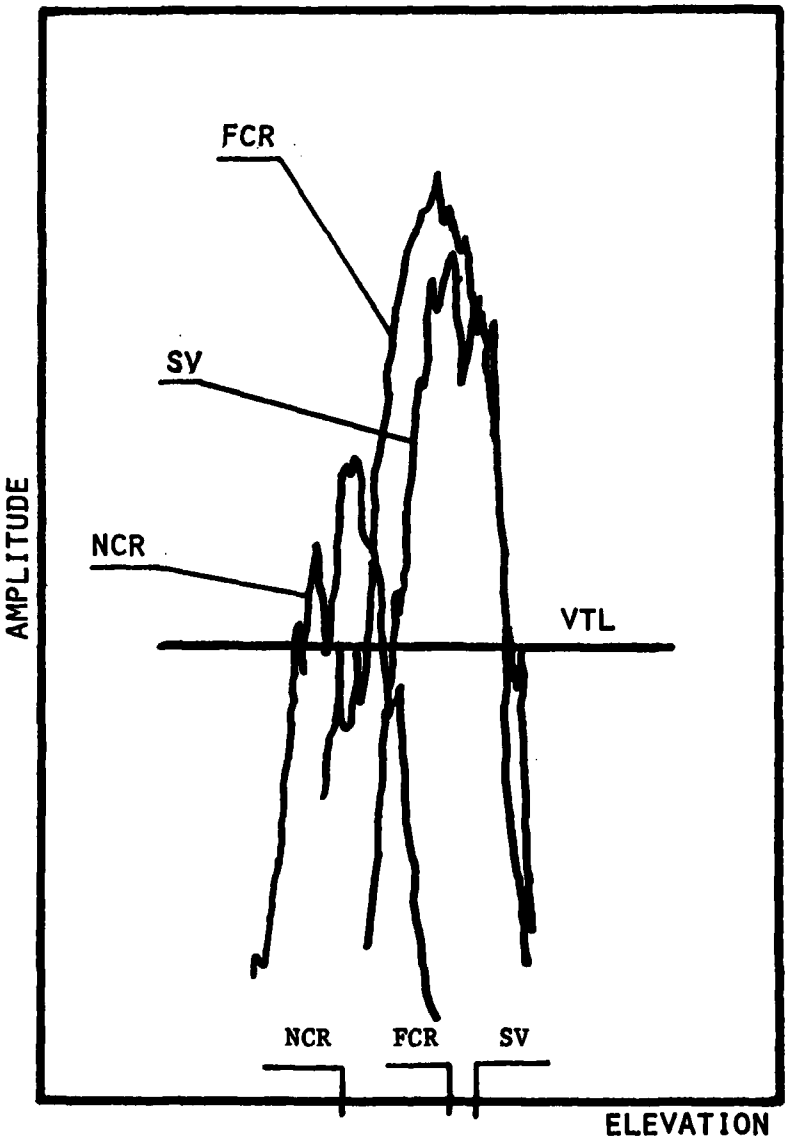

Figure 30. Radar elevation profiles: Run number D-1.

RANGE (METERS)		ELEVATION ANGLE (MRAD BELOW HORIZ)
1315	SHOP VAN (SV)	2.35
354	FAR CORNER REFLECTOR (FCR)	4.51
299	NEAR CORNER REFLECTOR (NCR)	11.03

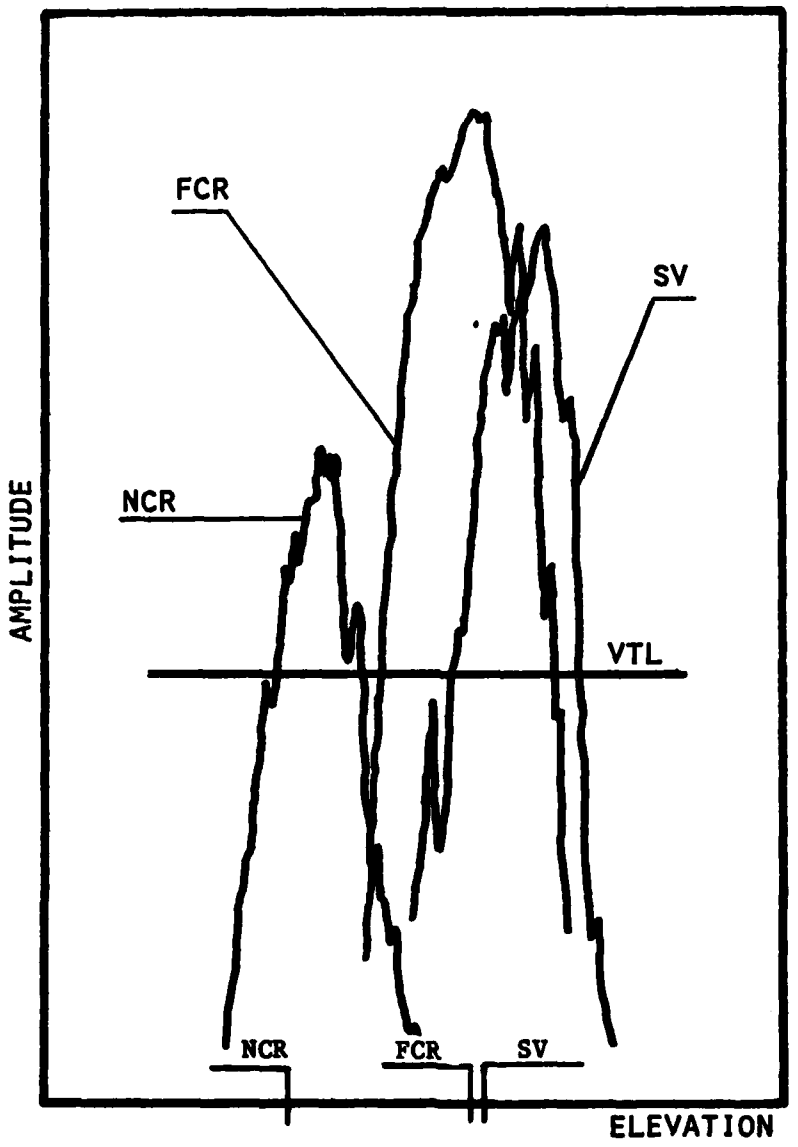

Figure 31. Radar elevation profiles: Run number D-2.

RANGE (METERS)		ELEVATION ANGLE (MRAD BELOW HORIZ)
1315	SHOP VAN (SV)	2.35
354	FAR CORNER REFLECTOR (FCR)	4.38
299	NEAR CORNER REFLECTOR (NCR)	10.98

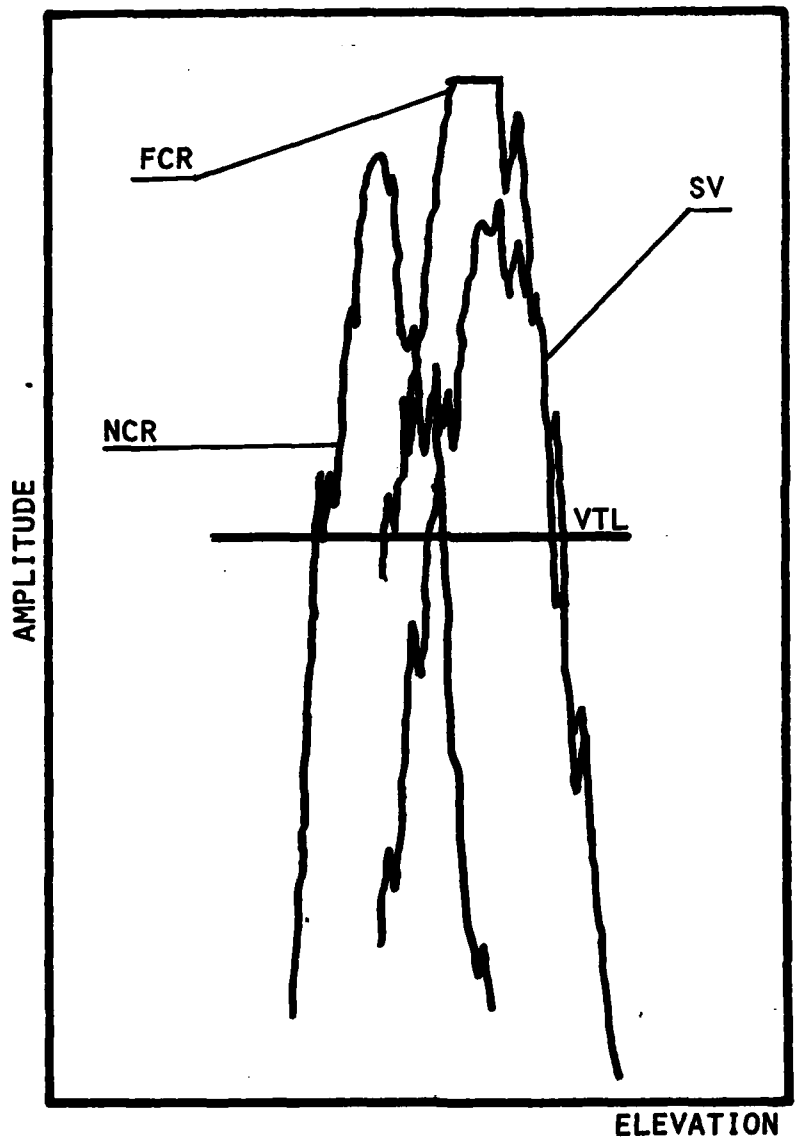

Figure 32. Radar elevation profiles: Run number D-3.

RANGE (METERS)		ELEVATION ANGLE (MRAD BELOW HORIZ)
1430	SHOP VAN (SV)	1.97
354	FAR CORNER REFLECTOR (FCR)	4.65
299	NEAR CORNER REFLECTOR (NCR)	11.02

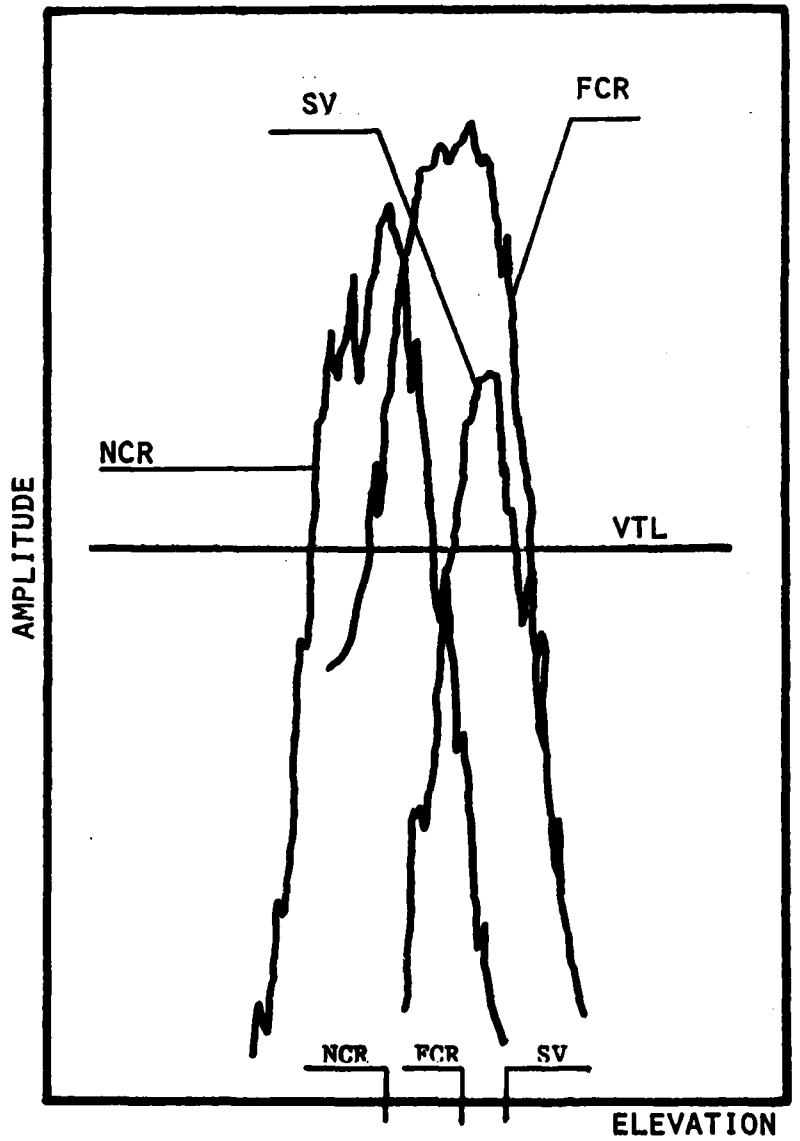

Figure 33. Radar elevation profiles: Run number E-1.

RANGE (METERS)		ELEVATION ANGLE (MRAD BELOW HORIZ)
1430	SHOP VAN (SV)	1.99
354	FAR CORNER REFLECTOR (FCR)	4.72
299	NEAR CORNER REFLECTOR (NCR)	11.01

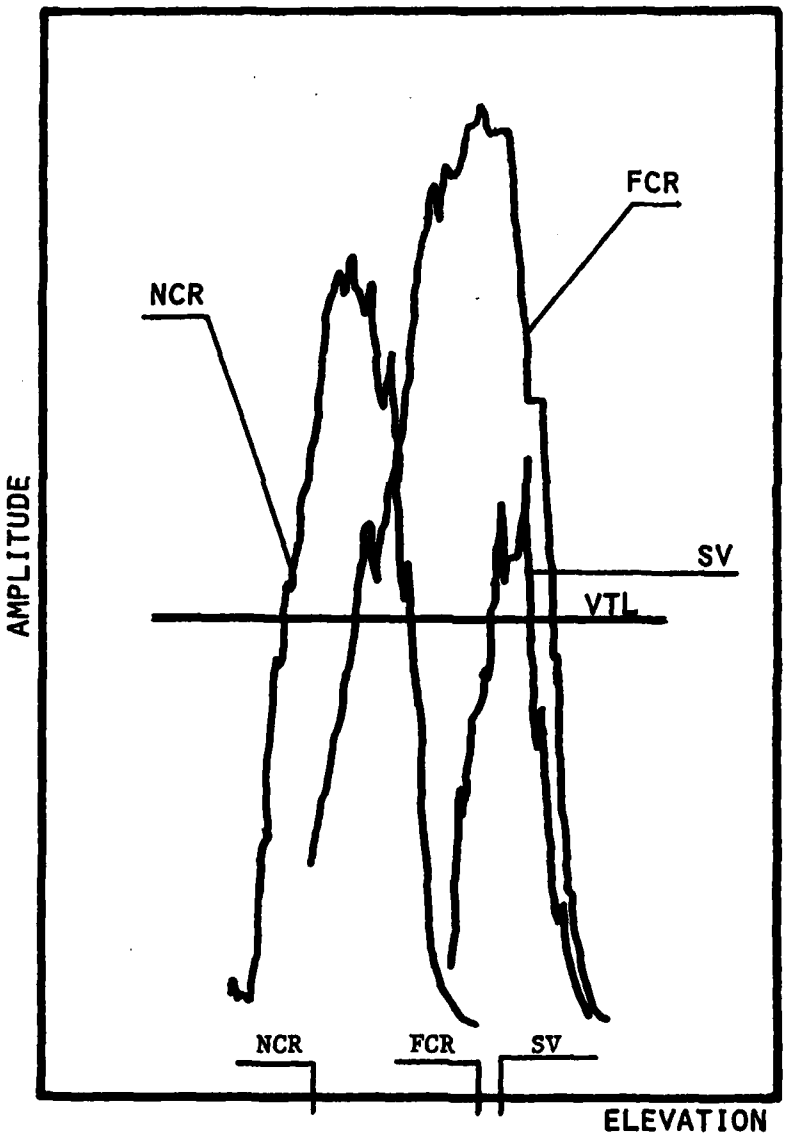

Figure 34. Radar elevation profiles: Run number E-2.

RANGE (METERS)		ELEVATION ANGLE (MRAD BELOW HORIZ)
1430	SHOP VAN (SV)	2.02
354	FAR CORNER REFLECTOR (FCR)	4.73
299	NEAR CORNER REFLECTOR (NCR)	11.04

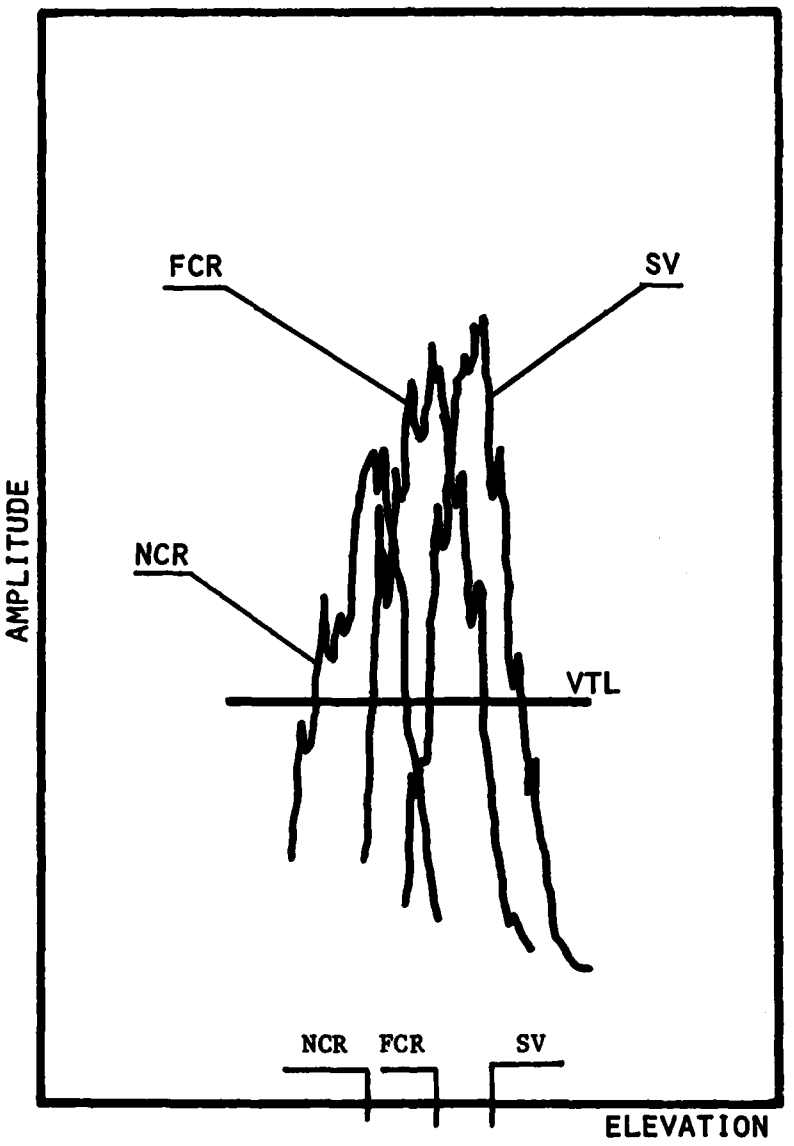

Figure 35. Radar elevation profiles: Run number E-3.

runs per test. The shop van was placed at a different range (from 438 meters to 1311 meters) for each test. For three of the tests (A, C, D), the shop van was oriented broadside to the boresight of the radar while for the remaining test (B), the shop van was oriented head-on to the boresight of the radar. A corner reflector was also placed in the field.

The test plan scenario for the azimuth beamsplitting experiments was as follows:

1. Locate the corner reflector in azimuth on B-scope display, electronically scan azimuth cursor across the corner reflector return and plot out a radar azimuth profile (RAP) on the X-Y plotter.

2. Align theodolite on corner reflector and set zero.

3. Locate shop van in azimuth on B-scope display and center scanning azimuth cursor on shop van return by moving entire radar console. The scanning cursor is considered centered on the return of the shop van when, as determined by the operator, the RAP of the shop van is centered over the RAP of the corner reflector.

4. Finally, measure the shop van's angular position relative to theodolite zero. (The azimuth angle of the shop van was taken to be the azimuth angle of the vertical line that intersects the leading edge of the middle of the three windows on the body of the van). If the radar has located the shop van accurately, then theodolite should be zeroed on the van.

This method increased the operator's beamsplitting accuracy over that obtained in the system integration tests. While still a subjective measurement, the operator's beamsplitting ability could now be judged by referring to the RAP's of the corner reflector and shop van for a given run and determining how well these two plots were superimposed.

The results of the azimuth beamsplitting experiments are given in Table VII. This table shows the azimuth position, $\Delta\phi$, of the shop van relative to the zero of the theodolite for all forty runs. The standard deviation in $\Delta\phi$ for the three tests where the shop van was broadside to the radar was approximately $\sigma(\Delta\phi) \simeq 0.5$ mrad, while for the test where the van was head on $\sigma(\Delta\phi) \simeq 0.8$ mrad. This represents, respectively, a 19:1 and a 12:1 beamsplit improvement in azimuth resolution.

TABLE VII: RESULTS OF AZIMUTH BEAMSPLITTING EXPERIMENTS (Field Tests)

RUN NUMBER	TEST A[†] $\Delta\phi$ (mrad)	TEST B[*] $\Delta\phi$ (mrad)	TEST C[††] $\Delta\phi$ (mrad)	TEST D[**] $\Delta\phi$ (mrad)
1	1.197	1.261	0.635	1.353
2	0.970	-0.650	1.673	1.493
3	0.999	-1.076	0.800	2.002
4	2.051	-0.378	2.031	2.376
5	1.576	-1.503	0.989	1.639
6	1.595	-0.339	1.687	2.390
7	1.319	0.412	1.508	1.508
8	1.081	0.679	1.794	1.770
9	1.251	0.330	1.590	2.400
10	0.000	-0.485	2.269	0.994
$\langle\Delta\phi\rangle$ (mrad)	1.204	-0.175	1.498	1.792
$\sigma(\Delta\phi)$ (mrad)	0.508	0.797	0.503	0.466

[†]Corner reflector range: 240 meters; Shop van range: 438 meters; Shop van orientation: Broadside

[*]Corner reflector range: 475 meters; Shop van range: 542 meters; Shop van orientation: Head-on

[††]Corner reflector range: 461 meters; Shop van range: 781 meters; Shop van orientation: Broadside

[**]Corner reflector range: 460 meters; Shop van range: 1311 meters; Shop van orientation: Broadside

The superimposed RAP's of the corner reflector and shop van for Tests C and D are shown in Figures 36 through 45.

Radar to EO Sensor Handoff Experiments

The radar to EO sensor handoff experiments consisted of three tests of 22 total runs using the visual azimuth beamsplitting technique and one test of eight runs using the electronic beamsplitter.

For the experiments in which the visual beamsplitting technique was used, the shop van target was located in azimuth by the radar in the same manner as in the azimuth beamsplitting experiments described earlier except the theodolite was not used. The test plan scenario for these tests was as follows:

1. Locate corner reflector in azimuth with EO sensor and align corner reflector stand with the "zero line" of the grid system on the monitor. Adjust special effects generator so that radar's B-scope is now displayed on the monitor.

2. Locate corner reflector in azimuth on B-scope display, electronically scan azimuth cursor across the corner reflector return and plot out a RAP on the X-Y plotter.

3. Locate shop van in azimuth on B-scope display and center scanning azimuth cursor on shop van return by moving entire radar console. The scanning cursor is considered centered on the return when the RAP of the shop van is centered over the RAP of the corner reflector.

4. Adjust special effects generator so that the EO sensor's scene of view is now displayed on monitor and note placement of shop van with respect to the "zero line" of the grid system.

Results of these tests are shown in Figures 46 through 67. On the left side of each figure are the superimposed RAP's of the corner reflector and shop van as they appeared on the X-Y plotter. On the right side of each figure is a picture of the corresponding scene of view of the EO sensor with the grid system superimposed. These pictures are taken from the video taped record of the experiments. The zero line of the grid system represents the shop van's location as determined by the radar using the visual beamsplitting technique. Notice that not only is this line on the target in every experimental run, but is usually centered on the target.

The test plan scenario for the experiments in which the electronic beamsplitter was used as follows:

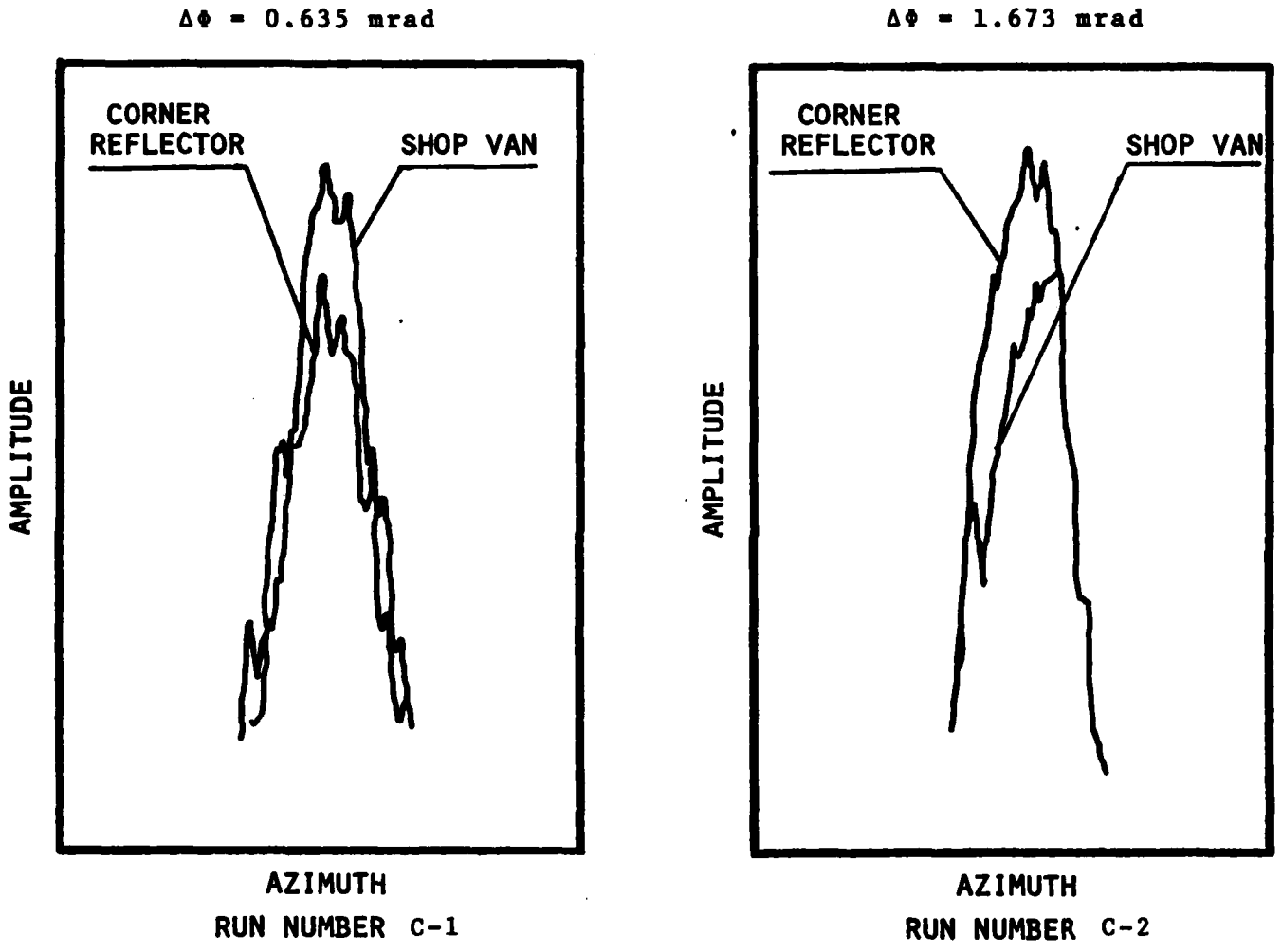

Figure 36. Radar azimuth profiles: Runs number C-1 and C-2

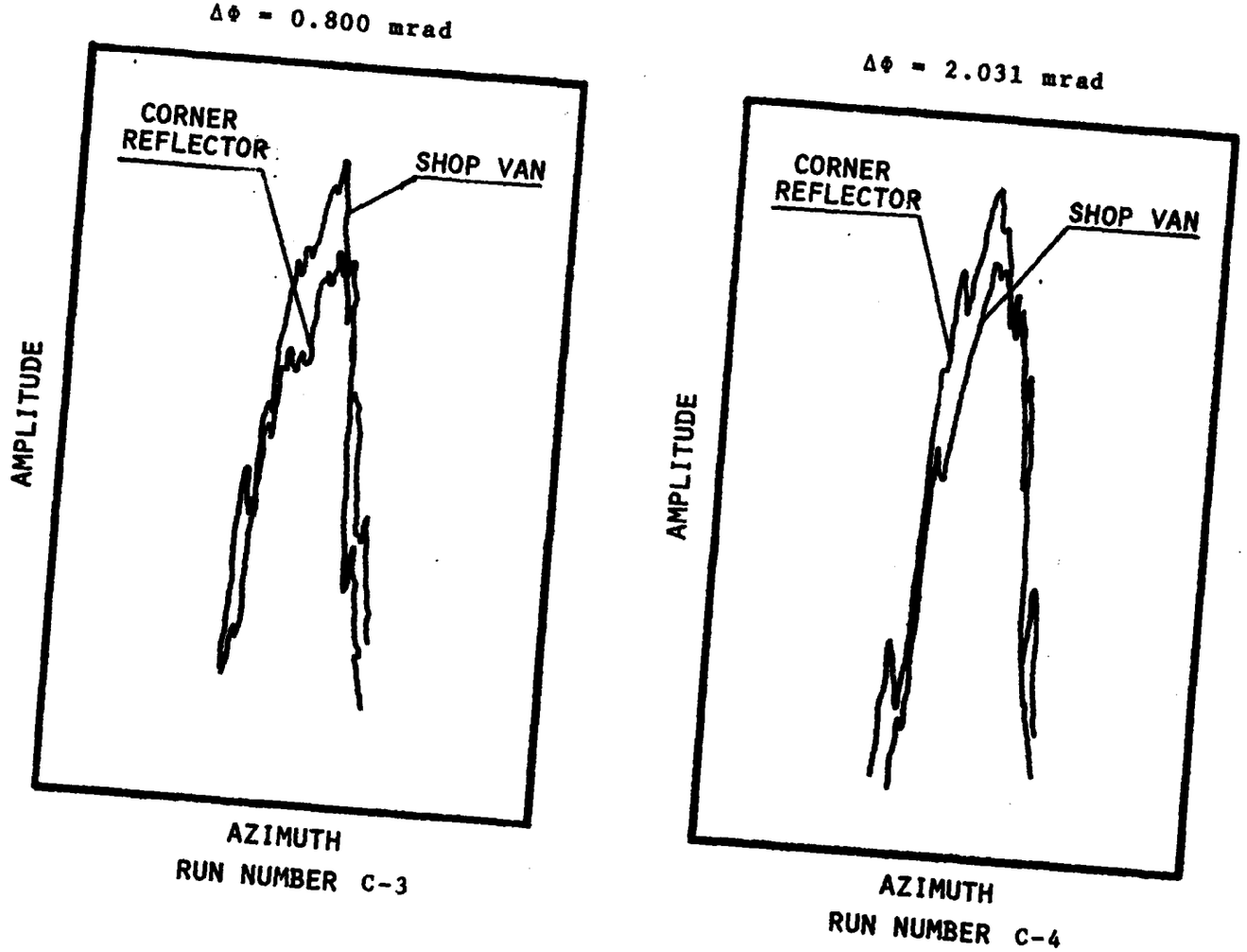

Figure 37. Radar azimuth profiles: Runs number C-3 and C-4

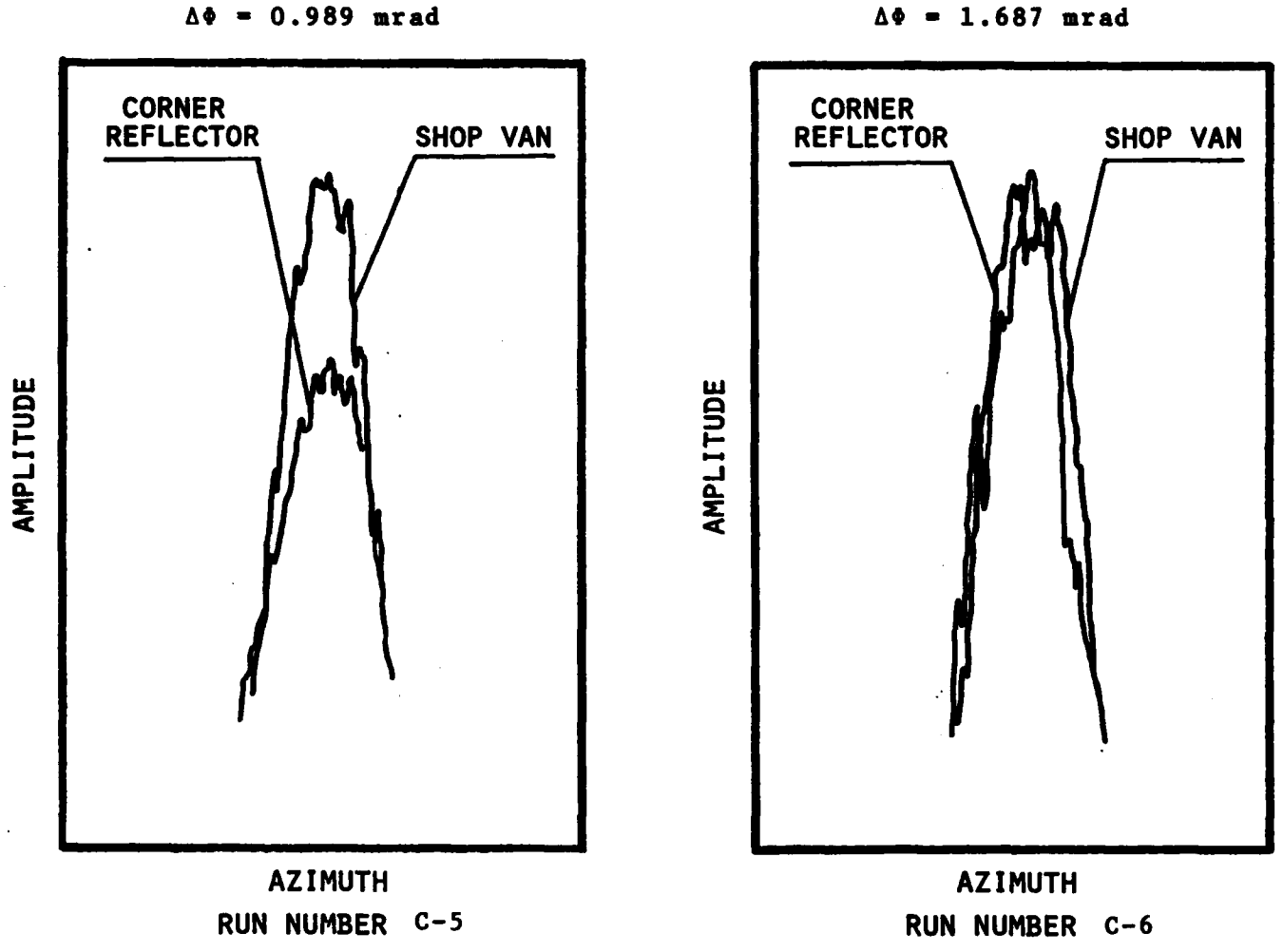

Figure 38. Radar azimuth profiles: Runs number C-5 and C-6

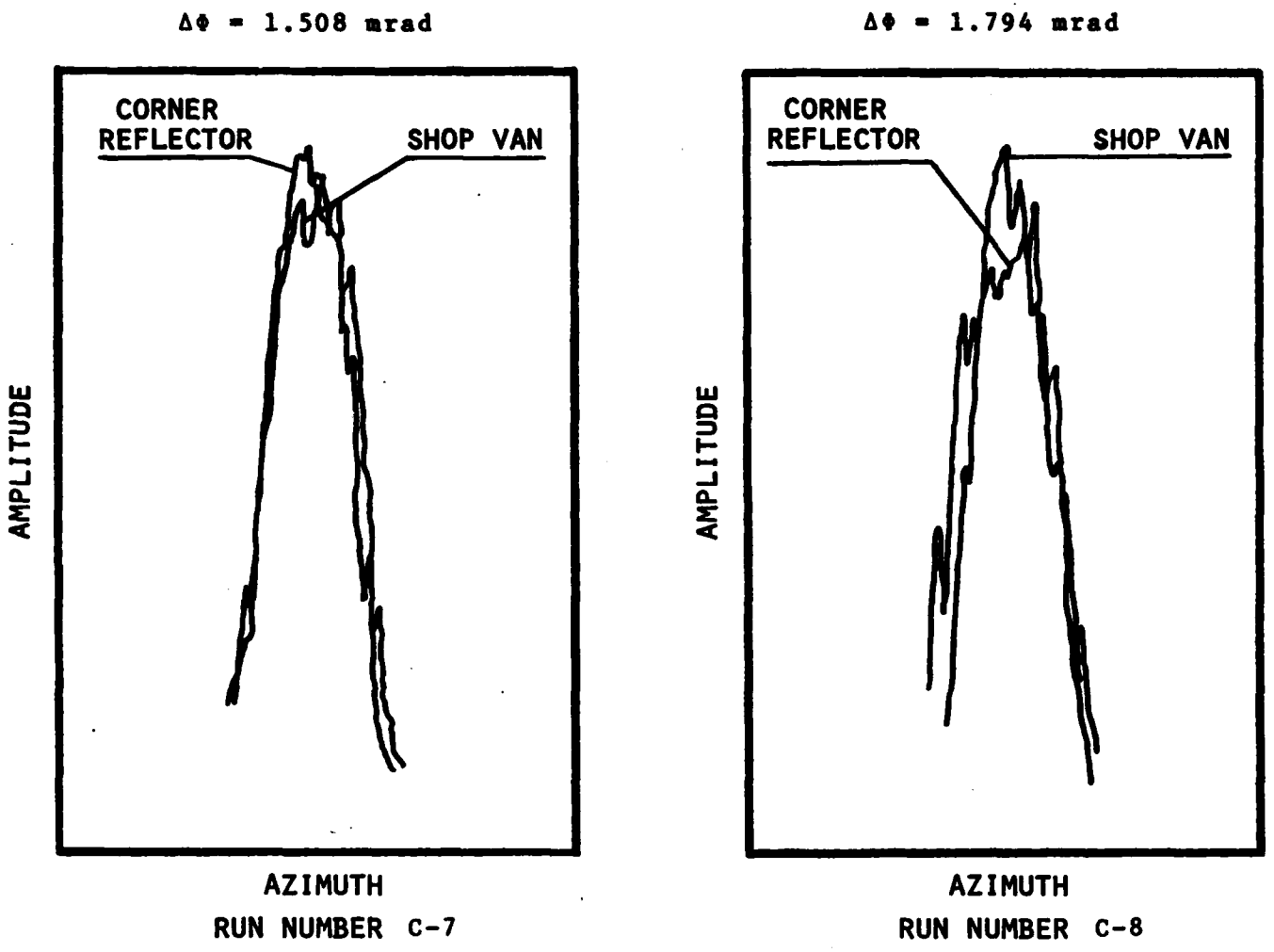

Figure 39. Radar azimuth profiles: Runs number C-7 and C-8

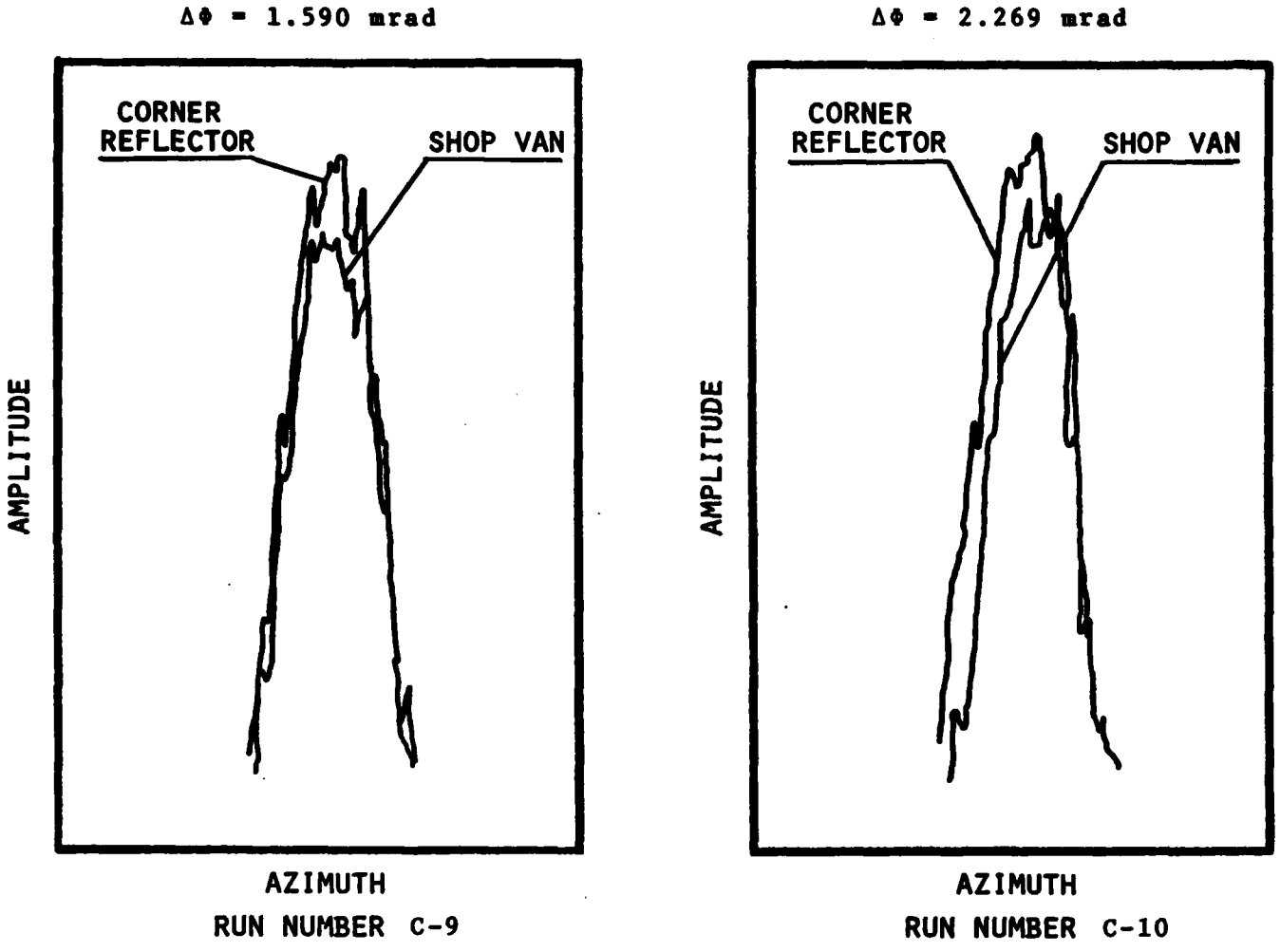

Figure 40. Radar azimuth profiles: Runs number C-9 and C-10

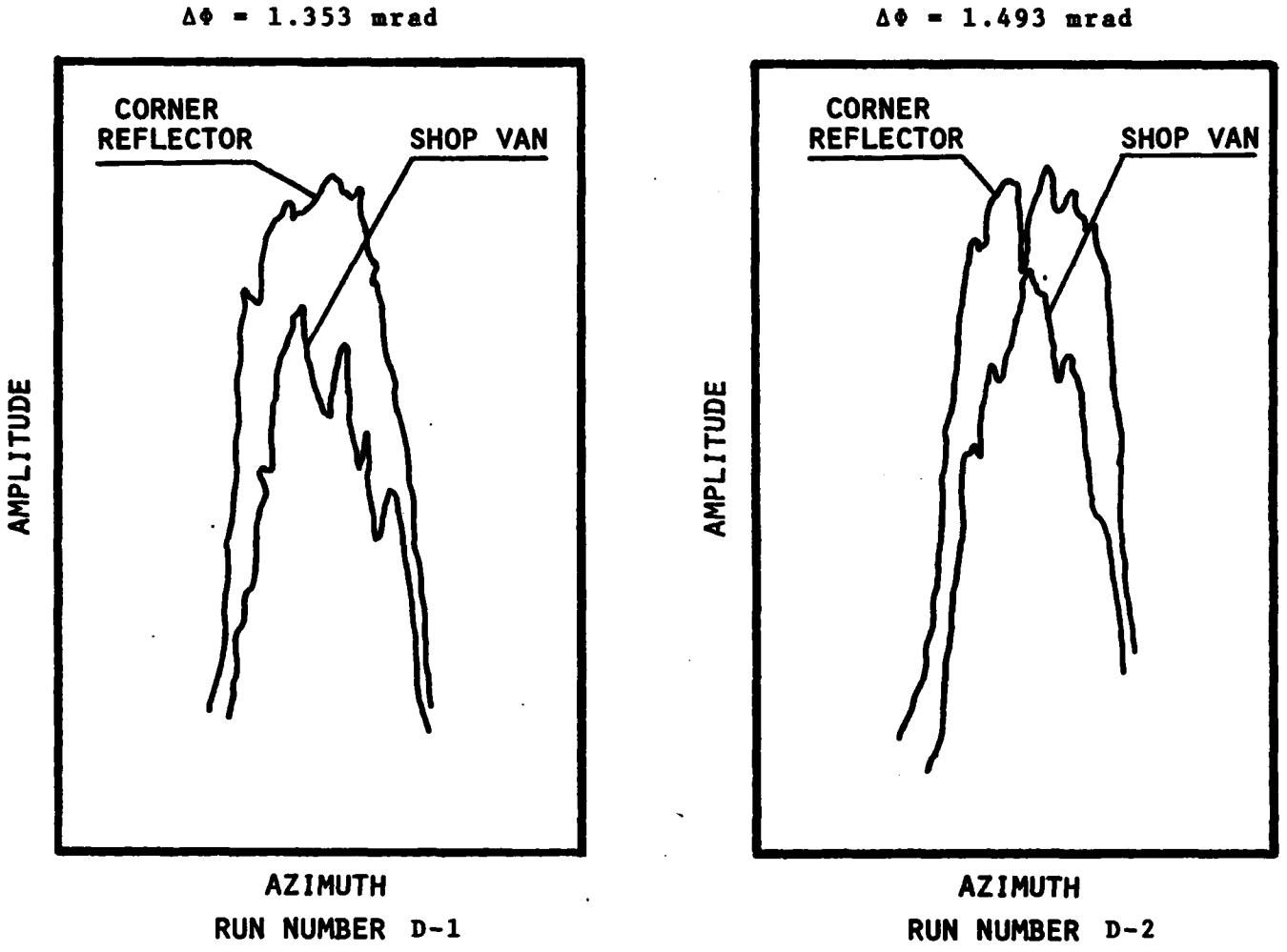

Figure 41. Radar azimuth profiles: Runs number D-1 and D-2

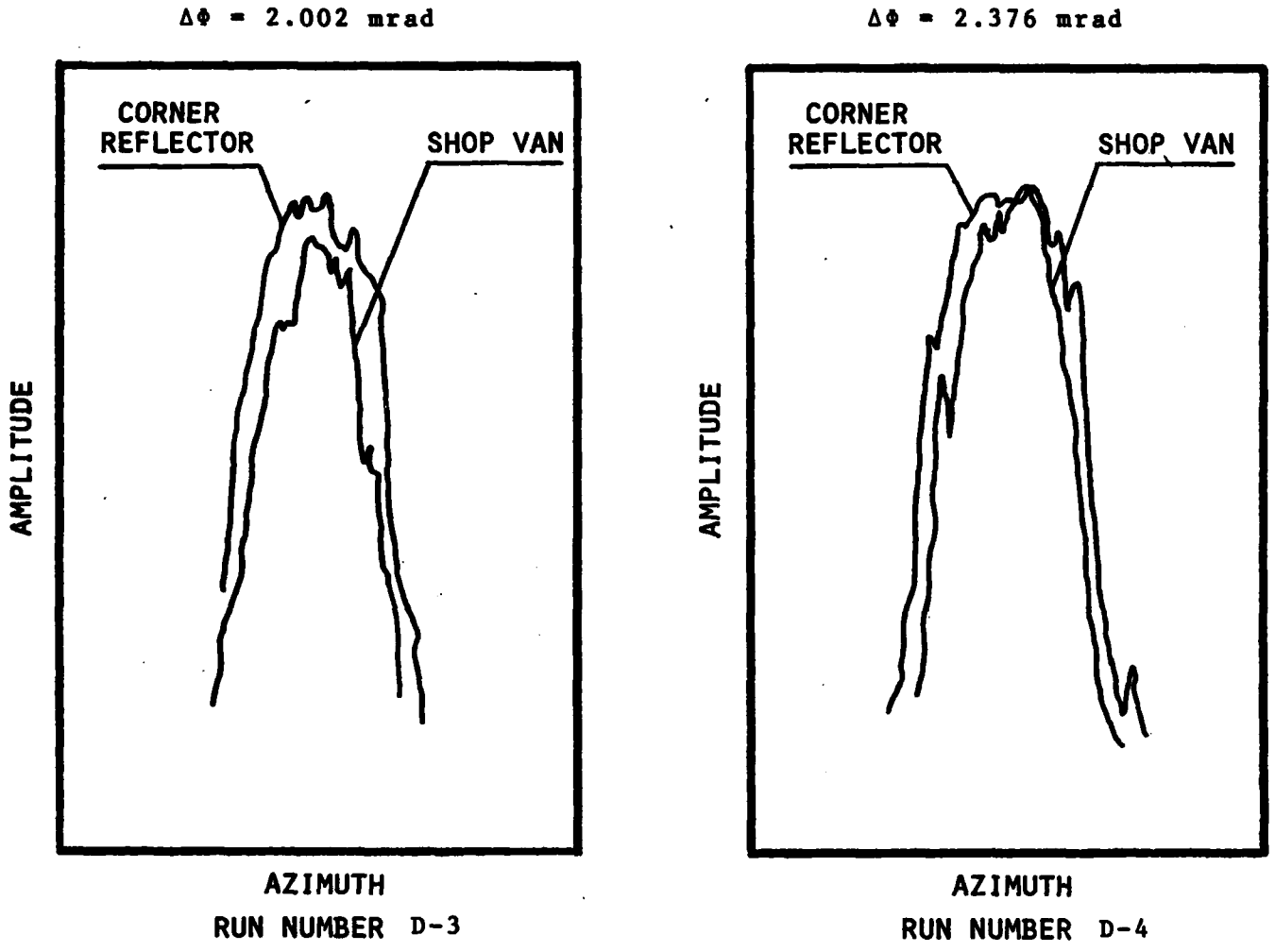

Figure 42. Radar azimuth profiles: Runs number D-3 and D-4

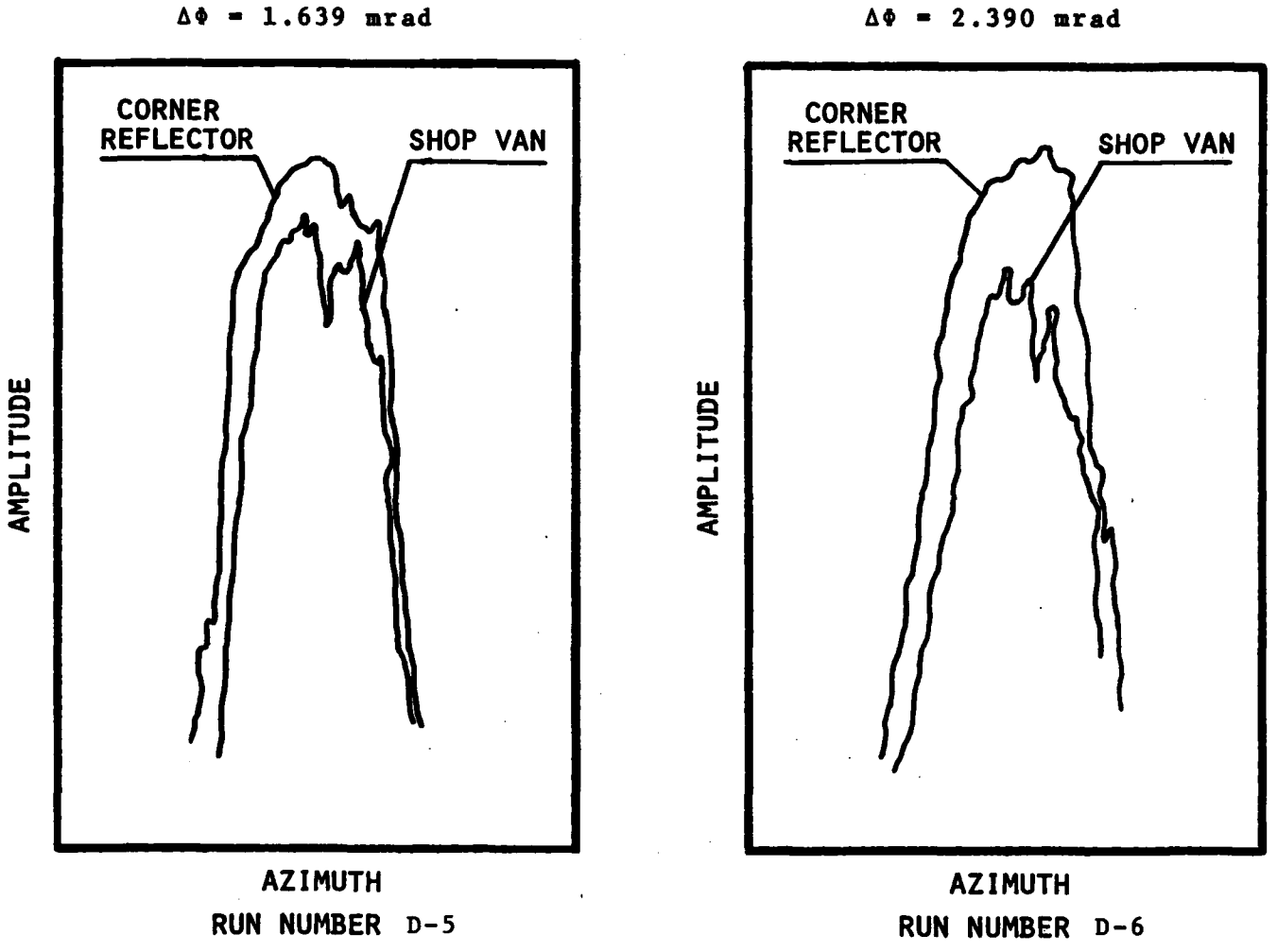

Figure 43. Radar azimuth profiles: Runs number D-5 and D-6

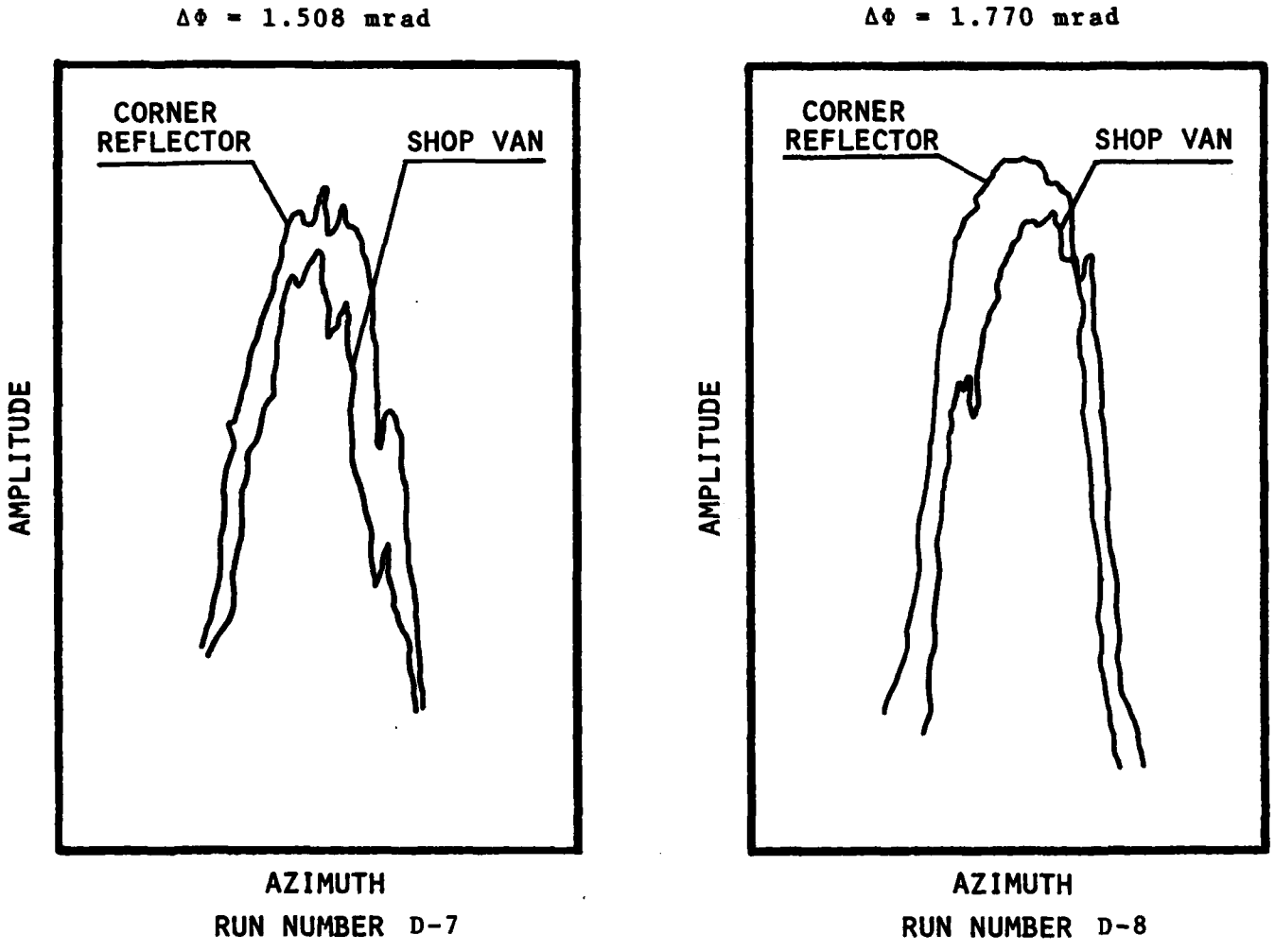

Figure 44. Radar azimuth profiles: Runs number D-7 and D-8

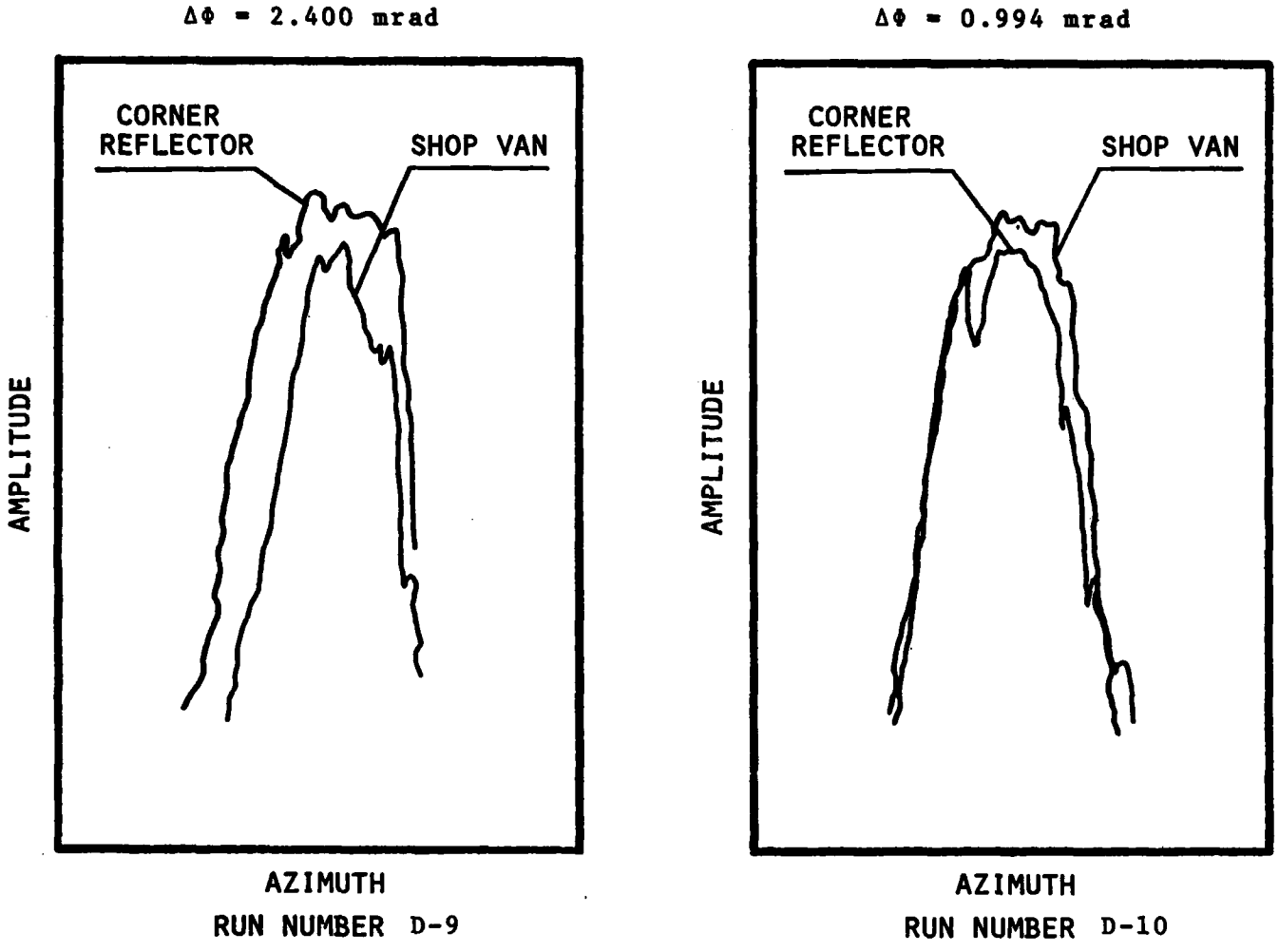

Figure 45. Radar azimuth profiles: Runs number D-9 and D-10

CORNER REFLECTOR RANGE: 526 METERS.

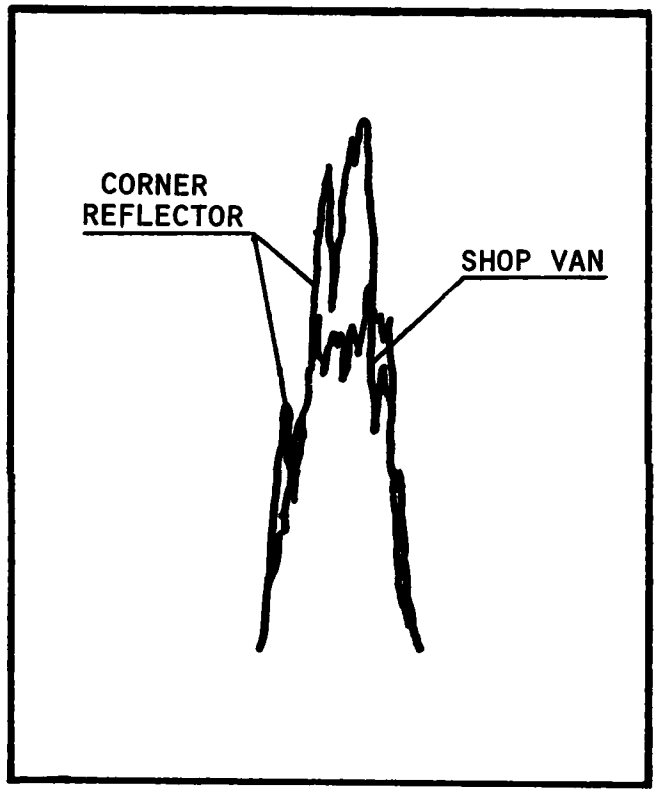

AZIMUTH PROFILES OF CORNER REFLECTOR AND SHOP VAN.

SHOP VAN RANGE: 805 METERS

VERTICAL LINES ARE ONE MILLIRADIAN APART.
ZERO LINE REPRESENTS TARGET LOCATION AS DETERMINED BY THE RADAR.

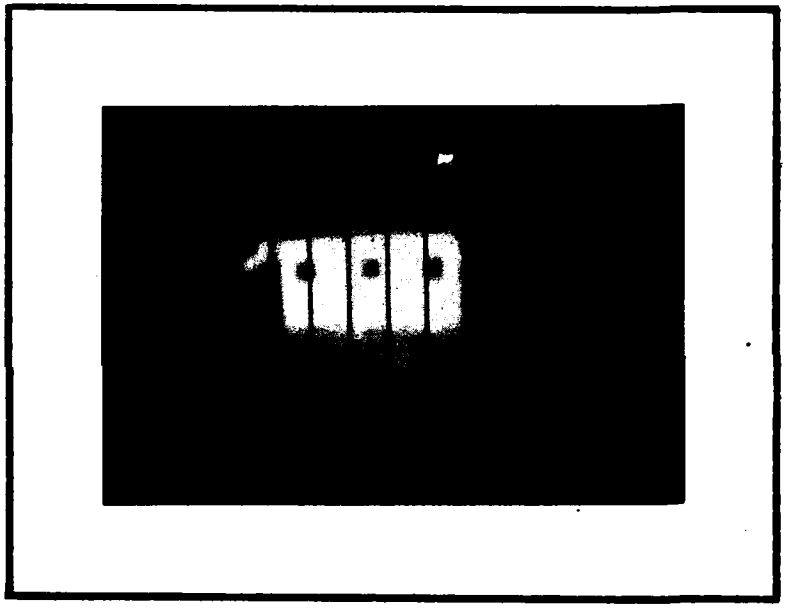

TV VIDEO OF SHOP VAN.

Figure 46. Radar azimuth profiles and TV video: Run number A-1

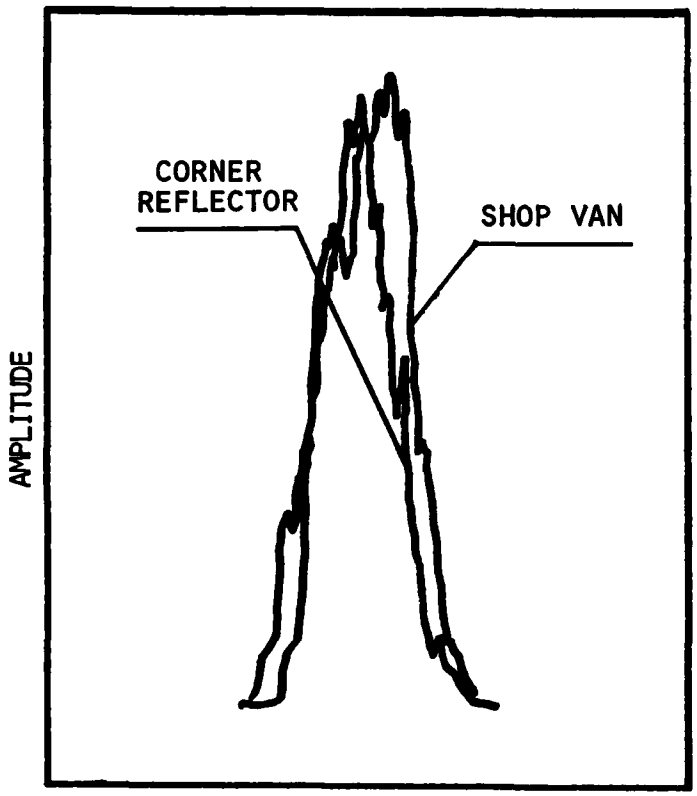

AZIMUTH PROFILES OF CORNER REFLECTOR AND SHOP VAN.

SHOP VAN RANGE: 805 METERS

VERTICAL LINES ARE ONE MILLIRADIAN APART.
ZERO LINE REPRESENTS TARGET LOCATION AS DETERMINED BY THE RADAR.

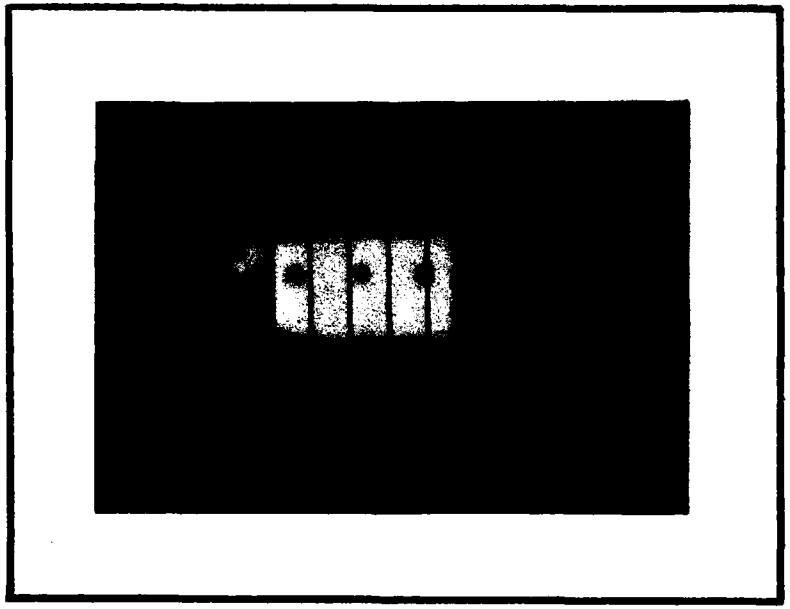

TV VIDEO OF SHOP VAN.

Figure 47. Radar azimuth profiles and TV video: Run number A-2

CORNER REFLECTOR RANGE: 526 METERS.

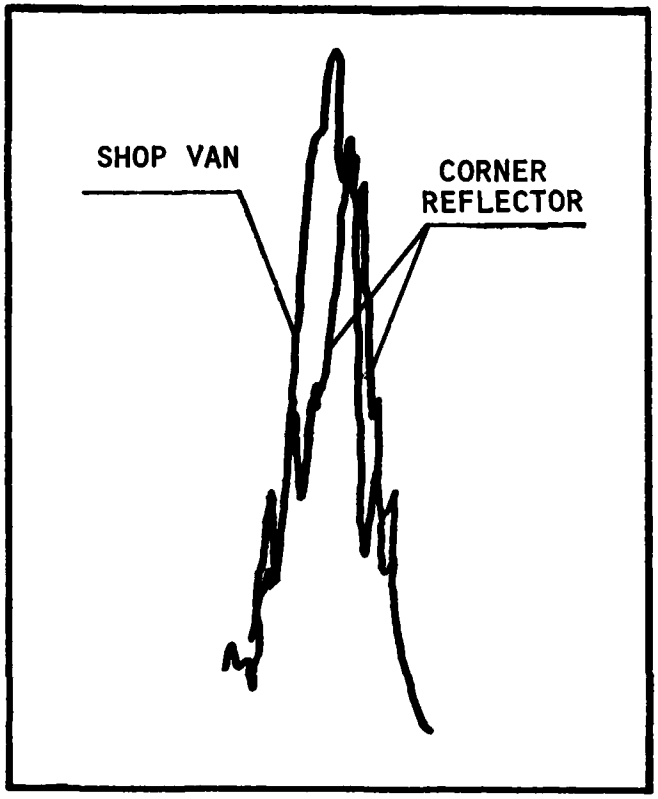

AZIMUTH PROFILES OF CORNER REFLECTOR AND SHOP VAN.

SHOP VAN RANGE: 805 METERS

VERTICAL LINES ARE ONE MILLIRADIAN APART.
ZERO LINE REPRESENTS TARGET LOCATION AS DETERMINED BY THE RADAR.

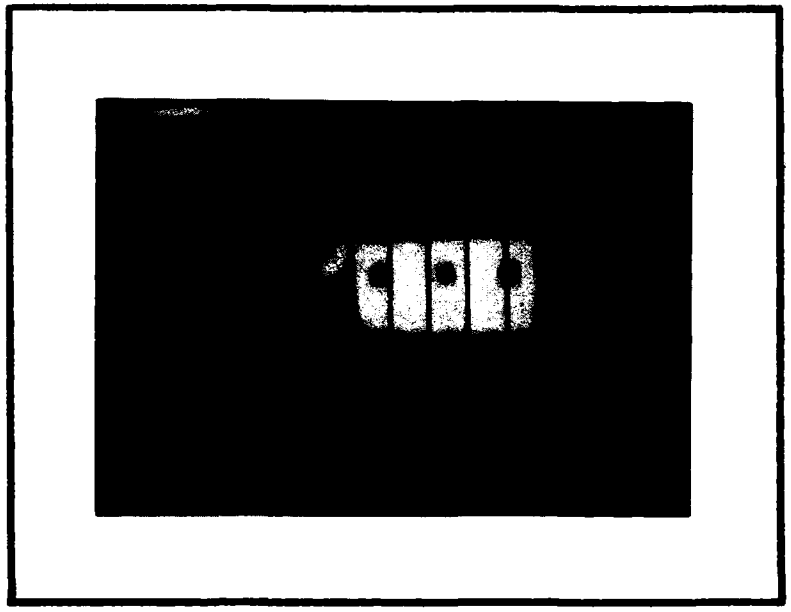

TV VIDEO OF SHOP VAN.

Figure 48. Radar azimuth profiles and TV video: Run number A-3

CORNER REFLECTOR RANGE: 526 METERS.

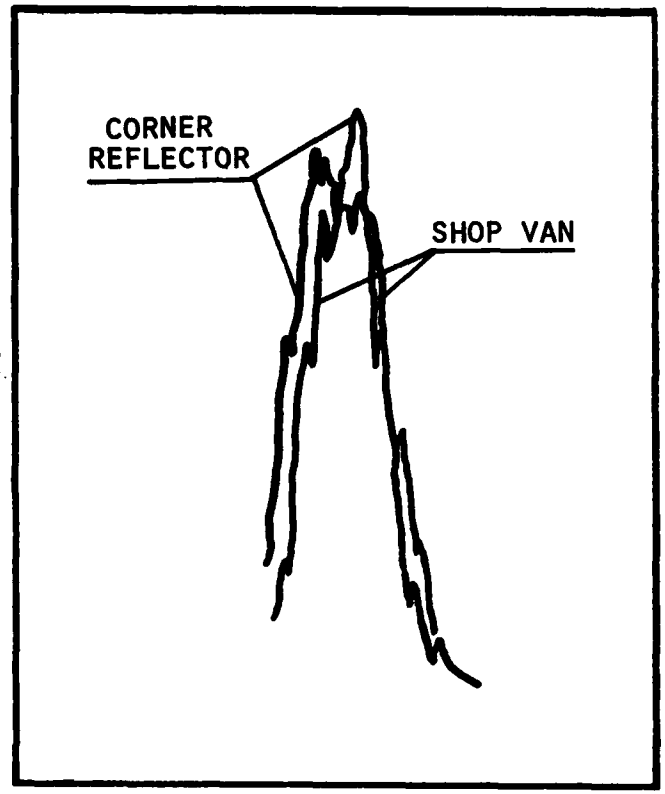

AZIMUTH PROFILES OF CORNER REFLECTOR AND SHOP VAN.

SHOP VAN RANGE: 805 METERS

VERTICAL LINES ARE ONE MILLIRADIAN APART.
ZERO LINE REPRESENTS TARGET LOCATION AS DETERMINED BY THE RADAR.

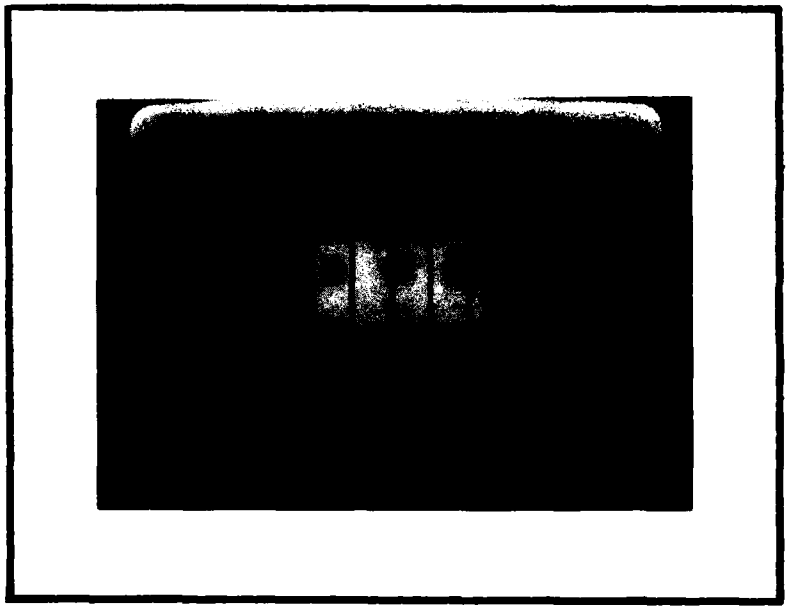

TV VIDEO OF SHOP VAN.

Figure 49. Radar azimuth profiles and TV video: Run number A-4

CORNER REFLECTOR RANGE: 526 METERS.

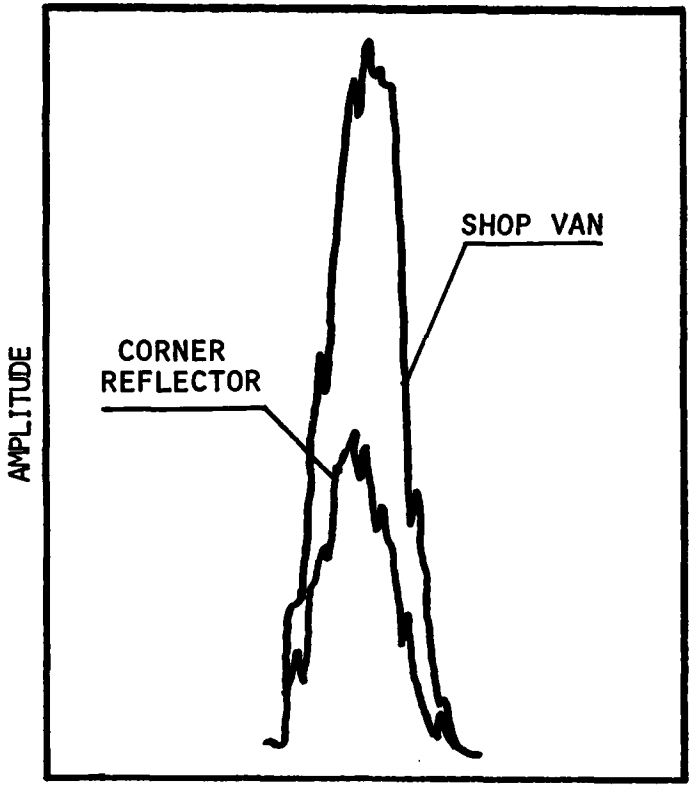

AZIMUTH PROFILES OF CORNER REFLECTOR AND SHOP VAN.

SHOP VAN RANGE: 805 METERS

VERTICAL LINES ARE ONE MILLIRADIAN APART.
ZERO LINE REPRESENTS TARGET LOCATION AS DETERMINED BY THE RADAR.

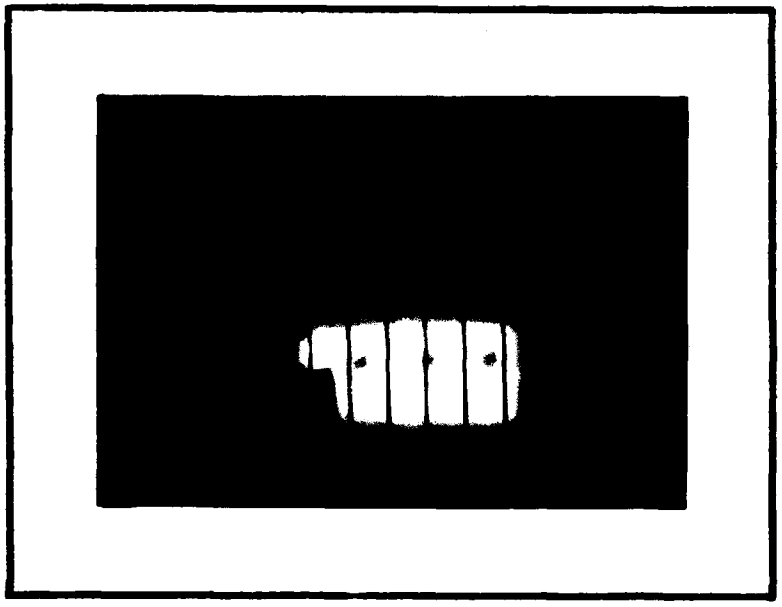

TV VIDEO OF SHOP VAN.

Figure 50. Radar azimuth profiles and TV video: Run number A-5

CORNER REFLECTOR RANGE: 526 METERS.

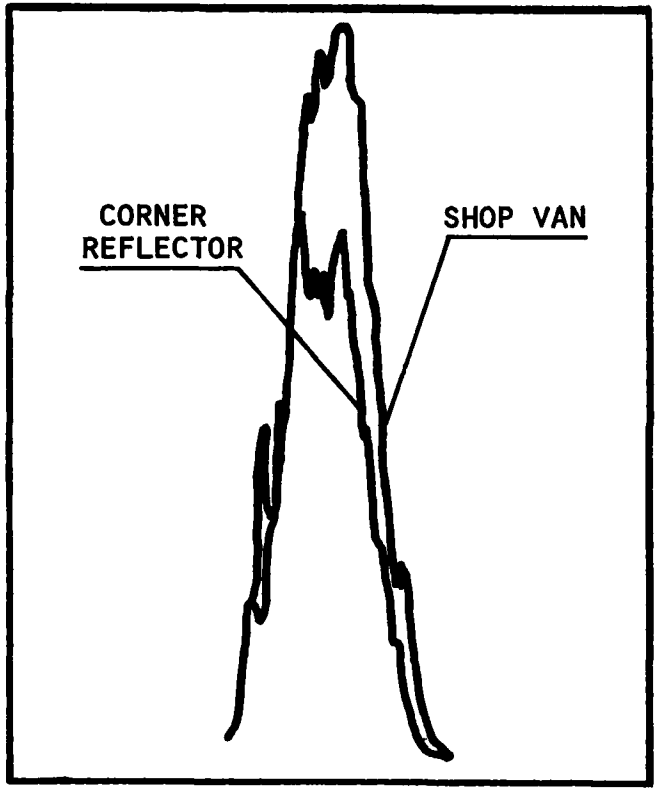

AZIMUTH PROFILES OF CORNER REFLECTOR AND SHOP VAN.

SHOP VAN RANGE: 805 METERS

VERTICAL LINES ARE ONE MILLIRADIAN APART.
ZERO LINE REPRESENTS TARGET LOCATION AS DETERMINED BY THE RADAR.

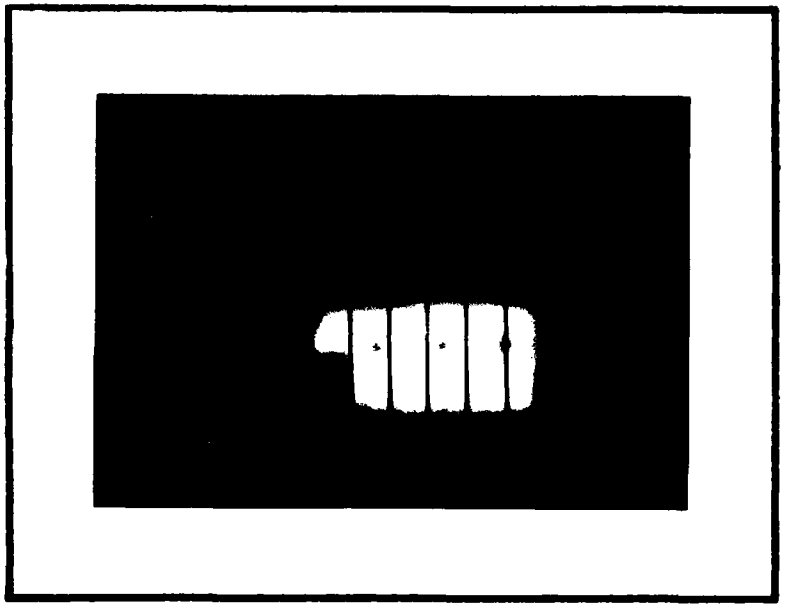

TV VIDEO OF SHOP VAN.

Figure 51. Radar azimuth profiles and TV video: Run number A-6

CORNER REFLECTOR RANGE: 526 METERS.

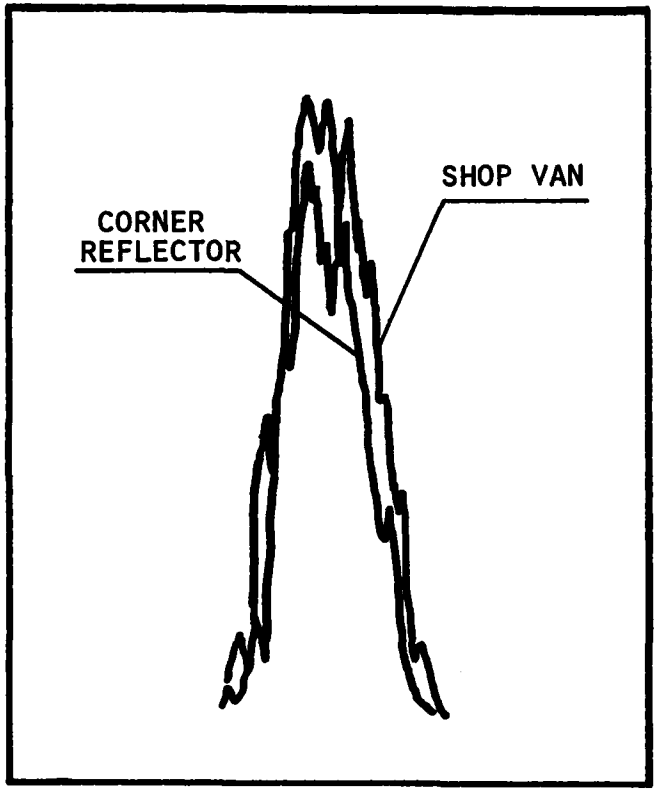

AZIMUTH PROFILES OF CORNER REFLECTOR AND SHOP VAN.

SHOP VAN RANGE: 805 METERS

VERTICAL LINES ARE ONE MILLIRADIAN APART.
ZERO LINE REPRESENTS TARGET LOCATION AS DETERMINED BY THE RADAR.

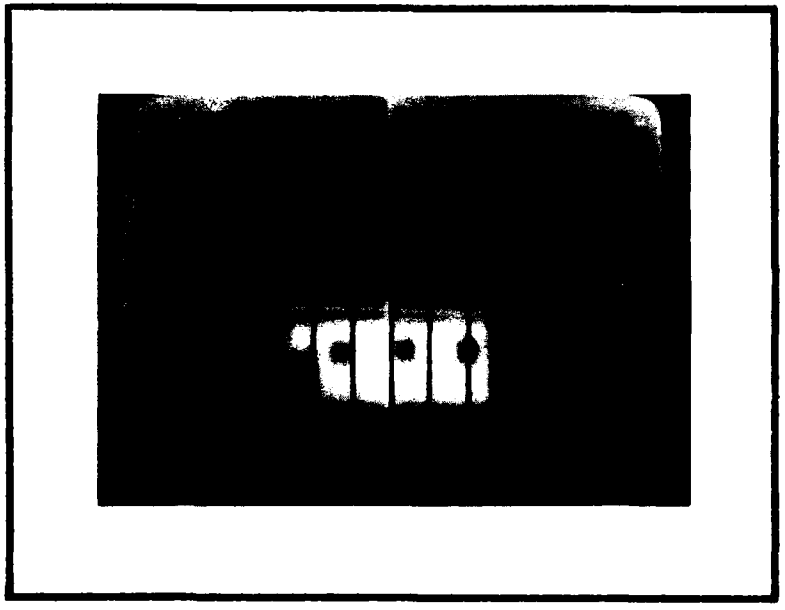

TV VIDEO OF SHOP VAN.

Figure 52. Radar azimuth profiles and TV video: Run number A-7

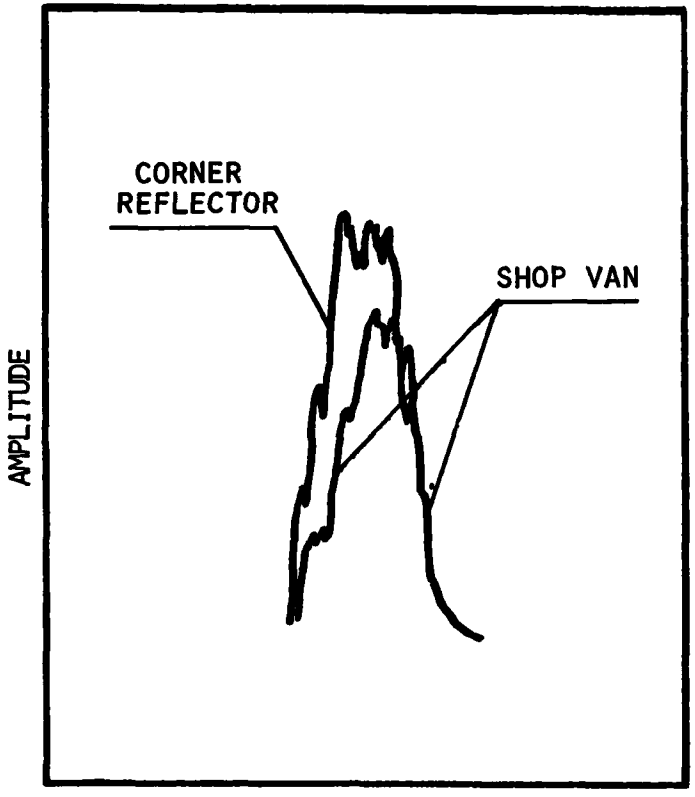

AZIMUTH PROFILES OF CORNER REFLECTOR AND SHOP VAN.

SHOP VAN RANGE: 1316 METERS

VERTICAL LINES ARE ONE MILLIRADIAN APART.
ZERO LINE REPRESENTS TARGET LOCATION AS DETERMINED BY THE RADAR.

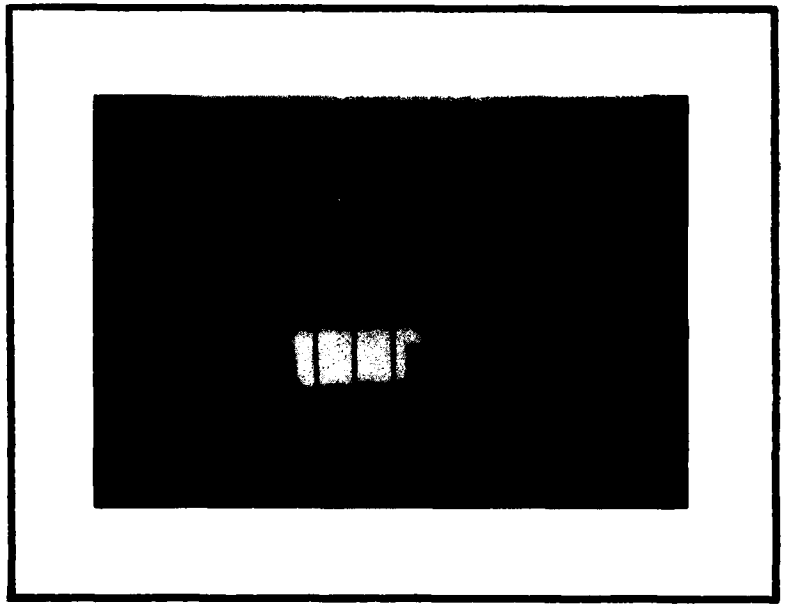

TV VIDEO OF SHOP VAN.

Figure 53. Radar azimuth profiles and TV video: Run number B-1

CORNER REFLECTOR RANGE: 526 METERS.

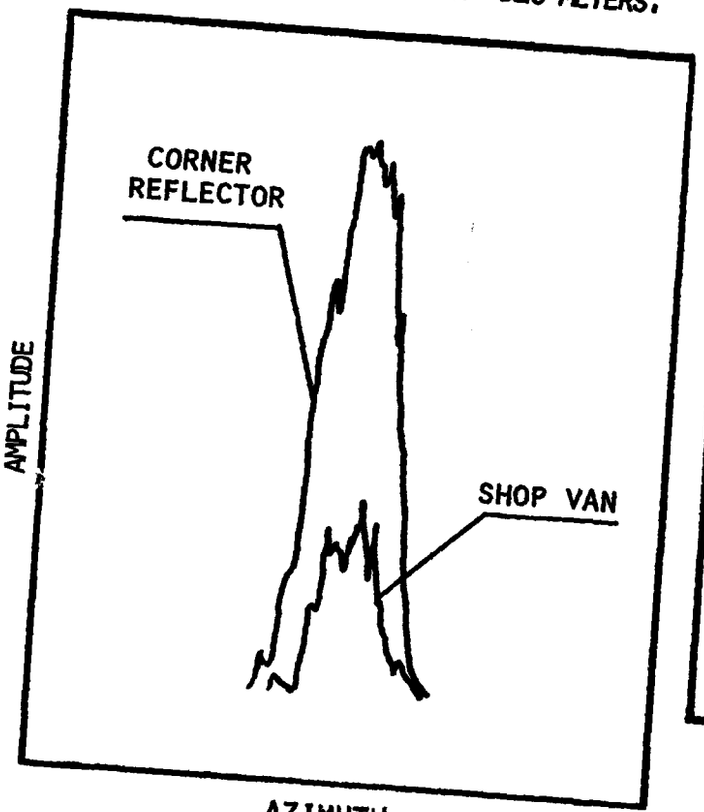

AZIMUTH PROFILES OF CORNER REFLECTOR AND SHOP VAN.

SHOP VAN RANGE: 1316 METERS

VERTICAL LINES ARE ONE MILLIRADIAN APART.
ZERO LINE REPRESENTS TARGET LOCATION AS DETERMINED BY THE RADAR.

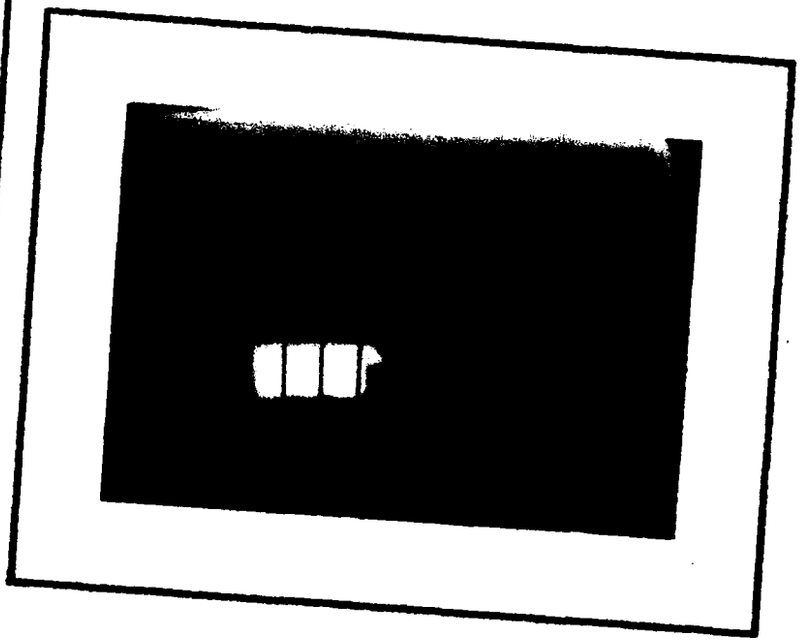

TV VIDEO OF SHOP VAN.

Figure 54. Radar azimuth profiles and TV video: Run number B-2

CORNER REFLECTOR RANGE: 526 METERS.

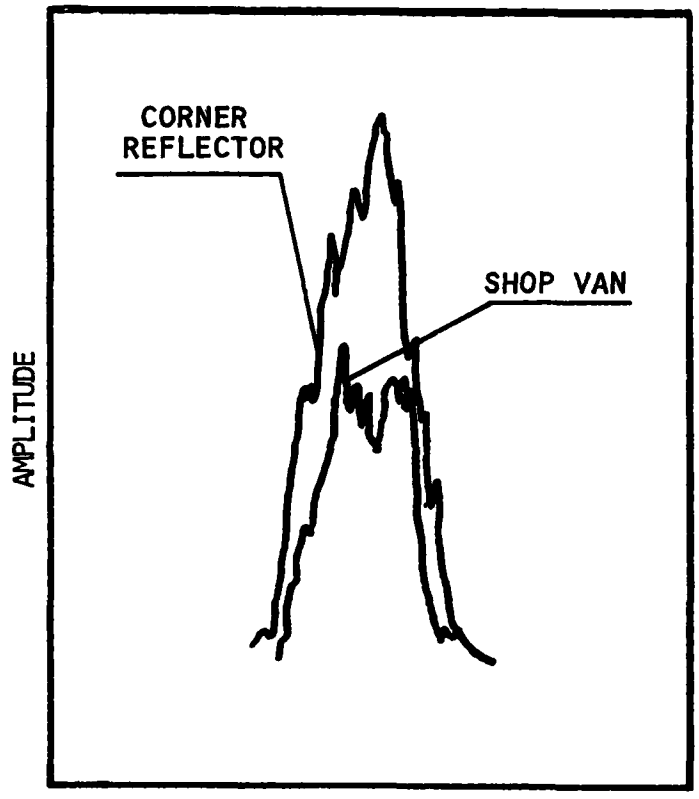

AZIMUTH PROFILES OF CORNER REFLECTOR AND SHOP VAN.

SHOP VAN RANGE: 1316 METERS

VERTICAL LINES ARE ONE MILLIRADIAN APART.
ZERO LINE REPRESENTS TARGET LOCATION AS DETERMINED BY THE RADAR.

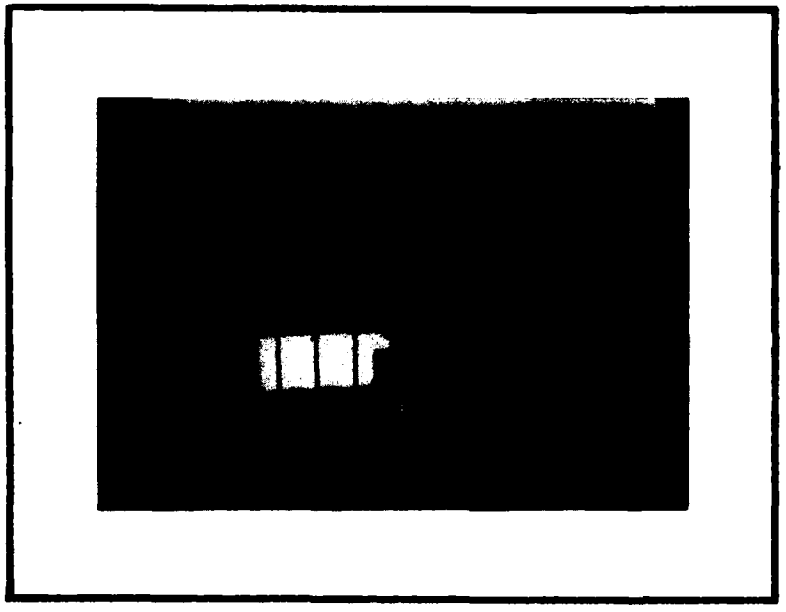

TV VIDEO OF SHOP VAN.

Figure 55. Radar azimuth profiles and TV video: Run number B-3

CORNER REFLECTOR RANGE: 526 METERS.

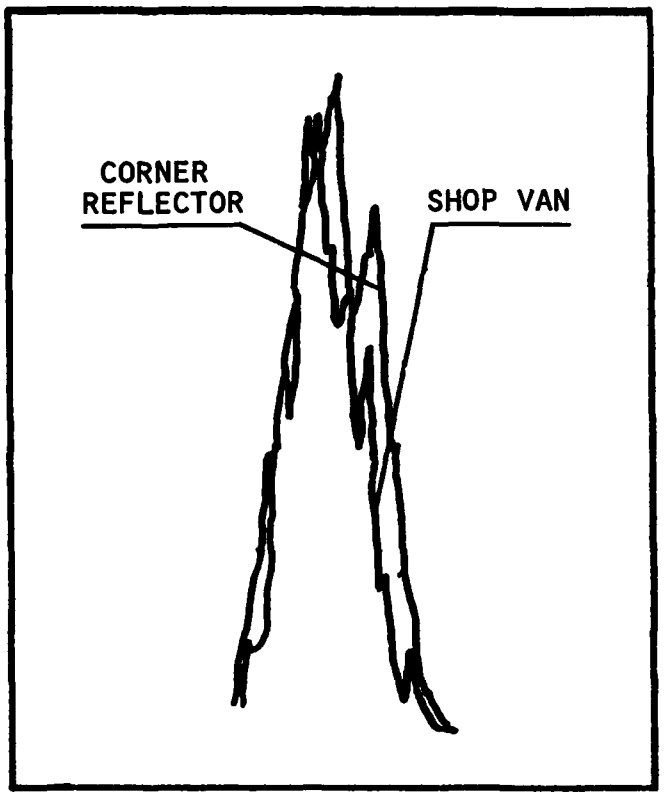

AZIMUTH PROFILES OF CORNER REFLECTOR AND SHOP VAN.

SHOP VAN RANGE: 1316 METERS

VERTICAL LINES ARE ONE MILLIRADIAN APART.
ZERO LINE REPRESENTS TARGET LOCATION AS DETERMINED BY THE RADAR.

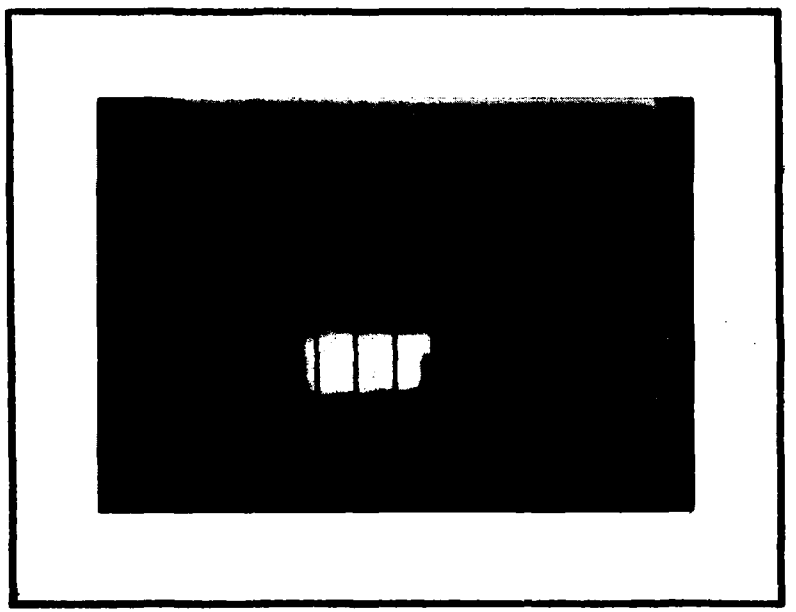

TV VIDEO OF SHOP VAN.

Figure 56. Radar azimuth profiles and TV video: Run number B-4

CORNER REFLECTOR RANGE: 526 METERS.

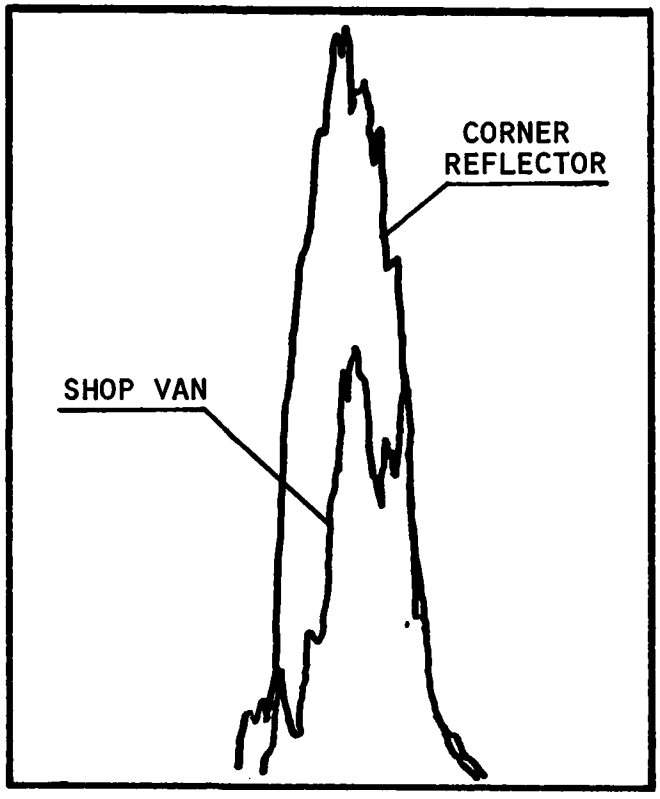

AZIMUTH PROFILES OF CORNER REFLECTOR AND SHOP VAN.

SHOP VAN RANGE: 1316 METERS

VERTICAL LINES ARE ONE MILLIRADIAN APART.
ZERO LINE REPRESENTS TARGET LOCATION AS DETERMINED BY THE RADAR.

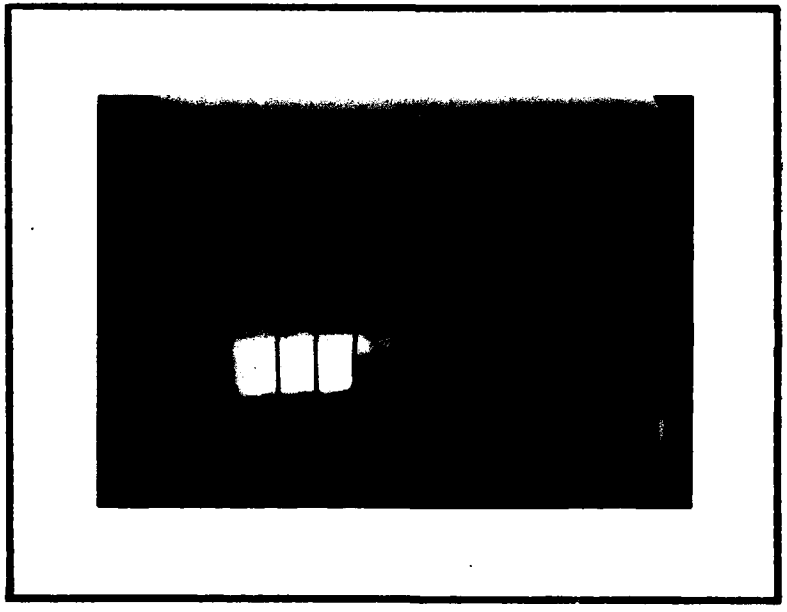

TV VIDEO OF SHOP VAN.

Figure 57. Radar azimuth profiles and TV video: Run number B-5

CORNER REFLECTOR RANGE: 526 METERS.

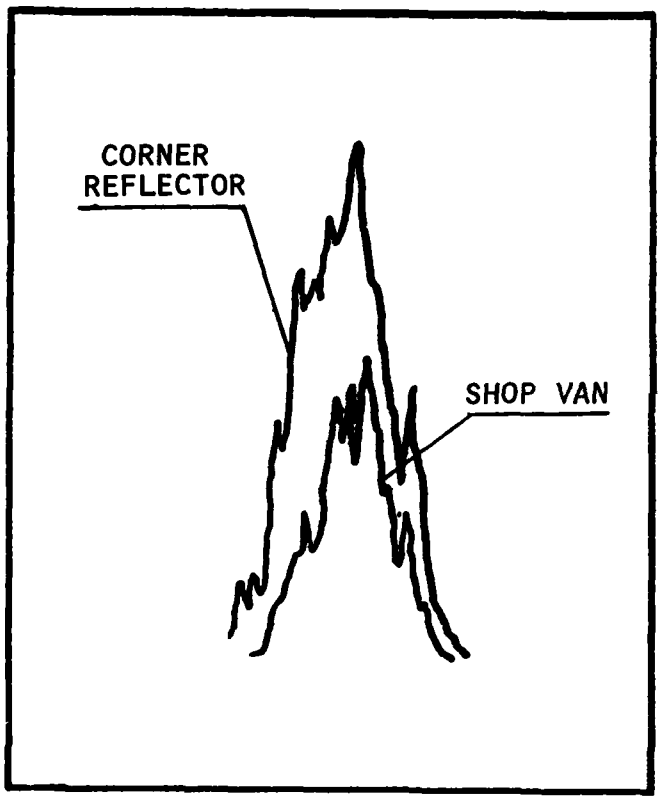

AZIMUTH PROFILES OF CORNER REFLECTOR AND SHOP VAN.

SHOP VAN RANGE: 1316 METERS

VERTICAL LINES ARE ONE MILLIRADIAN APART.
ZERO LINE REPRESENTS TARGET LOCATION AS DETERMINED BY THE RADAR.

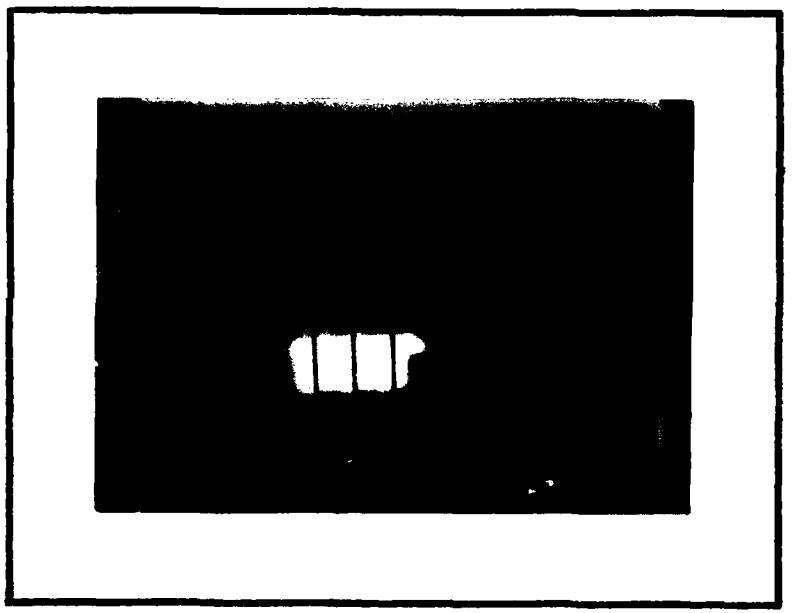

TV VIDEO OF SHOP VAN.

Figure 58. Radar azimuth profiles and TV video: Run number B-6

AD-A146 393 RADAR BEAMSPLITTING EXPERIMENTS AND FEASIBILITY DEMONSTRATION OF A COMBIN.. (U) GEORGIA INST OF TECH ATLANTA ENGINEERING EXPERIMENT STATION W A HOLM ET AL. 2/2

UNCLASSIFIED JUL 78 GIT/EES-A-2047-000 SBI-AD-E001 604 F/G 17/9 NL

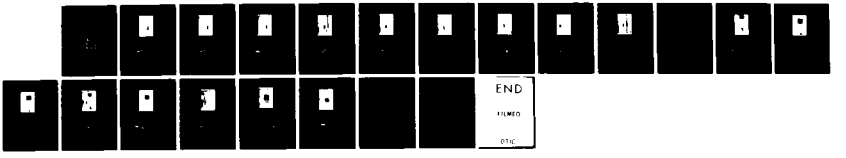

END

FILMED

DTIC

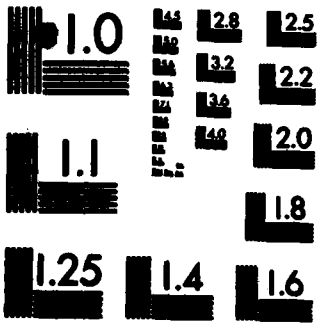

OPY RESOLUTION TEST CHART

CORNER REFLECTOR RANGE: 526 METERS.

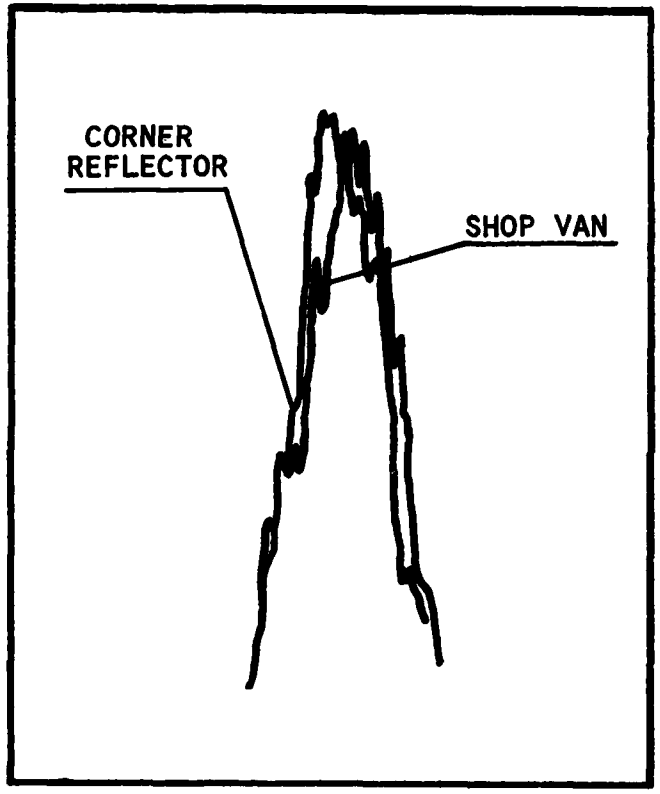

AZIMUTH PROFILES OF CORNER REFLECTOR AND SHOP VAN.

SHOP VAN RANGE: 1316 METERS

VERTICAL LINES ARE ONE MILLIRADIAN APART.
ZERO LINE REPRESENTS TARGET LOCATION AS DETERMINED BY THE RADAR.

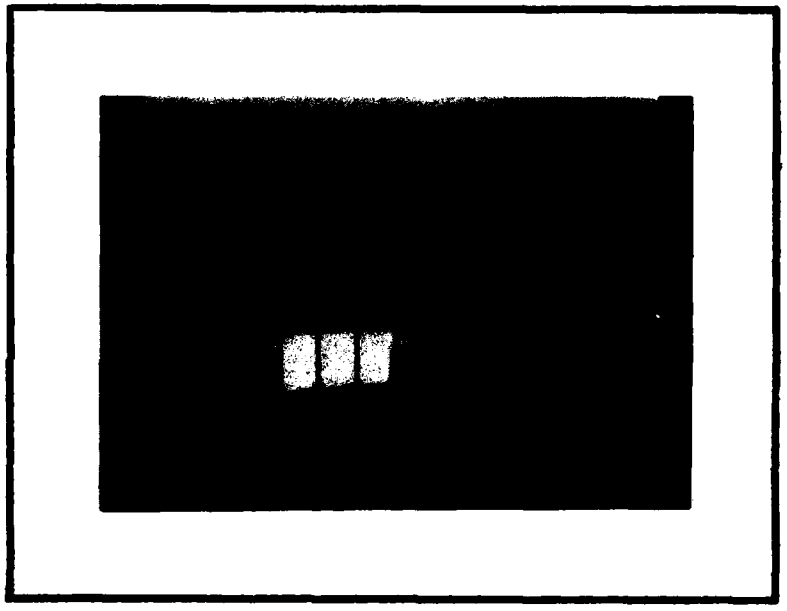

TV VIDEO OF SHOP VAN.

Figure 59. Radar azimuth profiles and TV video: Run number B-7

SHOP VAN RANGE: 1316 METERS

VERTICAL LINES ARE ONE MILLIRADIAN APART.
ZERO LINE REPRESENTS TARGET LOCATION AS DETERMINED BY THE RADAR.

CORNER REFLECTOR RANGE: 526 METERS.

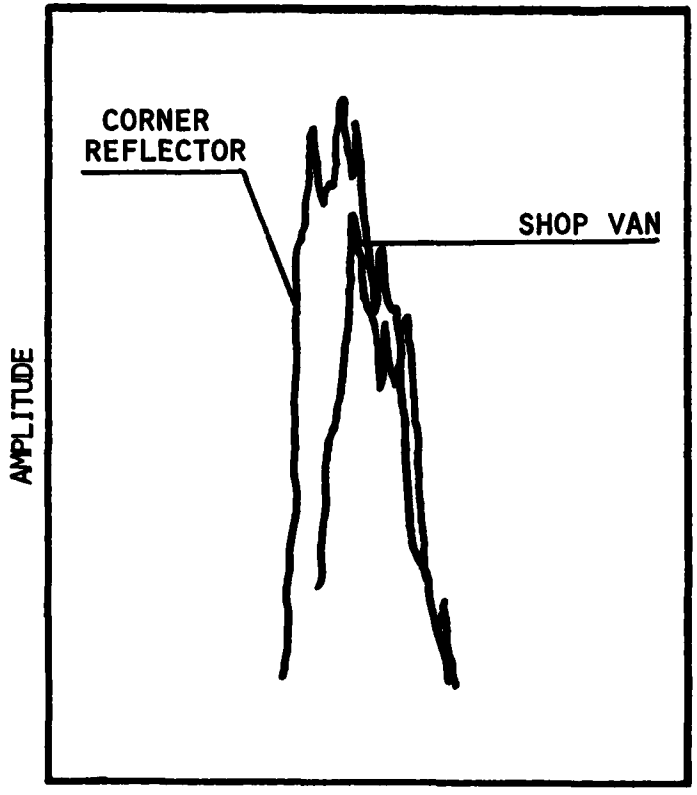

AZIMUTH PROFILES OF CORNER REFLECTOR AND SHOP VAN.

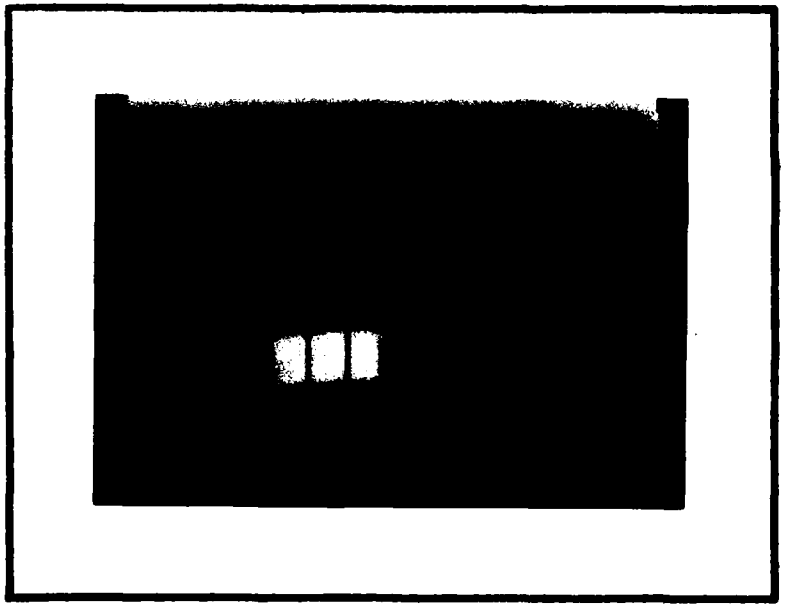

TV VIDEO OF SHOP VAN.

Figure 60. Radar azimuth profiles and TV video: Run number B-8

CORNER REFLECTOR RANGE: 526 METERS.

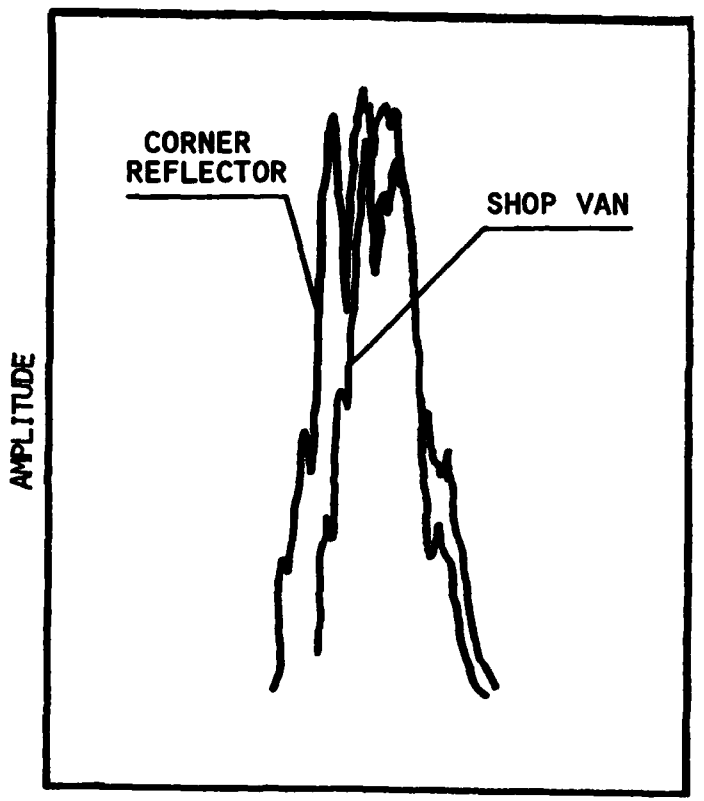

AZIMUTH PROFILES OF CORNER REFLECTOR AND SHOP VAN.

SHOP VAN RANGE: 1316 METERS

VERTICAL LINES ARE ONE MILLIRADIAN APART.
ZERO LINE REPRESENTS TARGET LOCATION AS DETERMINED BY THE RADAR.

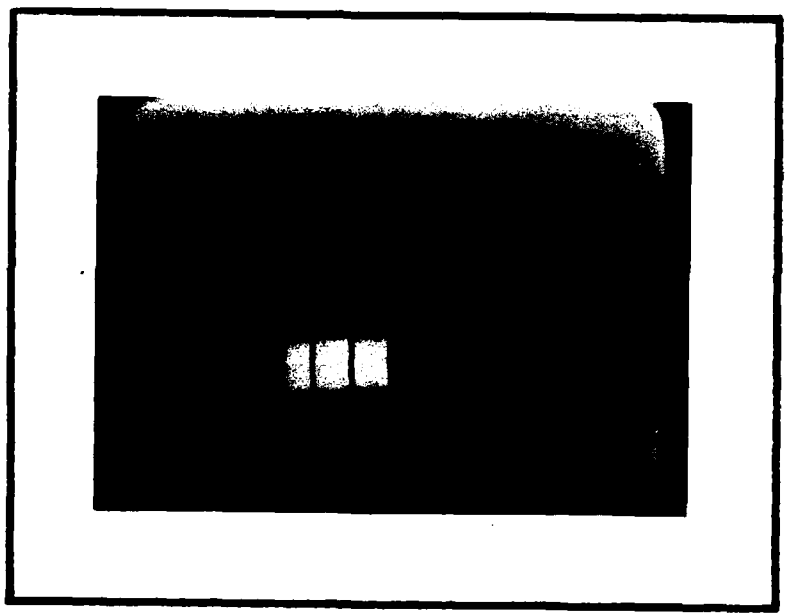

TV VIDEO OF SHOP VAN.

Figure 61. Radar azimuth profiles and TV video: Run number B-9

CORNER REFLECTOR RANGE: 526 METERS.

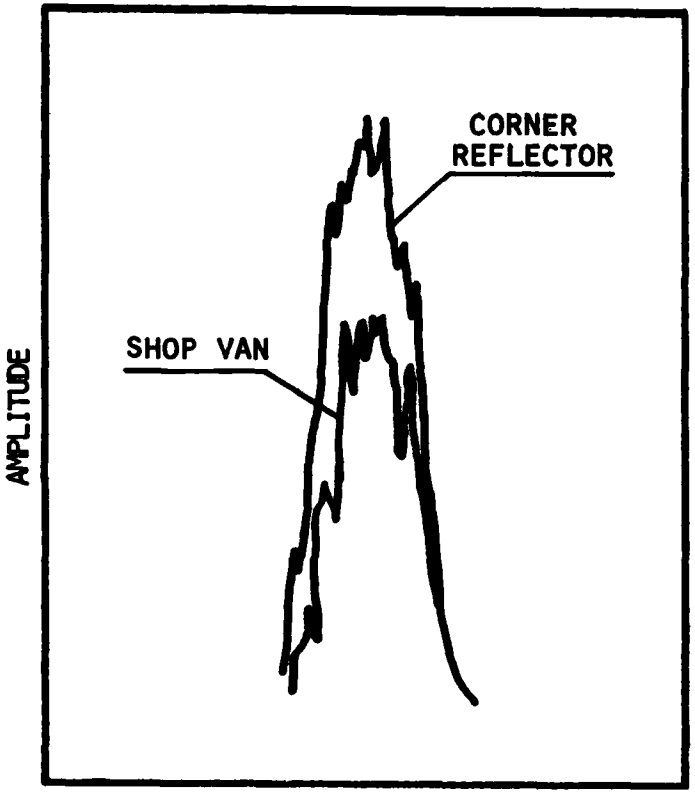

AZIMUTH PROFILES OF CORNER REFLECTOR AND SHOP VAN.

SHOP VAN RANGE: 1420 METERS

VERTICAL LINES ARE ONE MILLIRADIAN APART.
ZERO LINE REPRESENTS TARGET LOCATION AS DETERMINED BY THE RADAR.

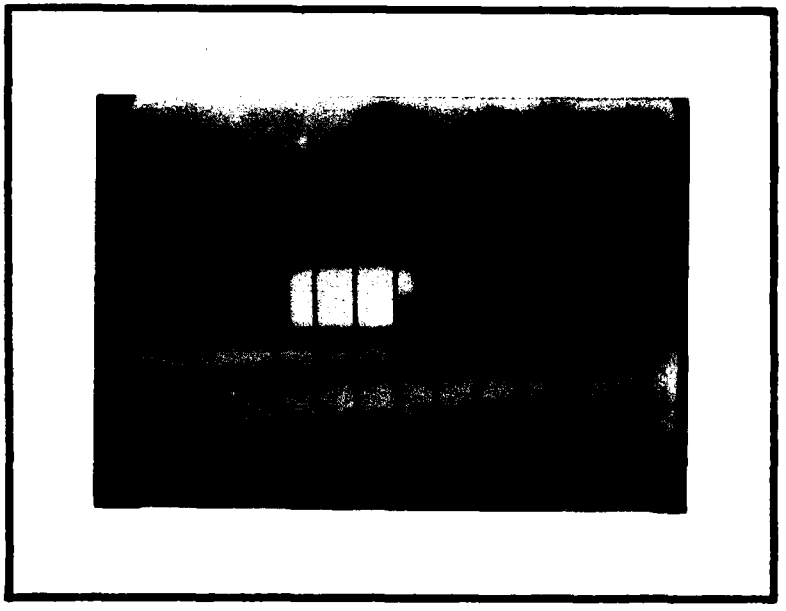

TV VIDEO OF SHOP VAN.

Figure 62. Radar azimuth profiles and TV video: Run number C-1

CORNER REFLECTOR RANGE: 526 METERS.

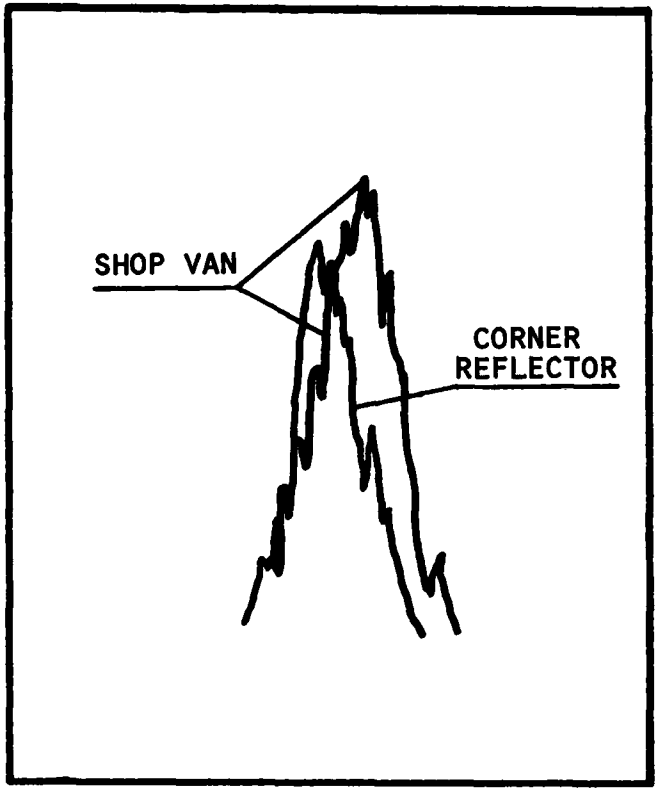

AZIMUTH PROFILES OF CORNER REFLECTOR AND SHOP VAN.

SHOP VAN RANGE: 1420 METERS

VERTICAL LINES ARE ONE MILLIRADIAN APART.
ZERO LINE REPRESENTS TARGET LOCATION AS DETERMINED BY THE RADAR.

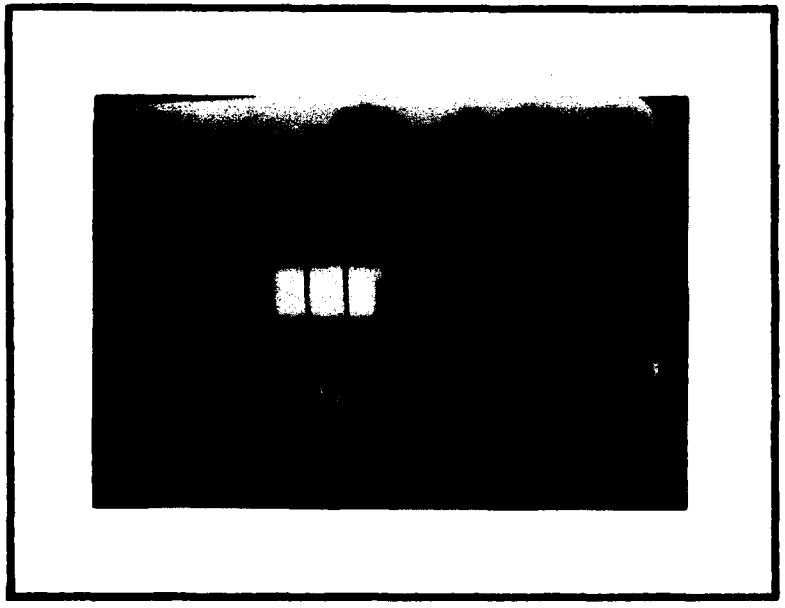

TV VIDEO OF SHOP VAN.

Figure 63. Radar azimuth profiles and TV video: Run number C-2

CORNER REFLECTOR RANGE: 526 METERS.

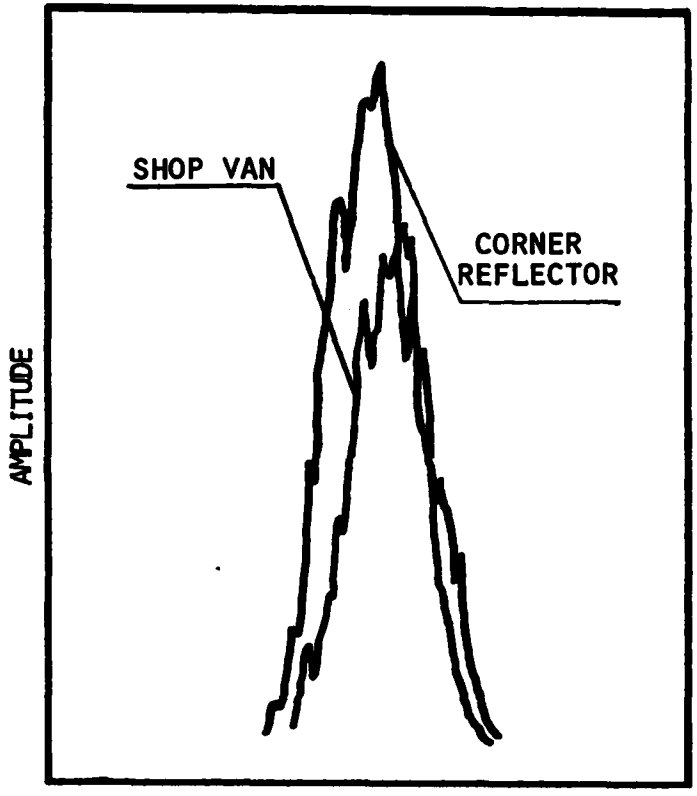

AZIMUTH PROFILES OF CORNER REFLECTOR AND SHOP VAN.

SHOP VAN RANGE: 1420 METERS

VERTICAL LINES ARE ONE MILLIRADIAN APART.
ZERO LINE REPRESENTS TARGET LOCATION AS DETERMINED BY THE RADAR.

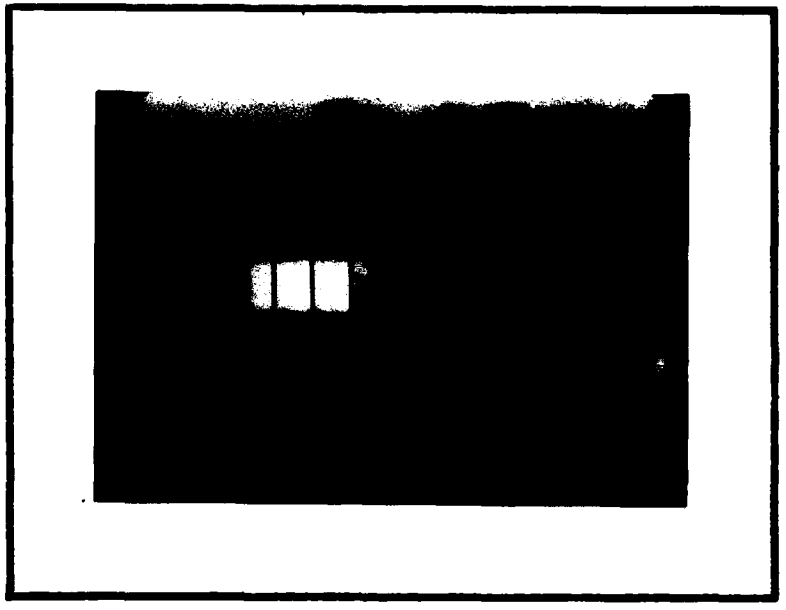

TV VIDEO OF SHOP VAN.

Figure 64. Radar azimuth profiles and TV video: Run number C-3

CORNER REFLECTOR RANGE: 526 METERS.

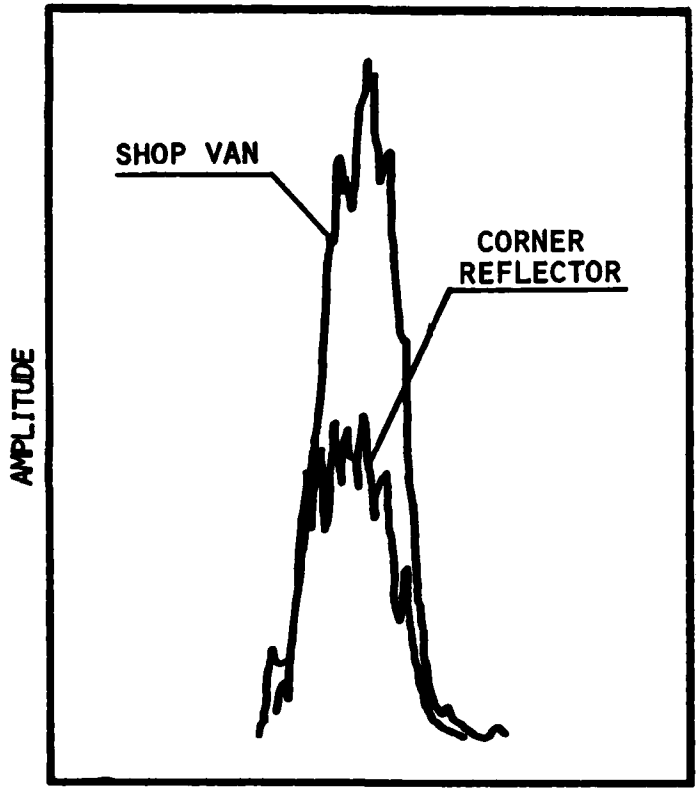

AZIMUTH PROFILES OF CORNER REFLECTOR AND SHOP VAN.

SHOP VAN RANGE: 1420 METERS

VERTICAL LINES ARE ONE MILLIRADIAN APART.
ZERO LINE REPRESENTS TARGET LOCATION AS DETERMINED BY THE RADAR.

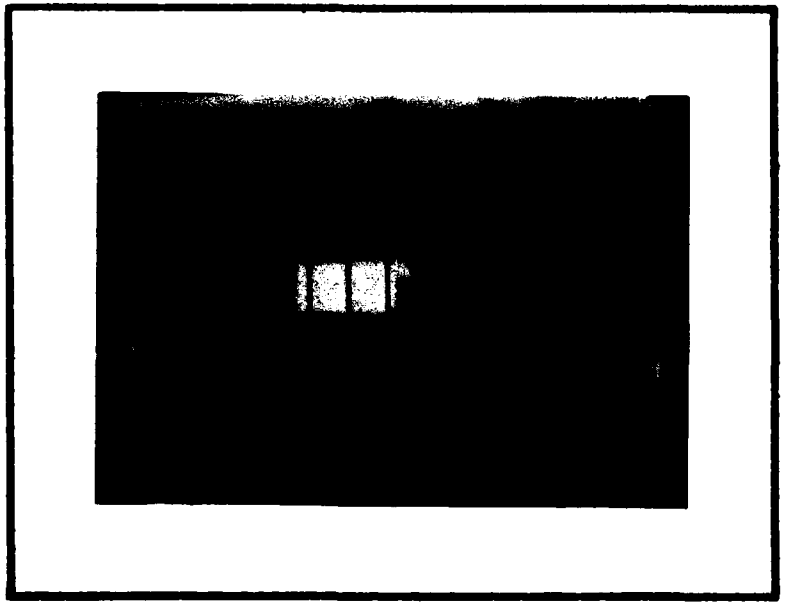

TV VIDEO OF SHOP VAN.

Figure 65. Radar azimuth profiles and TV video: Run number C-4

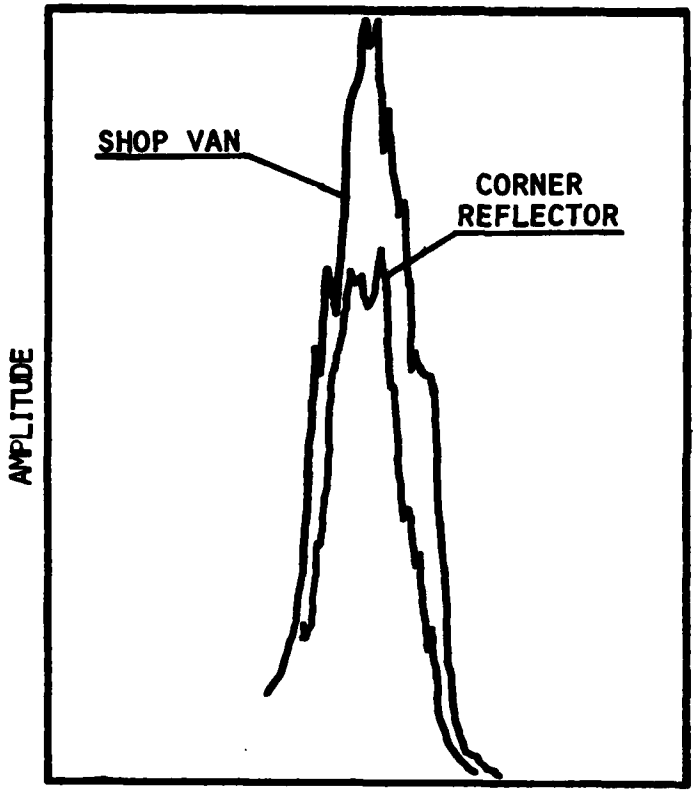

AZIMUTH PROFILES OF CORNER REFLECTOR AND SHOP VAN.

SHOP VAN RANGE: 1420 METERS

VERTICAL LINES ARE ONE MILLIRADIAN APART.
ZERO LINE REPRESENTS TARGET LOCATION AS DETERMINED BY THE RADAR.

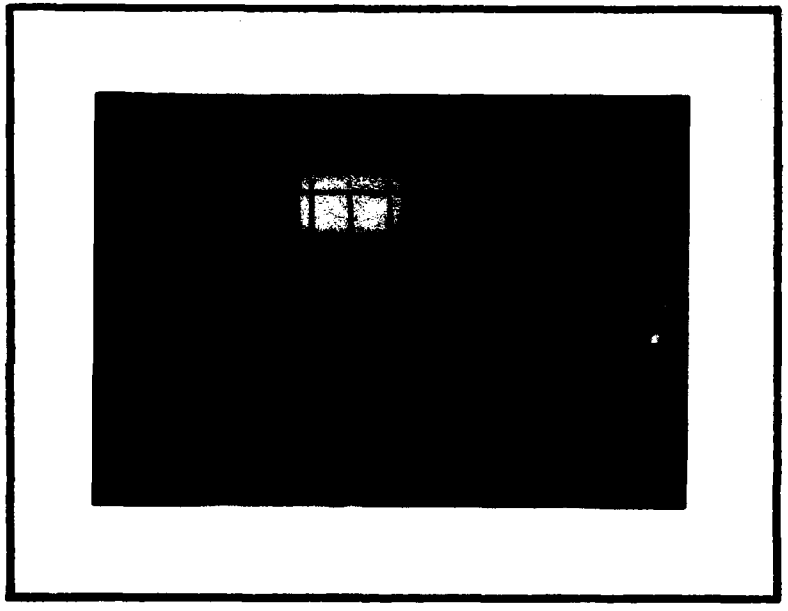

TV VIDEO OF SHOP VAN.

Figure 66. Radar azimuth profiles and TV video: Run number C-5

CORNER REFLECTOR RANGE: 526 METERS.

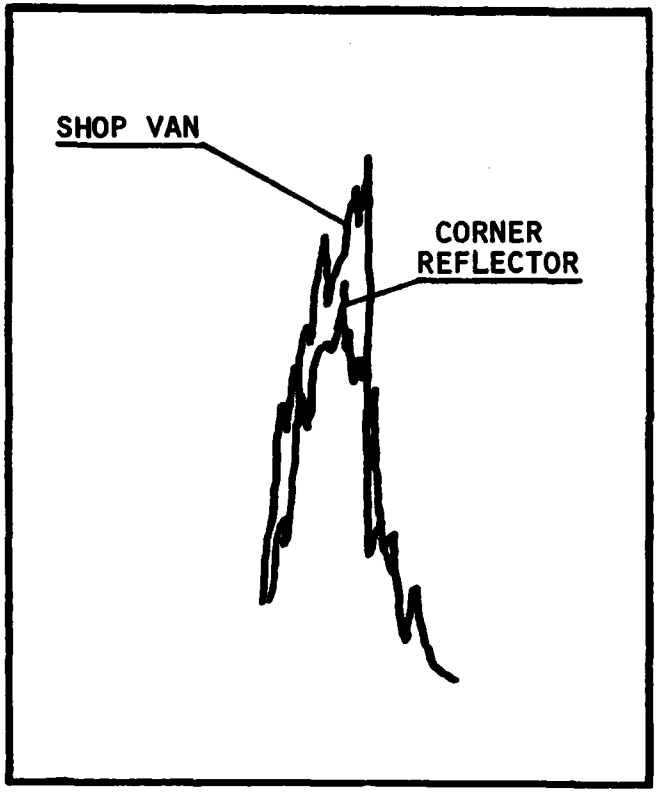

AZIMUTH PROFILES OF CORNER REFLECTOR AND SHOP VAN.

SHOP VAN RANGE: 1420 METERS

VERTICAL LINES ARE ONE MILLIRADIAN APART.
ZERO LINE REPRESENTS TARGET LOCATION AS DETERMINED BY THE RADAR.

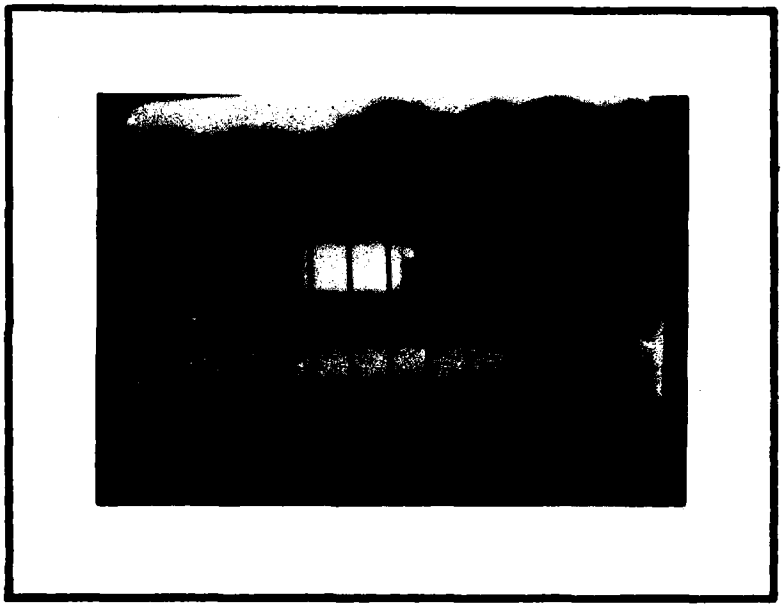

TV VIDEO OF SHOP VAN.

Figure 67. Radar azimuth profiles and TV video: Run number C-6

1. Locate corner reflector in azimuth with EO sensor and align corner reflector stand with the "zero line" of the grid system on the monitor. Adjust special effects generator so that the radar's B-scope is displayed on the monitor.

2. Locate corner reflector in azimuth on B-scope display, electronically scan azimuth cursor across the corner reflector return and plot out a RAP on the X-Y plotter.

3. Locate the center of the RAP of the corner reflector using the electronic beamsplitter and note the cursor voltage of this center.

4. Locate shop van in azimuth on B-scope display and center scanning azimuth cursor on shop van return by moving entire radar console. The scanning cursor is considered centered on the return when the center of the RAP of the shop van as determined by the electronic beamsplitter has a cursor voltage equal to that measured in step three above.

5. Adjust special effects generator so that the EO sensor's scene of view is now displayed on the monitor and note placement of shop van with respect to the "zero line" of the grid system.

Results of these tests are shown in Figures 68 through 75. The shop van was oriented at a 45° angle to radar's boresight. The poorer target locating ability of the electronic beamsplitter is evidenced in these figures by the pictures of the scene of view of the EO sensor taken from the video taped record.

CORNER REFLECTOR RANGE: 538 METERS.

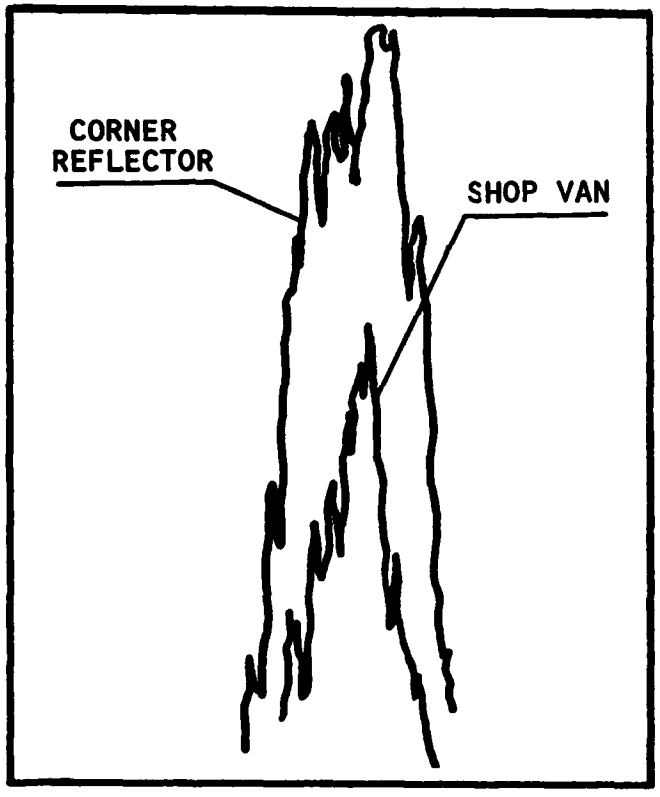

AZIMUTH PROFILES OF CORNER REFLECTOR AND SHOP VAN.

SHOP VAN RANGE: 538 METERS

VERTICAL LINES ARE ONE MILLIRADIAN APART.
ZERO LINE REPRESENTS TARGET LOCATION AS DETERMINED BY THE RADAR.

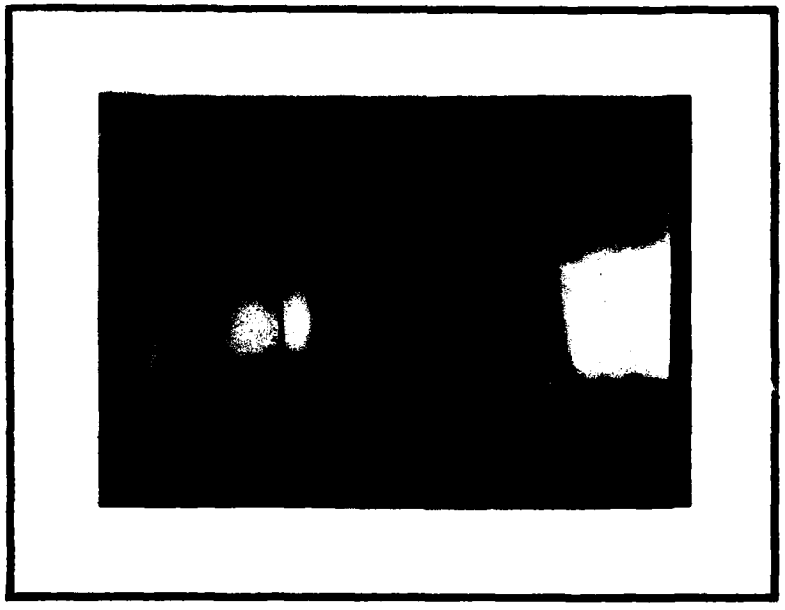

TV VIDEO OF SHOP VAN.

Figure 68. Radar azimuth profiles and TV video: Run number D-1.

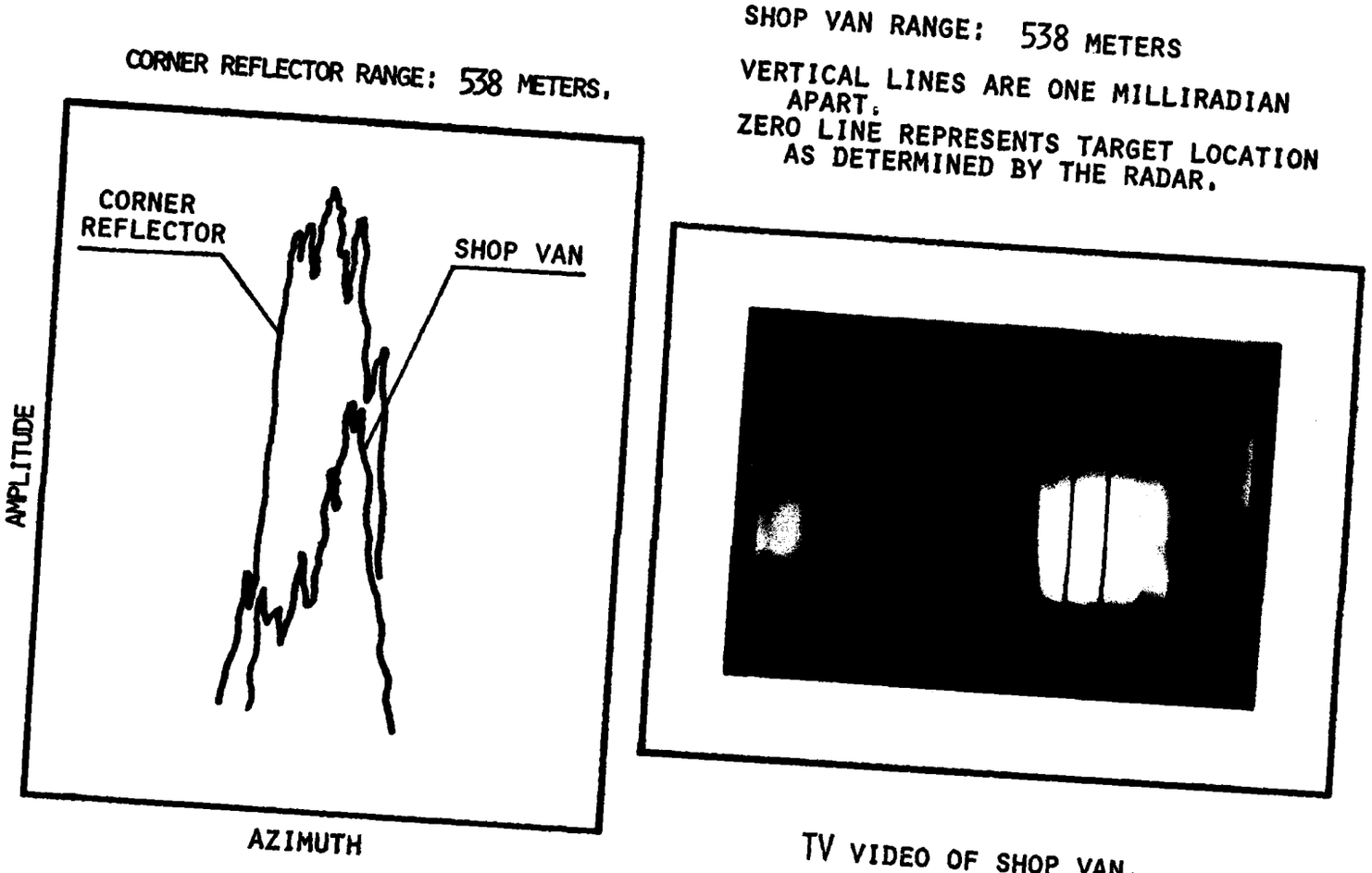

Figure 69. Radar azimuth profiles and TV video: Run number D-2.

CORNER REFLECTOR RANGE: 538 METERS.

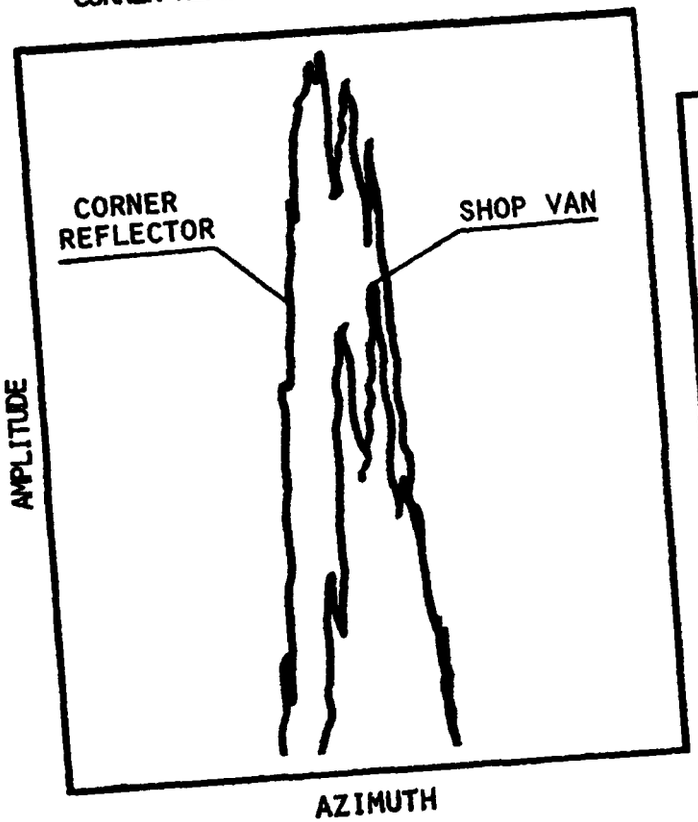

AZIMUTH PROFILES OF CORNER REFLECTOR AND SHOP VAN.

SHOP VAN RANGE: 538 METERS

VERTICAL LINES ARE ONE MILLIRADIAN APART.
ZERO LINE REPRESENTS TARGET LOCATION AS DETERMINED BY THE RADAR.

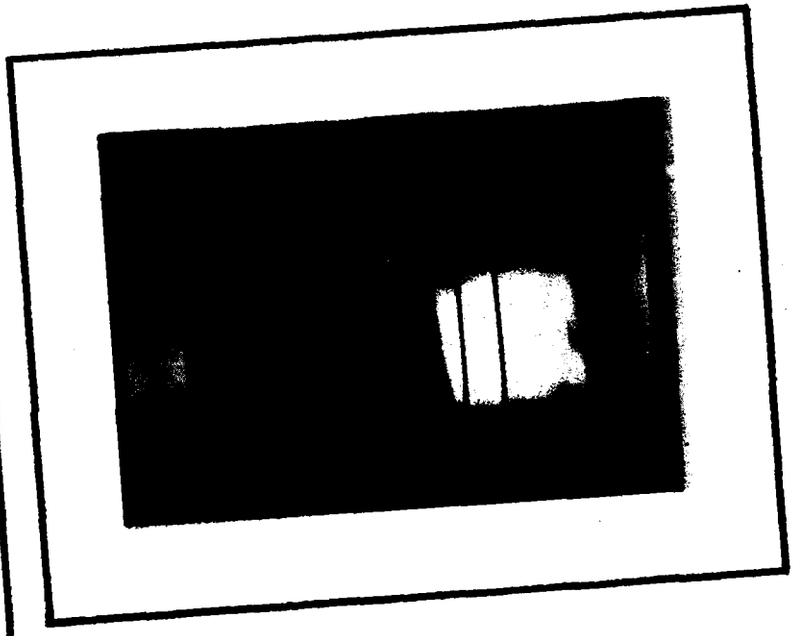

TV VIDEO OF SHOP VAN.

Figure 70. Radar azimuth profiles and TV video: Run number D-3.

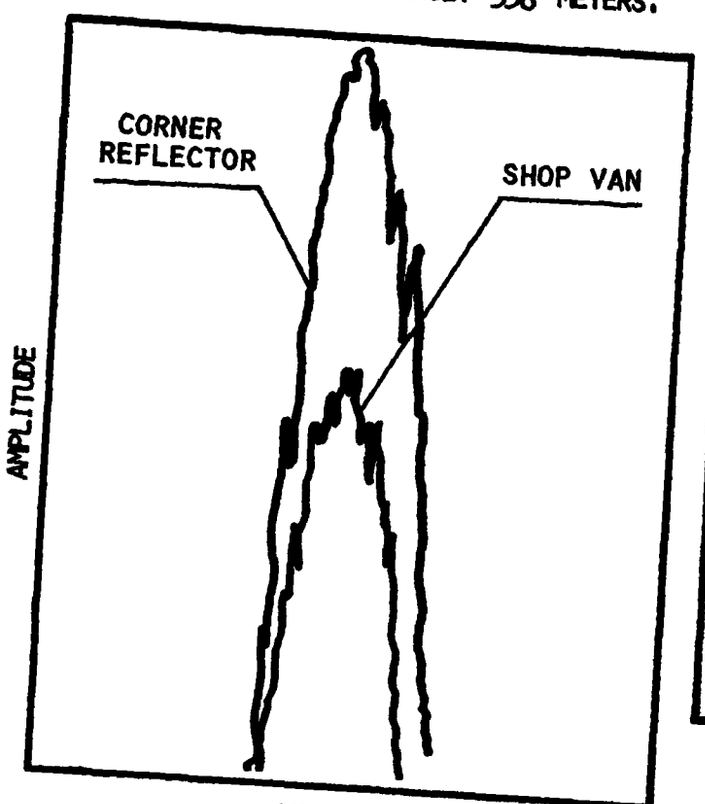

AZIMUTH PROFILES OF CORNER REFLECTOR AND SHOP VAN.

SHOP VAN RANGE: 538 METERS

VERTICAL LINES ARE ONE MILLIRADIAN APART.
ZERO LINE REPRESENTS TARGET LOCATION AS DETERMINED BY THE RADAR.

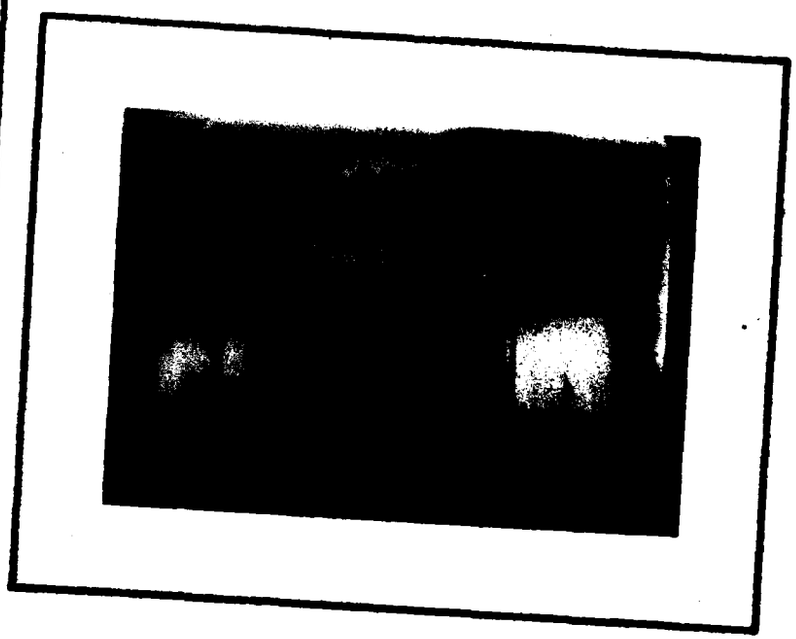

TV VIDEO OF SHOP VAN.

Figure 71. Radar azimuth profiles and TV video: Run number D-4.

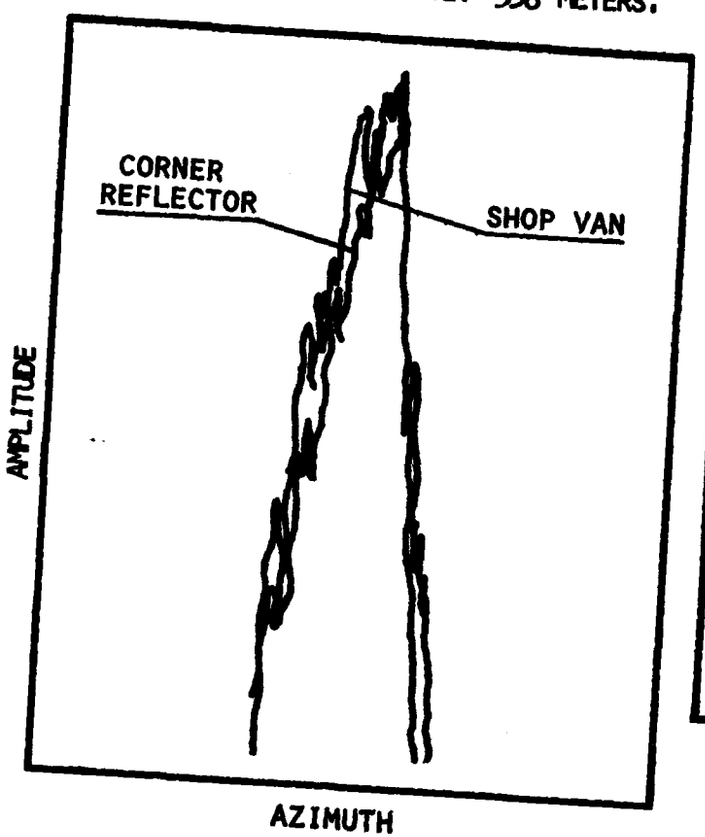

AZIMUTH PROFILES OF CORNER REFLECTOR AND SHOP VAN.

SHOP VAN RANGE: 538 METERS

VERTICAL LINES ARE ONE MILLIRADIAN APART.
ZERO LINE REPRESENTS TARGET LOCATION AS DETERMINED BY THE RADAR.

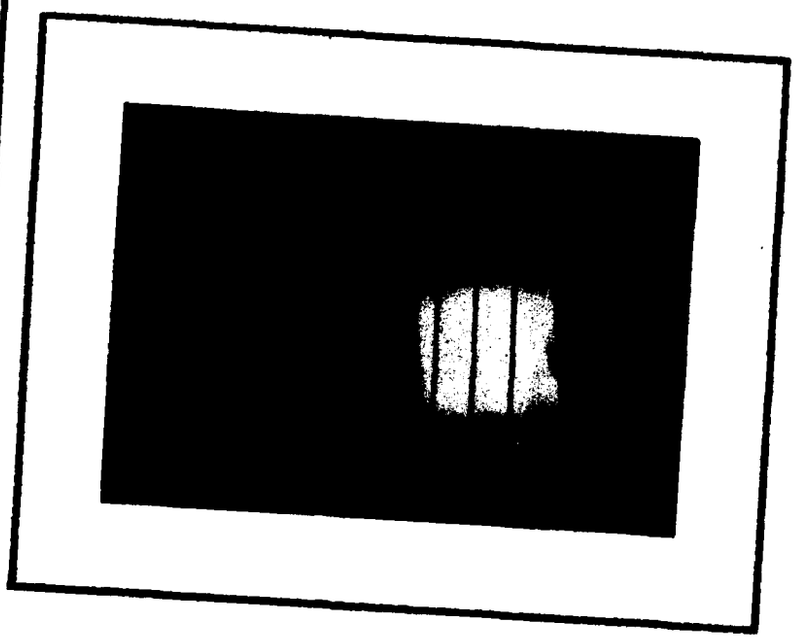

TV VIDEO OF SHOP VAN.

Figure 72. Radar azimuth profiles and TV video: Run number D-5.

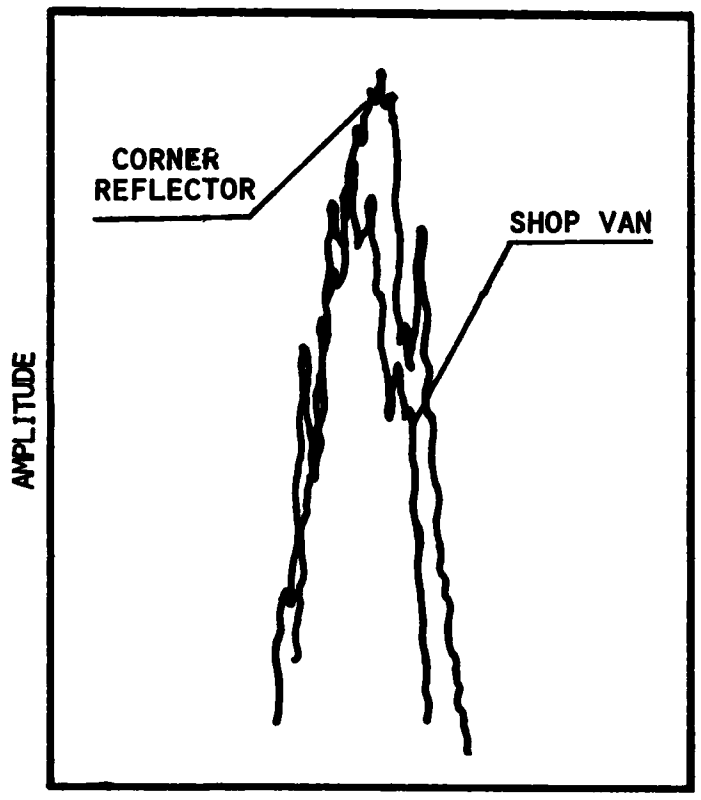

AZIMUTH PROFILES OF CORNER REFLECTOR AND SHOP VAN.

SHOP VAN RANGE: 538 METERS

VERTICAL LINES ARE ONE MILLIRADIAN APART.
ZERO LINE REPRESENTS TARGET LOCATION AS DETERMINED BY THE RADAR.

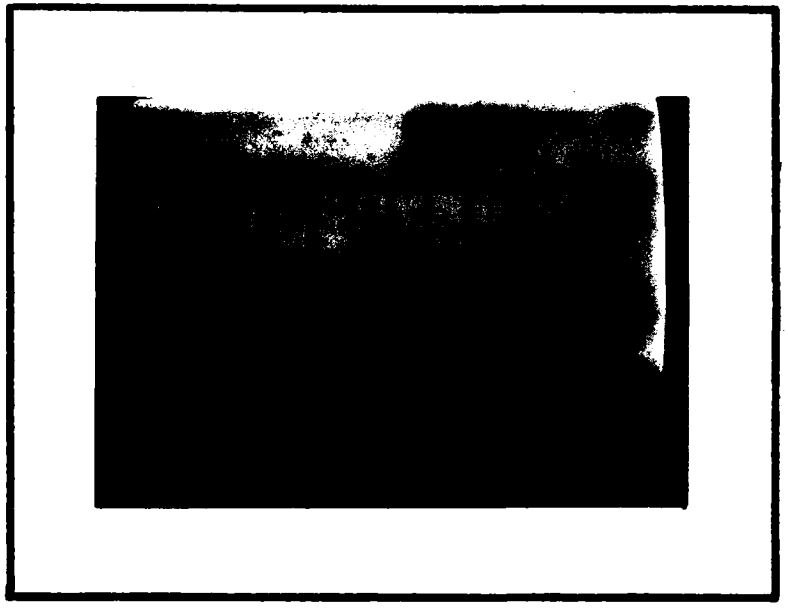

TV VIDEO OF SHOP VAN.

Figure 73. Radar azimuth profiles and TV video: Run number D-6.

CORNER REFLECTOR RANGE: 538 METERS.

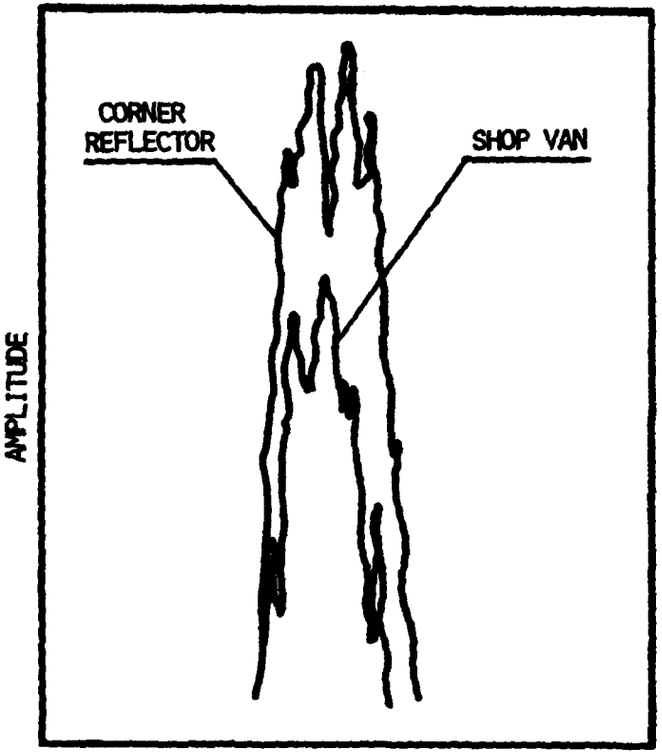

AZIMUTH PROFILES OF CORNER REFLECTOR AND SHOP VAN.

SHOP VAN-RANGE: 538 METERS

VERTICAL LINES ARE ONE MILLIRADIAN APART.
ZERO LINE REPRESENTS TARGET LOCATION AS DETERMINED BY THE RADAR.

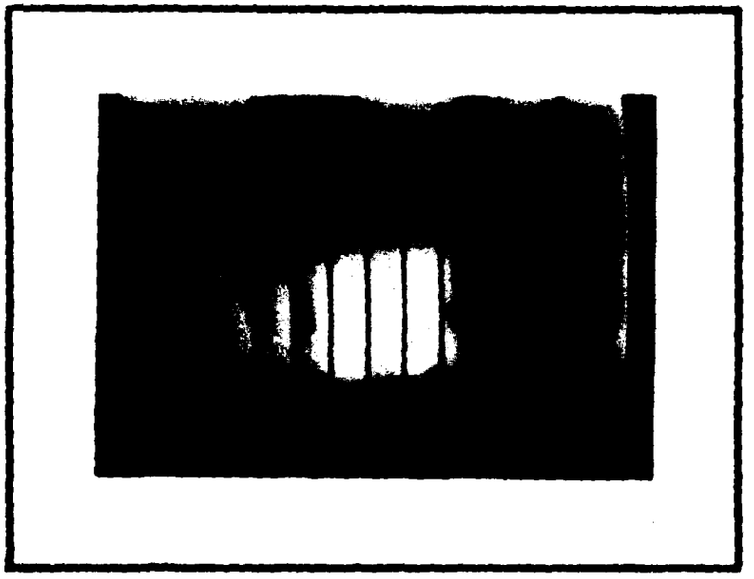

TV VIDEO OF SHOP VAN.

Figure 74. Radar azimuth profiles and TV video: Run number D-7.

CORNER REFLECTOR RANGE: 538 METERS.

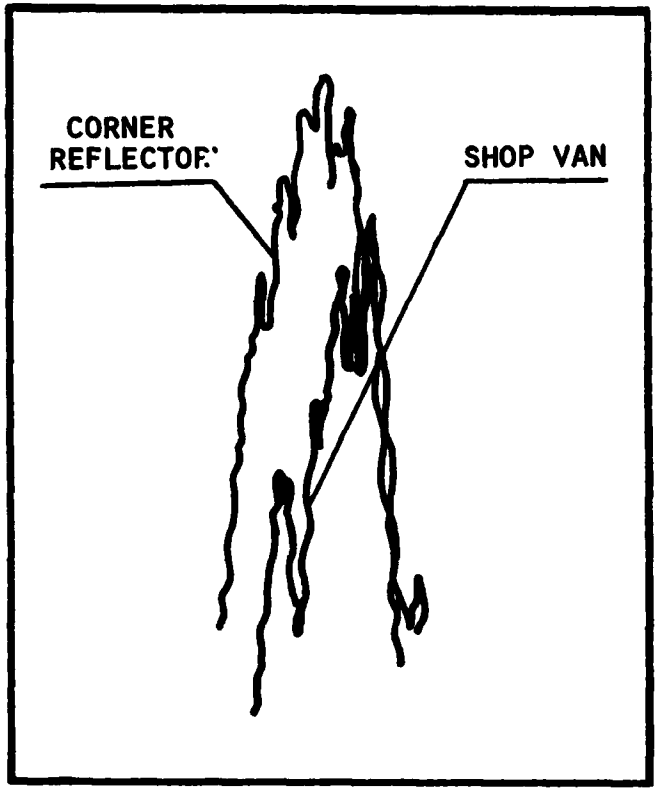

AZIMUTH PROFILES OF CORNER REFLECTOR AND SHOP VAN.

SHOP VAN RANGE: 538 METERS

VERTICAL LINES ARE ONE MILLIRADIAN APART.
ZERO LINE REPRESENTS TARGET LOCATION AS DETERMINED BY THE RADAR.

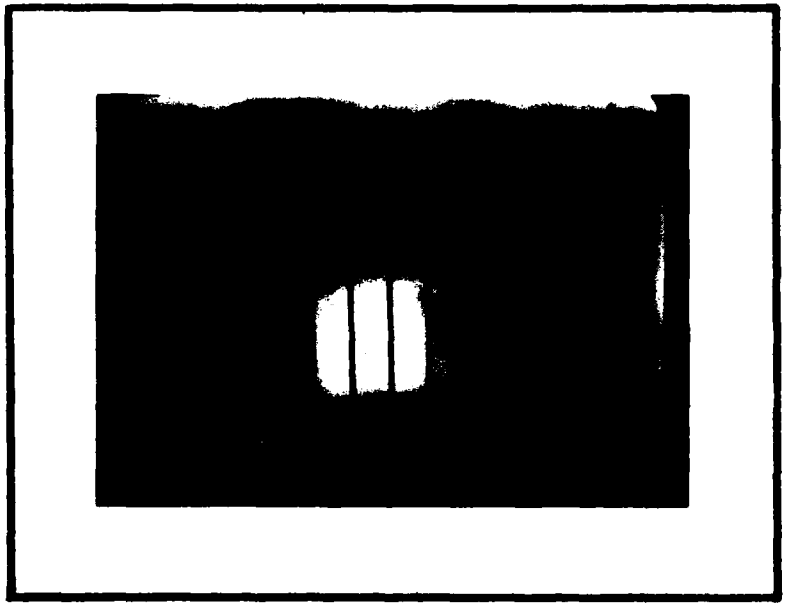

TV VIDEO OF SHOP VAN.

Figure 75. Radar azimuth profiles and TV video: Run number D-8.

V. CONCLUSIONS AND RECOMMENDATIONS

The experimental tests successfully demonstrated the feasibility of the dual mode sensor concept and provided empirical data for system definition and further research. The experiments indicate that the laser radar sensor should scan a 3 mrad by 3 mrad angle of view. This AOV is large enough so that the radar sensor can use beamsplitting techniques to direct the laser to the target such that the target will always be in the laser's field of view. Yet, this AOV is small enough to be easily handled by the laser's scanning optics for the frame rates desired.

Several problems encountered in the field tests were due to the physical location of the EO sensor. The EO sensor was located inside the radar shop van and aligned with the periscope/mirror system. The same location for the laser sensor is not deemed feasible due to space restrictions inside the van, difficulties in obtaining proper minor alignments to minimize optical aberrations and other problems. Therefore, the laser will be located on top of the radar's folded geodesic lens. In this way, the laser and the radar are still mechanically coupled in azimuth. Elevation coupling between the radar and laser will be handled electronically with the radar's elevation cursor driving a gimbaled mirror system for the laser.

The beamsplitting experiments proved to be very successful with 9:1 beamsplits both in azimuth and elevation readily obtained. Beamsplits as high as 19:1 in azimuth were also realized. The success of these experiments is important since the value of an appropriate beamsplitting technique cannot be overemphasized. In adverse environmental conditions when all EO sensors are ineffective, it is extremely important to have the appropriate beamsplitting technique available that would maximize the target locating ability of the radar.

The performance of the automatic electronic beamsplitter fabricated for these experiments was most encouraging. This electronic device involved hands-off operation and thus effectively removed the radar operator from the beam-

splitting exercise. Several improvements in operation of the beamsplitter could be achieved to maximize its performance. One factor that adversely affected all beamsplitting techniques was the instability of a target's return on the radar's display. Tests showed that a stationary target's return would jitter in azimuth as much as 20% of the return width. This effect could be minimized by having the electronic beamsplitter average over a number of sample returns.

The electronic beamsplitter suffered from resolution deficiencies due to its limited 8-bit processing. This problem can be easily rectified by using 12- to 16-bit processing. Also, sensitivity can be increased by using an adaptive threshold. The prototype circuit was implemented with TTL logic and arithmetic logic units (ALU's). In expanded future applications, it is recommended that microprocessor technology be employed to reduce circuit complexity and increase processing flexibility. In addition, the data rate requirements are well within the current state-of-the-art for 12- to 16-bit microprocessing units (e.g., IM6100, TMS9980, CP1600).

One other point worth noting concerns the role of the range cursor and its placement during automatic beamsplitting operations. The range cursor on the 70 GHz radar is excessively wide (in range). In fact, it is as wide as the return from a corner reflector at 450 meters. As a result, it is quite difficult to set the center of the range cursor directly over the target. To solve this problem, a circuit was designed and constructed that differentiated the video in range and detected zero crossings (in the analog domain) thereby allowing targets to be pinpointed in range. It was found that accurate range detection is central to accurate azimuthal beamsplitting. Any second generation beamsplitting processors should include this function as an automatic feature, where the range cursor is scanned like the azimuth cursor to <u>automatically</u> pinpoint target position in both range and azimuth.

END

FILMED

11-84

DTIC